AD-A158 950 THE PHYSICS O SPIN-POLARIZED ATOMIC VAPORS(U) 1/1
PRINCETON UNIV NJ W HAPPER ET AL. 1985
AFOSR-TR-85-0729 AFOSR-81-0104

UNCLASSIFIED F/G 20/8 NL

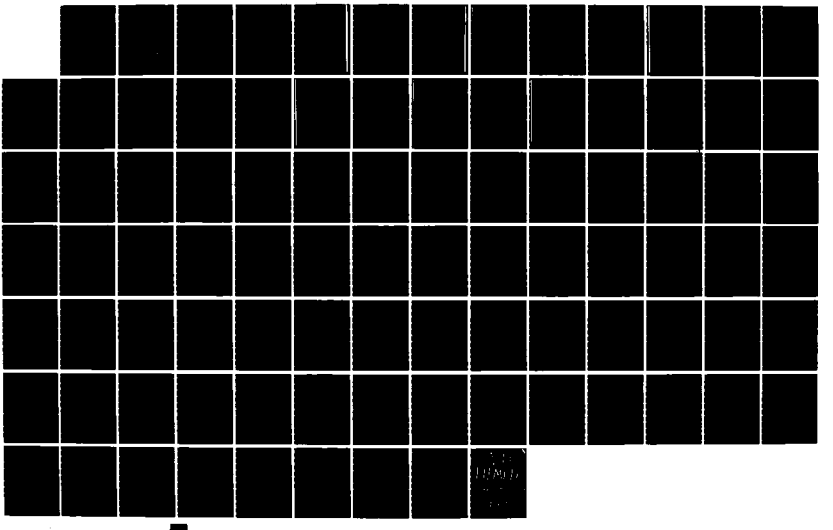

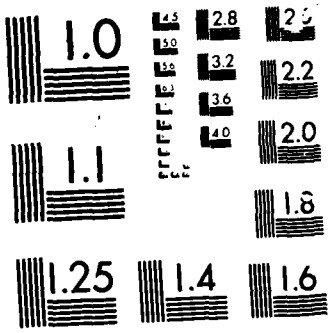

MICROCOPY RESOLUTION TEST CHART

AFOSR-TR- 85-0729

(2)

Scientific Report for Grant AFOSR-81-0104

for Periods Ending April 29, 1984 and March 29, 1985

Final 1 Mar 81 - 28 Feb 85

The major thrust of the work supported by this grant during the past year has been studies of spin polarized noble gases. The aim of the work has been to understand the gas-phase spin transfer, which in heavy noble gases is dominated by interactions in van der Waals molecules. We have measured the three body formation rates and the collisional breakup rates of these molecules. We have also measured the strengths of the major spin interactions in the molecules. We have developed a simple theory of the spin rotation interaction in alkali-noble-gas molecules. This is the first theory which successfully accounts for the observed spin rotation constants in heavy noble gases. More details about the results of our work can be found in the attached reprints and preprint.

While much of the work is basic physics there are also close ties between this work and various practical problems. Atomic frequency standards and nmr gyroscopes, are examples of applied areas which are closely related to our work.

The following personnel have participated in the work supported by this grant.

Dr. W. Happer, Principal Investigator

Dr. Z. Wu, Research Associate

Dr. J. Daniels, Visiting Faculty Member

Dr. M. Kitano, Research Associate

Mr. P. Mende, Graduate Student

Mr. T. Walker, Graduate Student

Princeton University
Princeton, NJ 08540

UNCLASSIFIED

SECURITY CLASSIFICATION OF THIS PAGE

REPORT DOCUMENTATION PAGE

AD-A158 950

1a. REPORT SECURITY CLASSIFICATION UNCLASSIFIED	1b. RESTRICTIVE MARKINGS
2a. SECURITY CLASSIFICATION AUTHORITY	3. DISTRIBUTION/AVAILABILITY OF REPORT Approved for public release; Distribution unlimited
2b. DECLASSIFICATION/DOWNGRADING SCHEDULE	
4. PERFORMING ORGANIZATION REPORT NUMBER(S)	5. MONITORING ORGANIZATION REPORT NUMBER(S) AFOSR TR- 85-0739
6a. NAME OF PERFORMING ORGANIZATION Princeton University 6b. OFFICE SYMBOL (If applicable)	7a. NAME OF MONITORING ORGANIZATION AFOSR/NP
6c. ADDRESS (City, State and ZIP Code) Office of Research and Project Administration Fifth floor, New South Building P.O. Box 36, Princetion Univ. N.J. 08544	7b. ADDRESS (City, State and ZIP Code) Building 410 Bolling AFB DC 20332-6448
8a. NAME OF FUNDING/SPONSORING ORGANIZATION AFOSR 8b. OFFICE SYMBOL (If applicable) NP	9. PROCUREMENT INSTRUMENT IDENTIFICATION NUMBER AFOSR-81-0104
8c. ADDRESS (City, State and ZIP Code) Building 410 Bolling AFB DC 20332-6448	10. SOURCE OF FUNDING NOS. PROGRAM ELEMENT NO. 61102F; PROJECT NO. 2301; TASK NO. A4; WORK UNIT NO.
11. TITLE (Include Security Classification) THE PHYSICS OF SPIN-POLARIZED ATOMIC VAPORS	
12. PERSONAL AUTHOR(S) W. Happer	
13a. TYPE OF REPORT FINAL	13b. TIME COVERED FROM 1 MAR 81 TO 28 FEB 85
14. DATE OF REPORT (Yr., Mo., Day)	15. PAGE COUNT 70
16. SUPPLEMENTARY NOTATION ANNUAL	
17. COSATI CODES FIELD / GROUP / SUB. GR.	18. SUBJECT TERMS (Continue on reverse if necessary and identify by block number)

19. ABSTRACT (Continue on reverse if necessary and identify by block number)

Studies have been made of spin polarized noble gases with the objective of understanding the gas-phase spin transfer in interactions in van der Waals molecules. Three body formation rates and the collisional breakup rates of these molecules have been measured in a number of species. The strengths of the major spin interaction in the molecules has also been measured, and a simple theory of the spin rotation interaction in alkali-noble-gas molecules has been developed. This is the first theory which successfully accounts for the observed spin rotation constants in heavy noble gases. This work will find application in atomic frequency standards and nmr gyroscopes.

20. DISTRIBUTION/AVAILABILITY OF ABSTRACT UNCLASSIFIED/UNLIMITED ☒ SAME AS RPT. ☒ DTIC USERS ☐	21. ABSTRACT SECURITY CLASSIFICATION UNCLASSIFIED
22a. NAME OF RESPONSIBLE INDIVIDUAL Dr. RALPH E. KELLEY	22b. TELEPHONE NUMBER (Include Area Code) (202)767-4909 22c. OFFICE SYMBOL NP

DD FORM 1473, 83 APR EDITION OF 1 JAN 73 IS OBSOLETE.

UNCLASSIFIED

SECURITY CLASSIFICATION OF THIS PAGE

Nuclear Alignment and Magnetic Moments of ^{133}Xe, $^{133}Xe^m$, and $^{131}Xe^m$ by Spin Exchange with Optically Pumped ^{87}Rb

F. P. Calaprice, W. Happer, D. F. Schreiber, M. M. Lowry, E. Miron, and X. Zeng
Princeton University, Princeton, New Jersey 08544
(Received 17 July 1984)

This paper reports the first demonstration of nuclear orientation of radioactive xenon atoms by spin exchange with polarized rubidium atoms. The nuclear tensor alignment, as measured by gamma-ray anisotropy, is about 30% of the maximum possible. The magnetic dipole moments for ^{133}Xe, $^{133}Xe^m$, and $^{131}Xe^m$ have also been measured by NMR spectroscopy. The methods developed here have possibilities for wide applications to nuclear and atomic studies of other radioactive rare-gas atoms.

PACS numbers: 21.10.Ky, 29.90.+r, 32.30.Bv

In this Letter we describe a new experimental method which has allowed us to produce for the first time large quantities of highly polarized nuclei of radioactive noble gases without the use of low temperatures, high magnetic fields, or Stern-Gerlach magnets. These nuclei have very long spin relaxation times, typically several minutes or longer, and it is therefore possible to obtain magnetic resonance linewidths of a few millihertz, and to make very precise measurements of the magnetic moments of these nuclei and of other small interactions of the nuclei with their environment.

In our work we polarize the nuclei of Xe by spin exchange with Rb atoms which have been electronically spin polarized by optical pumping with a dye laser. The overall spin reaction is

$$\mathrm{Rb}(\uparrow)+\mathrm{Xe}(\downarrow)\rightarrow \mathrm{Rb}(\downarrow)+\mathrm{Xe}(\uparrow), \quad (1)$$

where the arrows in parentheses represent spin directions.

The polarization of helium atoms by spin exchange with polarized Rb atoms was first observed by Bouchiat, Carver, and Varnum.[1] Grover[2] later demonstrated that the heavy-rare-gas atoms have much larger spin-exchange cross sections and large polarizations for the stable xenon isotopes have been observed. The details of the spin transfer (1) are complicated and most of the spin transfer occurs in RbXe van der Waals molecules.[3] A third body, a N_2 molecule in our experiments, is needed to form the RbXe molecules. The N_2 also quenches the fluorescence of the optically pumped Rb atoms and prevents the reabsorption of fluorescence, which destroys the Rb spin polarization.

The three Xe isotopes were oriented by spin exchange with polarized ^{87}Rb and the resulting nuclear alignment was measured by observing γ-ray anisotropies.[4-6] The angular distribution of γ rays emitted from oriented nuclei can be expressed in a series of even Legendre polynomials $P_k(\cos\theta)$,

$$W(\theta)=1+A_2P_2(\cos\theta)+A_4P_4(\cos\theta)+\ldots, \quad (2)$$

where θ is the angle between the orientation axis and the direction of the γ ray. The coefficient A_k can be expressed as a product, $A_k=\rho_kF_k$, of orientation parameter ρ_k and a function F_k which depends on the spin sequence and multipolarity.[7] The tensor-orientation parameters are defined by

$$\rho_k=(2J+1)^{1/2}\sum_m(-1)^{J-m}\times C(J\,J\,k;m\,-m\,0)a_m, \quad (3)$$

where C is the Clebsch-Gordan coefficient and a_m is the population of the m state, normalized to unity, $\sum a_m=1$.

The $\frac{11}{2}^-$ isomers $^{131}Xe^m$ and $^{133}Xe^m$ decay to the $\frac{3}{2}^+$ ground states. The leading multipolarity should be $M4$ but $E5$ is also allowed. However, the $E5$ is expected to be small for a single neutron transition ($h_{11/2}\rightarrow d_{3/2}$) and has not been observed in other experiments. We therefore assume a pure $M4$ decay and the series accordingly terminates at $k=8$, with F_0, F_2, F_4, F_6, and F_8 given by 1, -0.8890, $+0.4434$, $+0.0320$, and -0.2624, respectively. A useful feature of this decay is that the γ intensity along the orientation axis is zero if the initial nuclei are all in the $m=+\frac{11}{2}$ state.

The ^{133}Xe nucleus, with spin $\frac{3}{2}^+$, decays by allowed Gamon-Teller β emission to $\frac{5}{2}^+$ levels of ^{133}Cs at 81 keV and 161 keV. These states then decay to the $\frac{7}{2}^+$ ground state by γ emission with $E2/M1$ mixing ratios given by[8] $\delta_{81}=-0.152(2)$ and $\delta_{161}=+0.61(2)$. The initial nuclear orientation of the $\frac{3}{2}^+$ ^{133}Xe is transferred to the $\frac{5}{2}^+$ states by β decay, resulting in alignment $\rho_2(\frac{5}{2}^+)=(\sqrt{14}/5)\rho_2(\frac{3}{2}^+)$ and $\rho_4(\frac{5}{2}^+)=0$. Thus, only the Legendre polynomial P_2 contributes to the angular distribution and with $F_2(81\ \mathrm{keV})=0.06714$ and $F_2(161\ \mathrm{keV})=0.8028$ we have $A_2(81\ \mathrm{keV})=-0.0502\rho_2(\frac{3}{2}^+)$ and $A_2(161\ \mathrm{keV})=+0.601\rho_2(\frac{3}{2}^+)$.

The experimental apparatus is illustrated in Fig. 1. The tunable, Kr^+ laser pumped, dye laser produces

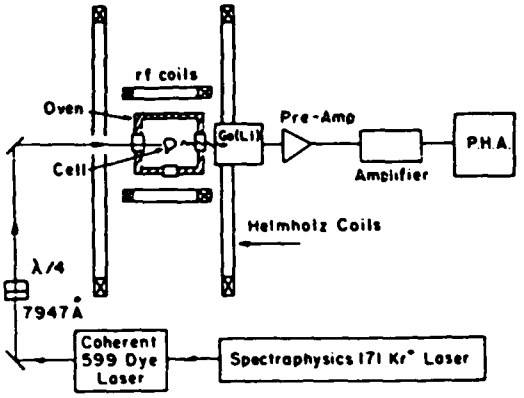

FIG. 1. The experimental apparatus for polarizing Xe isotopes.

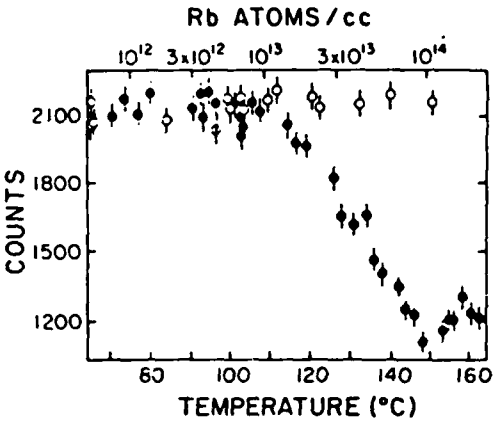

FIG. 2. The count rate from the 164 keV $M4$ γ ray of $^{131}Xe^{m}$ vs cell temperature. The open points were taken with the laser off. The solid points, taken with the laser on, decrease as the Rb density increases, demonstrating significant nuclear orientation.

0.4 W of linearly polarized light at the rubidium D_1 wavelength, 7947 nm, with a bandwidth of ~ 30 GHz. The laser beam is expanded and passed through a $\lambda/4$ plate which converts the light to circular polarization. The second mirror is movable, allowing the cell to be illuminated either with laser light or by a rubidium lamp. The cells, Pyrex-glass spheres with an inner diameter of 1 cm, were filled with a few milligrams of ^{87}Rb metal, about 10 μCi of ^{133}Xe (containing traces of $^{133}Xe^{m}$ and $^{131}Xe^{m}$), and 50 Torr of N_2 gas. The cell was mounted inside an oven heated by flowing hot air. A magnetic field was maintained in the propagation direction of the laser light by three Helmholz coil pairs. A smaller pair of coils near the cell was used to drive magnetic-resonance transitions in the audio- and radio-frequency range.

The γ-ray energy spectrum was measured with a Ge(Li) detector, positioned at $\theta = 0°$, and a multichannel pulse-height analyzer. The intensities in the four peaks at 81 keV, 161 keV, 164 keV, and 233 keV were corrected for background and decay and recorded for each optical pumping and NMR condition. The washout of the angular correlation due to finite detector size is $\sim 5\%$ for the $P_2(\cos\theta)$ term.

Figure 2 illustrates the intensity of the 164 keV line of the $\frac{11}{2}^-$ $^{131}Xe^{m}$ isomer, with laser on and laser off, as a function of cell temperature, or equivalently, Rb density. At room temperature there is no observable difference in count rates indicating no appreciable Xe nuclear alignment. As the temperature is increased the Rb density increases which increases the collision frequency of a Xe atom with polarized Rb atoms. At a temperature of ~ 110°C (Rb density of $\sim 10^{13}$ atoms/cm^3), the spin-exchange rate is fast enough to produce noticeable alignment of the xenon nuclei. As the temperature is increased further the γ-ray count rate decreases, as expected with increasing nuclear alignment, reaches a minimum at about 150 °C (10^{14} atoms/cm^3), and then levels off. The maximum fractional change in count rate (ratio of count rate with laser on and laser off) is 0.56, indicating substantial but not complete polarization of the Xe nuclei. The saturation of alignment which occurs at 150 °C is not completely understood at this time but is thought to be due to failure to maintain complete polarization of the Rb atoms at high density (10^{14} atoms/cm^3). At this density, spin destroying Rb-Rb collisions could reduce the Rb spin polarization. To characterize the nuclear orientation we assume that the magnetic substates have an equilibrium Boltzmann distribution given by $P_m \propto e^{\beta m}$ which is determined by a dimensionless spin-temperature parameter β. The maximum alignment achieved (~ 150 °C) then corresponds to a temperature $\beta = 0.38$. At this temperature the dominant term is the rank-2 alignment for which $\rho_2(\frac{11}{2}^-) \cong 0.51$ while the next term has $\rho_4(\frac{11}{2}^-) \cong 0.04$. The value of $\rho_2(\frac{11}{2}^-)$ if all nuclei were in the $m = +\frac{11}{2}$ state is 1.74. Our result is 29% of this value.

Although we illustrate only the $^{131}Xe^{m}$ data we obtain substantially the same alignment for both $\frac{11}{2}^-$ isomers, $^{131}Xe^{m}$ and $^{133}Xe^{m}$. The spin $\frac{3}{2}^+$ ^{133}Xe, however, behaves a little differently. We find that the alignment begins to be noticeable at a slightly lower temperature, namely ~ 100 °C instead of 110 °C as obtained for the $\frac{11}{2}^-$ isomers. This is not unexpected since the gyromagnetic ratio of ^{133}Xe is larger than that for the $\frac{11}{2}^-$ isomers (see below) and this should enhance the spin-transfer process. The ^{133}Xe alignment increases with temperature up to 140 °C and then begins decreasing with higher temperature, unlike the $\frac{11}{2}^-$ isomer which seems to level off. At the peak in orientation the rank-2 alignment parameter is $\rho_2(\frac{3}{2}) \approx 0.28$ which corresponds to a spin-temperature parameter of $\beta(\frac{3}{2}) \approx 0.83$. If all ^{133}Xe nuclei were in

the $m = +\frac{1}{2}$ state the value of $\rho_2(\frac{1}{2})$ would be 1.0. We have achieved, therefore, about 30% of this maximum for ^{133}Xe.

The magnetic-dipole moments of the xenon isotopes were measured by NMR spectroscopy. A weak alternating magnetic field B_{rf} was applied tranverse to the static field B_0. The resonances were observed by scanning the frequency of the alternating field under conditions in which the cell was at ~ 150 °C and the Xe nuclei were oriented by the laser. When the rf frequency coincides with the nuclear-precession frequency the nuclear orientation is destroyed and the count rate changes. The resonance pattern for ^{131}Xe^m is illustrated in Fig. 3. We note that the 0.5-Hz width of the resonance is determined in this case by the strength of the rf field but much narrower resonances are possible at lower rf fields because of very long spin-relaxation times. To minimize the effects of long-term drifts in the magnetic field, the data were taken in three sets of resonance pairs, namely, ^{133}Xe-^{131}Xe^m, ^{133}Xe^m-^{131}Xe^m, and ^{87}Rb-^{131}Xe^m. The resonance data for each pair were also interwoven so that the ratio of the two resonance frequencies would be accurate. The resonance frequencies are given in Table I.

The frequencies for Zeeman transitions of ^{87}Rb, which were used for field calibration, were measured by observing changes in the light transmitted through the cell when the rf field induced Zeeman transitions in the $F = 2$ multiplet. A rubidium lamp was used for these measurements because the laser light is too noisy. Since the low light intensity of the lamp is unable to penetrate the dense Rb vapor at ~ 150 °C the cell had to be quickly cooled to ~ 90 °C for the measurements.

The ^{87}Rb Zeeman transitions are not resolved at the field used (≈ 2 G). The observed resonance line is thus a superposition of all four transitions in the multiplet $F = 2$. The line has an asymmetric shape which reverses with the circular polarization of the light. An average over all four transitions and both polarization states yields the frequency given in Table I. This corresponds to a field experienced by the Rb atoms of $B_0 = 2.151\,72(5)$ G. There is an additional small contribution to the field experienced by the xenon atoms due to collisions with polarized Rb atoms. From independent studies[9] we estimate that this field would be $B_{Rb\text{-}Xe} = 3.09(30) \times 10^{-3}$ G with 100% polarization at the Rb density corresponding to a cell temperature of 147 ± 5 °C. As a result of the uncertainty in the Rb polarization at high density, we take the average field to be 75% ± 25% of this maximum value. (Collisions of Xe with other Xe atoms and with N_2 molecules can be expected to cause a frequency shift of 10^{-4} Hz or less, based on the work of Brinkman *et al.*[10]) The total field experienced by the Rb atoms in run 3 is therefore $B_{Xe} = 2.154\,04(80)$ G. This value was used to determine the magnetic moment of ^{131}Xe^m from the data of run 3. Runs 1 and 2 then determine the magnetic moments of ^{133}Xe and ^{133}Xe^m. Table II summarizes the magnetic-moment values with and without the correction for atomic diamagnetism. We have not determined the signs of the moments. Previous results are also given in Table II. The present results are substantially more accurate for the $\frac{11}{2}^-$ isomers than the previous values which were obtained by low-temperature methods. Our ^{133}Xe result agrees reasonably well with a preliminary value obtained by laser hyperfine studies in excited Xe states.

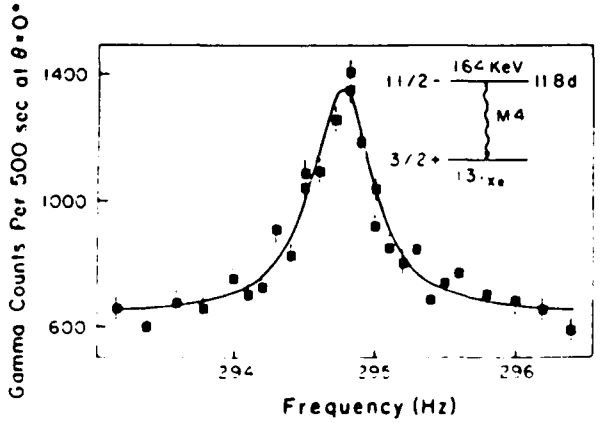

FIG. 3. The NMR pattern for the $\frac{11}{2}^-$ isomer ^{131}Xe^m. The 0.5-Hz width of the resonance is due to power broadening.

TABLE I. Centroid frequencies for spin resonances.

Run	Xe	ν_x (Hz)	$\nu(^{131}\text{Xe}^m)$ (Hz)	$\nu_x/\nu(^{131}\text{Xe}^m)$
1	^{133}Xe	884.442(77)	294.781(6)	3.000 34(27)
2	^{133}Xe^m	321.077(45)	294.850(8)	1.088 95(16)
3	^{87}Rb	1505 291(32)	294.753(8)	5106.96(18)

TABLE II. Magnetic moments.

Isotope	$\lvert\mu_{uncorr}\rvert$ (μ_N)	$\lvert\mu_{corr}\rvert$[a] (μ_N)	$\mu_{previous}$
^{131}Xe^m	0.987 34(38)	0.994 35(38)	−0.80(10)[b]
^{133}Xe	0.807 92(32)	0.813 65(32)	0.8125(3)[c]
^{133}Xe^m	1.075 16(45)	1.082 79(45)	−0.87(12)[b]

[a]Corrected for diamagnetism with $1/(1-\sigma) = 1.007092$. See Ref. 11.
[b]Reference 12.
[c]Reference 13.

These methods can be extended to other radioactive Xe isotopes and very likely to radioactive isotopes of Kr and Rn. The already high spin polarization can certainly be increased by more careful attention to wall relaxation and to the basic limits of optical pumping at high alkali-vapor densities. The radioactive isotopes have already been useful for studying spin polarization in samples which are too optically thick for conventional optical methods.

This work was supported in part by the U. S. Air Force Office of Scientific Research under Grant No. AFOSR-81-0104C and in part by the National Science Foundation.

[1]M. A. Bouchiat, T. R. Carver, and C. M. Varnum, Phys. Rev. Lett. 5, 373 (1960).

[2]B. C. Grover, Phys. Rev. Lett. 40, 391 (1978).

[3]C. H. Volk, T. M. Kwon, and J. G. Mark, Phys. Rev. A 21, 1549 (1980).

[4]J. M. Daniels, *Oriented Nuclei* (Academic, New York, 1965).

[5]U. Cappeller and W. Mazurkewitz, J. Magn. Reson. 10, 15 (1973).

[6]J. Bonn, G. Huber, H. J. Kluge, E. W. Otten, and D. Lode, Phys. Rev. A 272, 375 (1975).

[7]T. Yamazaki, Nucl. Data Sect. A 3, 1 (1960).

[8]K. S. Krane, At. Data Nucl. Data Tables 19, 364 (1977).

[9]D. Gonatas, Senior thesis, Princeton University, 1984 (unpublished).

[10]D. Brinkman, E. Brun, and H. H. Staub, Helv. Phys. Acta 35, 431 (1962).

[11]*Table of Isotopes*, edited by C. M. Lederer and V. S. Shirley (Wiley, New York, 1978), 7th Ed.

[12]R. E. Silvermans, R. Coussement, H. Pattyn, E. Schoeters, and L. Vanneste, Z. Phys. 267, 145 (1974).

[13]F. Schneider, W. Makat, E. Mathias, R. Wenz, and P. J. West, in *Lasers in Nuclear Physics*, edited by C. E. Bemis and H. K. Carter, Nuclear Science Research Conference Series Vol. 3 (Harwood Academic, Chur, 1982).

Polarization of the nuclear spins of noble-gas atoms by spin exchange with optically pumped alkali-metal atoms

W. Happer, E. Miron, S. Schaefer, D. Schreiber, W. A. van Wijngaarden, and X. Zeng
Department of Physics, Princeton University, Princeton, New Jersey 08544
(Received 16 December 1983)

The theory of spin exchange between optically pumped alkali-metal atoms and noble-gas nuclei is presented. Spin exchange with heavy noble gases is dominated by interactions in long-lived van der Waals molecules. The main spin interactions are assumed to be the spin-rotation interactions $\gamma\vec{N}\cdot\vec{S}$ between the rotational angular momentum $\vec{N}$ of the alkali-metal–noble-gas pair and the electron spin $\vec{S}$ of the alkali-metal atom, and the contact hyperfine interaction $\alpha\vec{K}\cdot\vec{S}$ between the nuclear spin $\vec{K}$ of the noble-gas atom and the electron spin $\vec{S}$. Arbitrary values for K and for the nuclear spin I of the alkali-metal atom are assumed. Precise formal expressions for spin transfer coefficients are given along with convenient approximations based on a perturbation expansion in powers of $(\alpha/\gamma N)^2$, a quantity which has been shown to be small by experiment.

I. INTRODUCTION

In this paper we discuss the theory of polarization transfer between the electron spins of alkali-metal atoms and the nuclear spins of noble-gas atoms in a gas. In 1960, Bouchiat, Carver, and Varnum[1] showed that the angular momentum could be transferred from the electron spins of optically pumped Rb atoms to the nuclear spins of ^{3}He in a gaseous mixture of the two elements. Unfortunately, the exchange times were extremely long, on the order of days, and the spin-exchange optical-pumping method was set aside in favor of the method of metastability exchange[2,3] where ^{3}He nuclei were polarized by hyperfine interactions with the electrons of the ^3S metastable state which have been polarized by optical pumping with 1.08-μm radiation. Leduc *et al.*[4,5] have shown that it is also possible to polarize the nuclei of ^{21}Ne by optically pumping the metastable states of neon and allowing metastability exchange collisions to carry the polarization to ground-state atoms. Presumably, similar polarization methods could work for other noble gases. A serious limitation to the method of metastability exchange is the need to operate at low gas pressures, a few Torr in the case of ^{3}He and a small fraction of a Torr for the heavier noble gases. Collisional decoupling of the fine structure in ^{3}He degrades the optical-pumping efficiency and collisional spin depolarization of the metastable states is a serious problem for the heavier noble gases. In contrast, the method of spin exchange with optically pumped alkali-metal atoms can be expected to work well at gas pressures of an atmosphere or more.

Renewed interest in spin-exchange optical pumping of noble-gas nuclei was generated when Grover[6] showed that the nuclei of ^{129}Xe could be polarized with remarkable efficiency by spin exchange with optically pumped Rb atoms. Subsequent work[7–9] has shown that spin-exchange rates between alkali-metal electron spins and the nuclei of heavy noble gases are completely dominated by interactions in van der Waals molecules. The basic process is illustrated in Fig. 1. A Rb atom and a Xe atom collide in the presence of a third body, a N_2 molecule in this example, and form a weakly bound van der Waals molecule. The molecule evolves freely for a time τ until it is broken up by a collision with a second N_2 molecule. During the relatively long molecular lifetime τ the weak coupling between the electron spin S of the alkali-metal atom, the rotational angular momentum N (not shown) of the molecule and the nuclear spin K of the noble-gas atom causes S to flip down and K to flip partway up. In contrast to electron spin exchange between $^2S_{1/2}$ atoms (alkali metals, H atoms, etc.), where the total electron spin of the colliding pair is very nearly conserved, only a small frac-

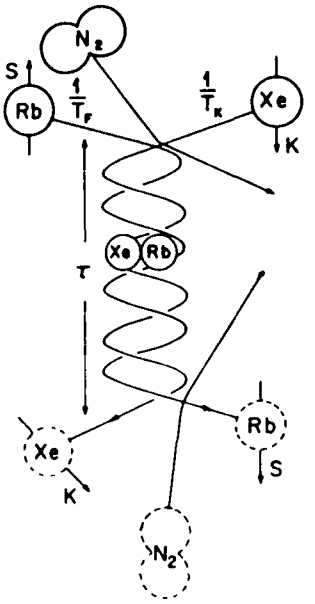

FIG. 1. Alkali-metal-atom–noble-gas molecules are formed in three-body collisions at a rate $(T_F)^{-1}$ per alkali-metal atom and $(T_K)^{-1}$ per noble-gas atom. They are broken up at a rate of $(\tau)^{-1}$ by collisions with other atoms or molecules.

tion ($<10\%$) of the spin lost by the alkali metal is transferred to the noble-gas nucleus. The rest is lost to N, the rotational motion of the alkali-metal atom and the noble-gas atom about each other.

It is noteworthy that the spin-exchange rates are extremely slow for noble gases in alkali-metal vapors because of the weakness of the spin interactions and the infrequency of three-body collisions. For example, the electron-electron spin-exchange rate constant for an alkali-metal atom in an alkali-metal-atom vapor is on the order of 10^{-9} cm^3 sec^{-1}. The nuclear-electron spin-exchange rate constant for a noble-gas atom in an alkali-metal-atom vapor is at most 10^{-14} cm^3 sec^{-1} (for ^{129}XeRb at about 15 Torr N_2 pressure) and the rate constant depends strongly on the third-body pressure.

Since the principal experimental facts about spin-exchange optical pumping of noble-gas nuclei are not widely known, we thought it would be useful to briefly review some of them here. A sketch of a typical apparatus used in our laboratory[10] is shown in Fig. 2. A source of pumping light which in Fig. 2 is a resonance lamp, but which can also be a tunable laser, is circularly polarized and is used to pump the D_1 transition of an alkali-metal atom. The time required to polarize the noble-gas nuclei depends on the cell temperature and on the gas pressure and composition in the cell. A few minutes of pumping are usually necessary. After the noble-gas nuclei are polarized, the subsequent evolution of the polarization can be monitored by removing the circular polarizer from the lamp and observing the circular dichroism of the vapor for D_1 resonance light. As indicated in Fig. 2, it is useful to adiabatically invert the nuclear spins of the noble-gas nuclei from time to time during the decay to eliminate problems due to slow drifts in the response of the detection system. A representative decay curve is shown in Fig. 3. By analyzing the data of Fig. 3 we find that the ^{129}Xe nuclei decay at a rate of 5.5×10^{-3} sec^{-1} after a loss of about 1% of the nuclear polarization per spin inversion has been taken into account. In Fig. 4 we show the measured dependence of the intrinsic decay rate of the noble-gas nuclear polarization on the alkali-metal atomic density, as deduced from the cell temperature and saturated vapor pressure formulas. Note that the noble-gas spin-polarization rate depends linearly on the alkali-metal number density. We may thus interpret the intercept of the curve in Fig. 4 as the relaxation rate due to collision with the walls. In Fig. 5 we show how the alkali-metal-

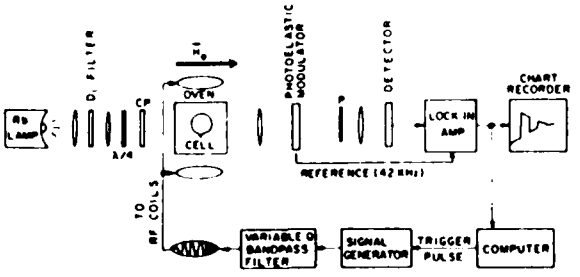

FIG. 2. Main parts of an apparatus to study spin-exchange optical pumping of noble gases. Detailed description of the apparatus is contained in the text and in Ref. 10.

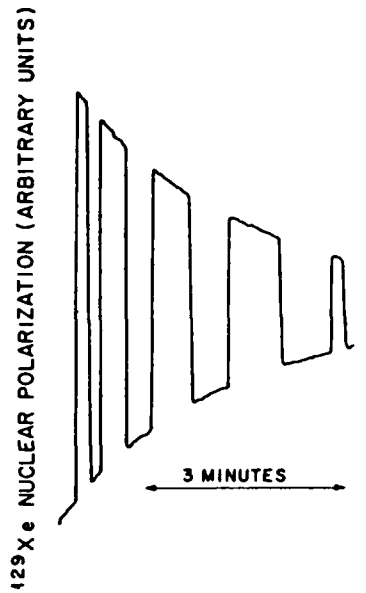

FIG. 3. A representative relaxation curve of ^{129}Xe nuclear spins in a cell containing 1 Torr ^{129}Xe, 35 Torr N_2, and a few droplets of ^{85}Rb metal. Cell temperature was 70.2 °C; the decay time of 181 sec is due to collisions with Rb atoms and with the cell walls. Each spin inversion destroys about 1% of the spin polarization.

induced relaxation depends on the third-body gas pressure, measured in units of a characteristic pressure p_0 which is discussed in more detail in connection with Eq. (156). The relaxation rate is a maximum at a pressure of about 15 Torr of N_2 and the rate diminishes for higher or

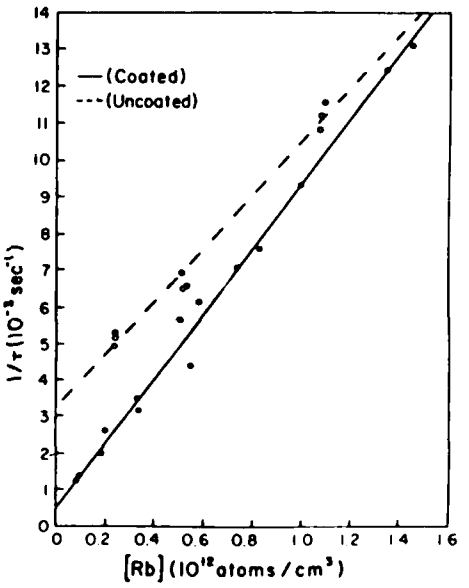

FIG. 4. Dependence of the ^{129}Xe spin-relaxation rate on the ^{87}Rb number density in an uncoated Pyrex cell containing 21 Torr of N_2 and in a silicone-coated Pyrex cell containing 14.9 Torr of N_2. Wall-induced relaxation rate is the intercept at [Rb]=0. Silicone-coated cells have much longer wall relaxation times for ^{129}Xe than uncoated cells (Ref. 10).

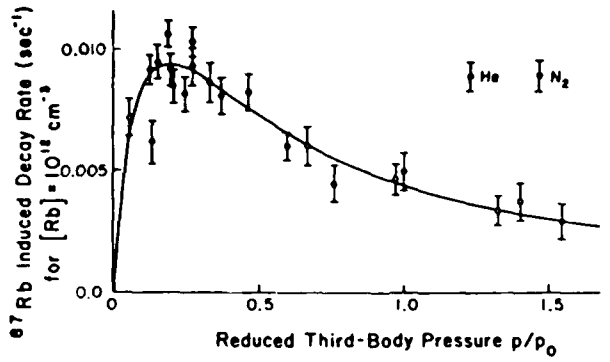

FIG. 5. Dependence of the ^{87}Rb-induced relaxation rate of ^{129}Xe spins on third-body pressures for cells containing $\frac{1}{2}$ Torr ^{129}Xe and operated at a temperature of 75 °C where [Rb] = 10^{14} cm^{-3}. Solid line is calculated from formula (82) (Ref. 11).

lower third-body pressures. Essentially the same relaxation rates are observed with He or N_2 as third bodies provided that the helium pressure is 1.6 times greater than the N_2 pressure.[11] Finally, in Fig. 6 we show the dependence of the alkali-metal-induced relaxation rate on the external field.[9] The relaxation rate is slowed down to values close to the wall-induced rate when a magnetic field of a few hundred gauss is applied to the sample. The width of the magnetic slowing-down curve increases with the third-body pressure. Data such as those of Fig. 6 show unequivocally that the relaxation of the noble-gas nuclear spins is completely dominated by long-lived van der Waals molecules. If the relaxation were caused by binary collisions, with correlation times on the order of 10^{-12} sec, magnetic fields on the order of 10^6 G would be needed to slow down the relaxation rate. Figure 6 shows that the correlation times of the interaction responsible for spin relaxation are on the order of 10^{-7} sec, the Larmor period of an electron spin in a field of 100 G. This long correlation time is almost certainly the collisionally limited lifetime of a van der Waals molecule.

Spin interactions between alkali-metal and noble-gas atoms also lead to significant polarization-dependent shifts in the magnetic resonance frequencies of the spins. Grover[6] has developed a widely used method to detect the spin polarization of noble gases at very small magnetic fields by observing the shifts which they produce in the magnetic resonance frequencies of alkali-metal atoms. A related method which works at large magnetic fields has been developed by McClelland.[12] A major advantage to the frequency-shift methods is their sensitivity to spin interactions of such short duration that negligible transfer of longitudinal spin occurs. Thus the frequency-shift method is especially useful for observing the effects of binary collisions. A disadvantage of frequency-shift methods is their great sensitivity to magnetic field fluctuations. A substantial investment in magnetic shielding is necessary for the successful application of frequency-shift methods.

In this paper we present the basic theory of spin exchange between alkali-metal atoms and noble-gas nuclei. We have made extensive experimental studies of spin-exchange optical pumping of noble-gas nuclei during the past several years and the development of the theory has been guided and constrained by experimental facts. A particularly important experimental result is that the spin-rotation interaction is usually much larger than the spin-exchange interaction. We have carried out experiments on the alkali-metal atoms ^{133}Cs, ^{85}Rb, ^{87}Rb, and ^{39}K with nuclear spins $I = \frac{7}{2}$, $\frac{5}{2}$, $\frac{3}{2}$ and $\frac{3}{2}$, respectively. We have also investigated ^{129}Xe and ^{131}Xe with nuclear spins $K = \frac{1}{2}$ and $\frac{3}{2}$. Consequently the theory has been cast in a form for which I and K are free parameters. We have also adhered as closely as possible to the notation of Bouchiat *et al.*[13,14] who first recognized the importance of van der Waals molecules for the spin relaxation of alkali-metal atoms in heavy noble gases but who did not address the question of spin-exchange polarization and relaxation of noble-gas nuclei. The theory presented here reduces to that of Bouchiat *et al.*[13] when the noble-gas nuclear spin K is zero.

Since our own experiments have been mostly concerned with isotopes of xenon where the spin relaxation is com-

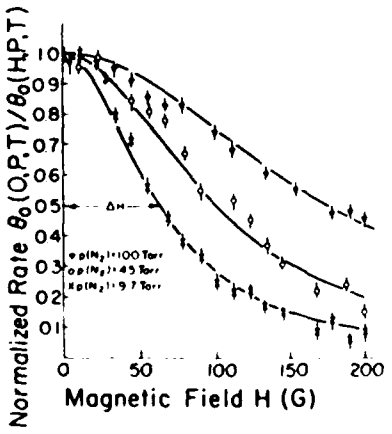

FIG. 6. Dependence of the ^{87}Rb-induced relaxation rate of ^{129}Xe spins on the magnitude of an external magnetic field H. Relaxation rate slows down substantially for fields of a few hundred gauss. Higher magnetic fields are needed to slow down the relaxation rates in cells with higher gas pressure (Ref. 9).

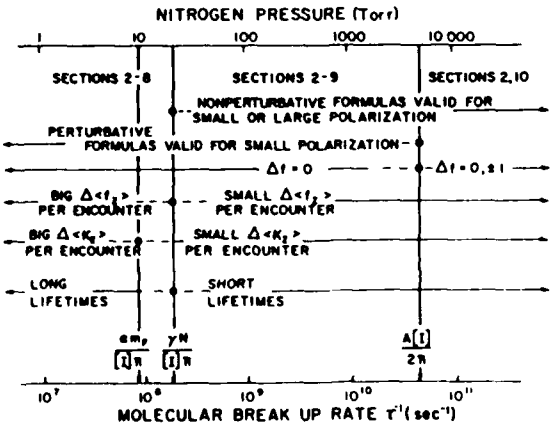

FIG. 7. An overview of the phenomena considered in this paper and of the ranges of validity of various approximations. Parameters A, γN, and am_F are to be interpreted as root-mean-square values.

pletely dominated by van der Waals molecules, we have stressed the relaxation due to molecules in this paper. However, we do discuss the simpler situation of relaxation due to binary collisions in Sec. X.

We derive formal expressions for spin-transfer and spin-relaxation rates of general validity but of such complexity that solutions by electronic computers are needed to compare with experiment. One goal of this paper has been to present simpler, easily evaluated formulas which are in good agreement with exact numerical results in clearly defined regimes of applicability. These regimes are delimited by the molecular breakup rates τ^{-1} which are equal (when multiplied by $\hbar$) to certain terms in the spin Hamiltonian. An overview of the main physical properties of these regimes and of the sections of the paper devoted to each regime is contained in Fig. 7.

II. BASIC THEORY

The simplest spin Hamiltonian which is consistent with currently known data on spin relaxation and spin transfer in mixtures of alkali-metal vapors and noble gases is

$$H = A\vec{I}\cdot\vec{S}+\gamma\vec{N}\cdot\vec{S}+\alpha\vec{K}\cdot\vec{S}+g_S\mu_B\vec{B}\cdot\vec{S} +g_I\mu_B\vec{B}\cdot\vec{I}+g_K\mu_B\vec{B}\cdot\vec{K}+\cdots . \quad (1)$$

The physical significance of the various angular momentum vectors of (1) is illustrated in Fig. 8. The electronic spin $\vec{S}$ of the alkali-metal atom in the molecule is coupled to the nuclear spin $\vec{I}$ of the alkali-metal atom by the magnetic dipole interaction $A\vec{I}\cdot\vec{S}$. The electron spin of the alkali-metal is also coupled to the rotational angular momentum $\vec{N}$ of the molecule by the spin-rotation interaction $\gamma\vec{N}\cdot\vec{S}$. The nuclear spin of $\vec{K}$ of the noble-gas atom is coupled to the electron spin of the alkali metal by the magnetic dipole interaction $\alpha\vec{K}\cdot\vec{S}$. An external magnetic field $\vec{B}$ couples to the magnetic moments of $\vec{S}$, $\vec{I}$, and $\vec{K}$ as shown in (1). The g factors g_I and g_K will be some 3 orders of magnitude smaller than g_S. All of the coupling coefficients $A,\gamma,\alpha,\ldots$ will depend somewhat on the vibrational and rotational state of the van der Waals molecule or on the intermolecular separation and velocity of an unbound colliding pair. We shall understand that subsequent formulas are to be averaged over appropriate molecular quantum states or collisional parameters.

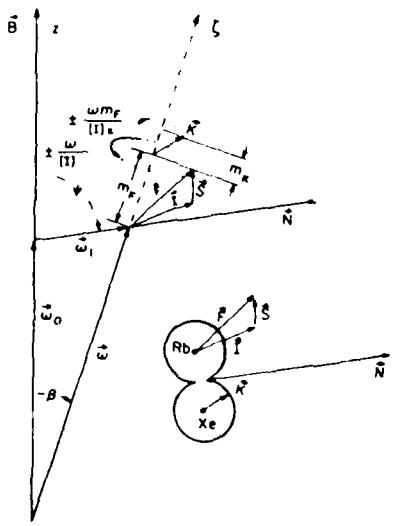

FIG. 8. Interacting spins of an alkali-metal–noble-gas van der Waals molecule. Nuclear spins of the alkali-metal and noble-gas atoms are denoted by I and K, respectively. Electron spin of the alkali-metal atom is S and the rotational angular momentum of the molecule is N. An external field B adds vectorially to the internal spin-rotation field to produce a net rotation velocity ω for the electron spin S of an alkali-metal atom without hyperfine structure. For alkali-metal atoms with a nuclear spin I the total angular momentum F rotates at a velocity $\pm\omega/(2I+1)$ about $\vec{\omega}$ for $F = I \pm \frac{1}{2}$. Finally, the nuclear spin K of the noble gas rotates at a velocity $\pm\omega m_f/[x(2I\pm1)]$ about $\vec{\omega}$ where m_f is the azimuthal quantum number of $\vec{F}$ and $x=\gamma N/\alpha$ is the Breit-Rabi field parameter defined in Eq. (55). Experiments show that $x^2 \gg 1$ for many alkali-metal–noble-gas pairs.

In the conventional notation introduced by Frosch and Foley[15] the magnetic dipole hyperfine coupling is written in the form

$$H_{\text{dipole}} = b\vec{K}\cdot\vec{S}+cK_RS_R , \quad (2)$$

where K_R and S_R are projections of the angular momentum operators $\vec{K}$ and $\vec{S}$ along the internuclear axis R. In subsequent calculations of spin-relaxation and spin-transfer processes it will be more convenient to write the interaction (2) as the sum of purely scalar and purely tensor parts

$$H_{\text{dipole}} = a\vec{K}\cdot\vec{S}+c\left[K_RS_R-\frac{\vec{K}\cdot\vec{S}}{3}\right], \quad (3)$$

where the relationship between a and the conventional Frosch-Foley parameters is

$$a = b+\frac{c}{3} . \quad (4)$$

We expect the purely scalar interaction $a\vec{K}\cdot\vec{S}$ to be relatively large in a van der Waals molecule because of the substantial overlap of the alkali-metal valence electron wave function with the noble-gas nucleus, as discussed by Herman.[16]

The purely tensor interaction is less effective in causing spin transfer and spin relaxation than the scalar interaction. For example, one can show that for binary collisions or for short-lived molecules the relaxation rates of $\langle K_z\rangle$ due to the two interactions are in the ratio

$$\frac{\mathscr{R}_{\text{tensor}}}{\mathscr{R}_{\text{scalar}}} = \frac{c^2}{18a^2} . \quad (5)$$

Although no direct information about the tensor interaction is available for alkali-metal–noble-gas van der Waals molecules, Herman[16] states, without giving numbers, that the tensor interaction is small relative to the scalar interaction for alkali-metal–noble-gas pairs. In this connection it is interesting to note that Childs, Cok, and Goodman[17] have made very precise spectroscopic studies of molecules like CaCl which are well described by the ionic structure Ca^+Cl^-. This ionic molecule is isoelect-

ronic to the van der Waals molecule KAr and it has the same $^2\Sigma_{1/2}$ ground-state symmetry. If the scalar and tensor coupling coefficients have similar relative sizes in alkali-metal–noble-gas molecules as in the alkaline-earth–halogen molecules studied by Childs *et al.*[17] there will be negligible contribution to the relaxation and spin-transfer processes from the tensor interaction. For example, in CaCl, Childs *et al.*[17] measure $b=19.2$ MHz and $c=12.5$ MHz, and therefore (5) implies that less than 2% of the relaxation of $\langle K_z\rangle$ would be caused by the tensor interaction. We have therefore omitted the tensor interaction from the Hamiltonian (1), and we shall ignore the contribution of the tensor interaction to the various spin-transfer rates in the subsequent discussions.

The rotational angular momentum $\vec{N}$ of (1) is typically on the order of 100 and it is so large compared to the other spins in the problem that we may regard N to be a fixed classical vector during the molecular lifetime which is limited by collisions to about 10^{-7} sec at 1 Torr of gas pressure. For convenience we introduce a rotation frequency

$$\vec{\omega}_1=\frac{\gamma\vec{N}}{\hbar} \tag{6}$$

to represent the effect of $\vec{N}$ on $\vec{S}$. In a like manner we introduce the rotational frequency due to the external field $\vec{B}$:

$$\vec{\omega}_0=\frac{g_S\mu_B\vec{B}}{\hbar} . \tag{7}$$

These frequencies are sketched in Fig. 8 along with their vector sum

$$\vec{\omega}=\vec{\omega}_0+\vec{\omega}_1=\omega\hat{\zeta} , \tag{8}$$

where $\hat{\zeta}$ is a unit vector along the direction of $\hat{\omega}$. Note that we may now write (1) as

$$H=A\vec{I}\cdot\vec{S}+\hbar\omega S_\zeta+\alpha\vec{K}\cdot\vec{S}+g_I\mu_B\vec{I}\cdot\vec{B}+g_B\mu_B\vec{K}\cdot\vec{B}+\cdots . \tag{9}$$

We shall find it convenient to introduce a laboratory coordinate system (x,y,z) whose z axis lies along the direction of the external magnetic field $\vec{B}$. The laboratory system will be used to describe the results of experimental measurements. We shall also find it convenient to introduce an orthonormal coordinate system (ξ,η,ζ) with the ζ axis defined by (8). As is shown in Fig. 8, the ζ axis is tilted by an angle β from the z axis. We see that the molecular Hamiltonian (9) is axially symmetric about ζ if we ignore the very small terms involving g_I and g_K, and it will therefore be expedient to calculate wave functions of (9) in the (ξ,η,ζ) coordinate system.

It will be convenient to calculate the spin-transfer and spin-relaxation rates in the interaction picture,[18,19] i.e., in a system for which the density matrices of the spins would be time independent if there were no interactions between the alkali-metal and noble-gas atoms. If an alkali-metal atom and a noble-gas atom are so far apart that they do not interact with each other the Hamiltonian H_n for the noninteracting pair would be

$$H_n=A\vec{I}\cdot\vec{S}+g_S\mu_BBS_z+g_I\mu_BBI_z+g_K\mu_BBK_z . \tag{10}$$

The interaction-picture density matrix σ is related to the Schrödinger picture density matrix ρ by

$$\rho=U_n\sigma U_n^{-1} , \tag{11}$$

where the evolution operator U_n is related to the noninteracting Hamiltonian (10) by

$$U_n=\exp(-iH_nt/\hbar) . \tag{12}$$

Since the alkali-metal atom and the noble-gas atom form molecules very infrequently, typically once every hundred seconds for a noble-gas atom, and since the more frequent binary collisions are of very short duration, typically 10^{-12} sec, it is an excellent approximation to write the density matrix of an alkali-metal–noble-gas pair at the instant of molecular formation, or just before a binary collision, as

$$\sigma_0=\sigma_{Rb}\sigma_{Xe} . \tag{13}$$

The initial density matrix (13) will evolve, after a time t, to

$$\sigma_{ev}=U_n^{-1}U\sigma_0U^{-1}U_n , \tag{14}$$

where U_n was defined in (12) and the evolution operator for an interacting pair as

$$U=\exp(-iHt/\hbar) . \tag{15}$$

Then the rate of change of some observable quantity M, for example, the spin K_z of a noble-gas nucleus, is

$$\frac{d}{dt}\langle M\rangle=\frac{1}{T(M)}\mathrm{Tr}[(\sigma_{ev}-\sigma_0)M]$$
$$=\frac{1}{T(M)}\mathrm{Tr}[(M_{ev}-M)\sigma_0] , \tag{16}$$

where the time-evolved operator is

$$M_{ev}=U^{-1}U_nMU_n^{-1}U \tag{17}$$

and the symbol Tr denotes a trace over all spin basis states of the alkali-metal–noble-gas pair. The rate of formation of van der Waals molecules per atom of the type associated with the observable M is denoted by $T^{-1}(M)$. For convenience we will set

$$T^{-1}(M)=T_F^{-1} \tag{18}$$

for any observable associated with an alkali-metal atom and

$$T^{-1}(M)=T_K^{-1} \tag{19}$$

for any observable associated with a noble-gas atom. We will normally find that $T_K\gg T_F$ because the number density of the noble-gas atoms greatly exceeds that of the alkali-metal atoms.

The density matrix of the noble-gas atoms can be written as

$$\sigma_{Xe}=[K]^{-1}+\frac{3(\vec{K})\cdot\vec{K}}{K(K+1)[K]}+\cdots . \tag{20}$$

We shall henceforth denote the statistical weight of any

ngular momentum quantum number, e.g., K, by

$$[K]=2K+1 . \tag{21}$$

he contribution from higher multipole moments,[19,20] hich we have denoted by ellipses, is small when the oble-gas nuclei are weakly polarized, the situation which revailed for most of the experiments described in this pa-er. Similarly, the density matrix of the alkali-metal toms is

$$\sigma_{\mathrm{Rb}}=\frac{1}{2[I]}+\sum_f \frac{3\langle \vec{f}\rangle\cdot\vec{f}}{f(f+1)[f]}+\cdots . \tag{22}$$

Here the sum is over the two possible values of the total ngular momentum quantum number of the alkali-metal tom, $f=I\pm\frac{1}{2}$. The projection of the total angular iomentum

$$\vec{F}=\vec{I}+\vec{S} \tag{23}$$

ithin each hyperfine multiplet is denoted by

$$\vec{f}=p(f)\vec{F}p(f) , \tag{24}$$

here the projection operators are

$$p(f=I\pm\tfrac{1}{2})=\frac{[f]\pm 4\vec{I}\cdot\vec{S}}{2[I]}=\frac{\hat{f}^2}{f(f+1)} . \tag{25}$$

n the future we shall call $f=a$ if $f=I+\frac{1}{2}$ and $f=b$ if $=I-\frac{1}{2}$. The corresponding operators from (24) will be enoted by $\vec{a}$ and $\vec{b}$. We shall henceforth use the nota-ion $\hat{f}^2$ to denote the square of the angular momentum perator. By substituting (13), (20), (22), and (17) into (16) /e find

$$\frac{d}{dt}\langle\vec{J}\rangle=\frac{1}{T(J)}\sum_L[q(J,L)\langle\vec{L}\rangle-\vec{S}(J,L)] , \tag{26}$$

here the symbols J and L can be a, b, or K, the labels of he three angular momenta which characterize the polari-ation of the alkali-metal and noble-gas atoms.

The spin-transfer coefficient is

$$q(J,L)=-\delta_{JL}+\frac{3}{2[I][K]L(L+1)W(L)}\times\mathrm{Tr}(U_n\vec{J}U_n^{-1}U\vec{L}U^{-1}) . \tag{27}$$

he terms $\vec{S}(J,L)$ describe the spin-polarization-ependent shifts of the magnetic resonance frequencies of ie alkali-metal and noble-gas atoms and they are given y

$$\vec{S}(J,L)=\frac{9\,\mathrm{Tr}(\vec{J}U_n^{-1}U\langle\vec{J}\rangle\cdot\vec{J}\vec{L}\cdot\langle\vec{L}\rangle U^{-1}U_n)}{J(J+1)[J]L(L+1)[L]} \tag{28}$$

he argument of the time-evolution operators U and U_n t, the lifetime of the van der Waals molecule before col-sional breakup. The weights $W(L)$ are defined by

$$W(a)=\frac{[a]}{2[I]} ,$$
$$W(b)=\frac{[b]}{2[I]} , \tag{29}$$
$$W(K)=1 .$$

They may be thought of as the probabilities $W(L)$ for finding an unpolarized atom in the angular momentum state L. We have neglected in (26) terms $\vec{S}(J',L')$ with $J'\neq J$ and $L'\neq J$. The coefficients of these terms are negligibly small under conditions of interest for this work. Finally, we note the special case $\vec{S}(a,b)=\vec{S}(b,a)=0$ which occurs because there are no terms with products of $\langle\vec{a}\rangle$ and $\langle\vec{b}\rangle$ in σ_0 of (13).

The lifetime of a van der Waals molecule may depend weakly on the rotational and vibrational state of the molecule. However, we shall make the simplifying assumption that, independent of the state of the molecule, the probability to find the lifetime between t and $t+dt$ is

$$P(t)dt=\tau^{-1}e^{-t/\tau}dt , \tag{30}$$

where τ is the mean lifetime of the molecule. When (27) and (28) are averaged over (30) the oscillatory time factors of the operators U and U_n are converted into resonance denominators appropriate to the matrix elements of the numerators, as we shall show in the next few sections.

III. FORMAL AVERAGE OVER THE DIRECTION OF N FOR NEGLIGIBLY SMALL MAGNETIC FIELD $B\ll\gamma N/\mu_B$

We consider the situation where (see Fig. 8)

$$\omega_0\ll\omega_1 . \tag{31}$$

For RbXe molecules this corresponds to fields of a few gauss or less. Then neither the eigenvalues nor eigenvectors [expressed in the (ξ,η,ζ) system of coordinates] of (1) will depend appreciably on the direction of $\vec{N}$, and the average over all directions of $\vec{N}$ reduces the tensor $q(J,L)$ to the scalar

$$q(J,L)=\frac{1}{2[I][K]}\sum_{i,j}\frac{-(\omega_{ij}\tau)^2}{1+(\omega_{ij}\tau)^2}\frac{\langle i|\vec{J}|j\rangle\cdot\langle j|\vec{L}|i\rangle}{L(L+1)W(L)} \tag{32}$$

and the frequency-shift terms reduce to the vector cross products

$$\vec{S}(J,L)=s(J,L)\langle\vec{J}\rangle\times\langle\vec{L}\rangle , \tag{33}$$

where the scalar coefficients are

$$s(J,L)=\frac{3}{4[I][K]}\sum_{i,j}\frac{i\omega_{ij}\tau}{1+(\omega_{ij}\tau)^2}\times\frac{\langle j|\vec{I}|i\rangle\cdot\langle i|(\vec{J}\times\vec{L})|j\rangle}{J(J+1)L(L+1)W(J)W(L)} . \tag{34}$$

The basis states $|i\rangle$ and $|j\rangle$ are eigenstates of the Ham-

Experimental determination of the rate constants for spin exchange between optically pumped K, Rb, and Cs atoms and ^{129}Xe nuclei in alkali-metal—noble-gas van der Waals molecules

X. Zeng, Z. Wu, T. Call, E. Miron, D. Schreiber, and W. Happer
Department of Physics, Princeton University, Princeton, New Jersey 08544
(Received 28 February 1984)

By analyzing the measured spin-relaxation transients of ^{129}Xe nuclear spins and alkali-metal-atomic spins in mixtures of alkali-metal-atom vapors, Xe gas, and larger amounts of N_2 gas, we have determined the three-body formation rates and the spin-transfer probabilities for alkali-metal—noble-gas van der Waals molecules. Three parameters, in addition to the spin quantum numbers of the alkali-metal and noble-gas nuclei, are needed to predict the spin-transfer rates. These parameters, which we have determined from experimental measurements, are $x=\gamma N/\alpha$, the ratio of the spin-rotation interaction γN to the spin-exchange interaction α; p_0, the third-body pressure for which the molecular breakup rate τ^{-1} is equal to the spin-rotation frequency $\gamma N/h$; and Z, the three-body rate constant for forming van der Waals molecules.

I. INTRODUCTION

ı 1960 Carver and Bouchiat[1] first showed that it was ible to transfer angular momentum from optically ıped alkali-metal-atom vapors to the nuclei of ^{3}He gas spin-exchange collisions. However, the spin-transfer s were discouragingly slow, and the spin-exchange s section was estimated[2] to be about 10^{-26} cm^2. In 3 Grover[3] showed that much faster spin-transfer rates d be obtained from the heavy noble gas ^{129}Xe, and the s appeared to be consistent with a cross section of ^{19} cm^2. Subsequent work by Volk *et al.*[4] showed that h of the spin transfer occurred in loosely bound li-metal—noble-gas van der Waals molecules. Bhas- *et al.*[5] showed that a large part of the alkali-metal- ı spin angular momentum was wasted by being sformed into rotational angular momentum of the li—noble-gas pair about each other. A comprehensive ry of the spin-transfer and spin-relaxation processes lkali—noble-gas systems was developed by Happer *l.*[6]

ecause most of the spin transfer between alkali-metal ıs and heavy noble gases occurs in van der Waals ecules, it is not possible to describe the process with a ɔle spin-exchange cross section. Three steps are in- ed in the spin exchange, the formation of a van der ls molecule in a three-body collision, the evolution of spins during the lifetime of the van der Waals mole- , and the collisional breakup of the molecule as illus- d in Fig. 1. If the alkali-metal-atom spin polariza- is described by a high spin temperature, the rates of ıge of the small longitudinal spin polarizations $\langle F_z\rangle$ $\langle K_z\rangle$ of the alkali-metal atoms and noble-gas atoms, ectively, are described by the equations[6]

$$\frac{d}{dt}\langle F_z\rangle=\frac{1}{T_F}[q(F,F)\langle F_z\rangle+q(F,K)\langle K_z\rangle]\,, \tag{1}$$

$$\frac{d}{dt}\langle K_z\rangle=\frac{1}{T_K}[q(K,K)\langle K_z\rangle+q(K,F)\langle F_z\rangle]\,, \tag{2}$$

where $1/T_F$ and $1/T_K$ are the molecular formation rates per alkali-metal atom and noble-gas atom, respectively. The spin-transfer coefficient $|q(F,F)|$ is the probability that the alkali-metal-atom spin polarization will be destroyed during the lifetime of the van der Waals molecule, and the coefficient $q(F,K)$ is the fraction of the nuclear spin of the noble-gas atom which is transferred to the alkali-metal atom during the lifetime of the molecule. The coefficients $q(K,K)$ and $q(K,f)$ have analogous meanings.

The spin-transfer coefficients depend on the product $H\tau$ of the molecular spin interaction Hamiltonian H and the mean, collisionally limited lifetime τ of the molecule.

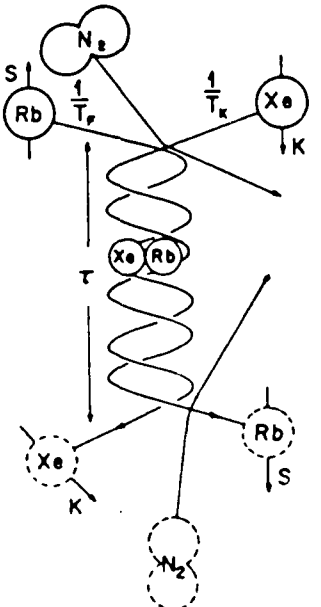

FIG. 1. Alkali-metal—noble-gas van der Waals molecules are formed in three-body collisions at a rate of T_F^{-1} per alkali-metal atom and T_K^{-1} per noble-gas atom. They are broken up at a rate of τ^{-1} by collisions with other atoms or molecules.

with the width obtained from the perturbation formulas (94) and (97). The zero-pressure width ΔH_0 is obtained by numerical evaluation of (97). The high-pressure width obtained from (94) is

$$\Delta H = \frac{\gamma N[I]}{g s \mu_B} \frac{p}{p_0} . \tag{166}$$

We have used the simple hyperbolic formula

$$\Delta H = \left[(\Delta H_0)^2 + \left[\frac{\gamma N[I]}{g s \mu_B} \frac{p}{p_0} \right]^2 \right]^{1/2} \tag{167}$$

to interpolate between the low- and high-pressure expressions for ΔH. The agreement between the perturbation formula and the numerical formula is excellent. The effect of a distribution of N is to decrease the predicted width by some 15%.

In Fig. 17 we show how the low-pressure width ΔH_0 depends on the coupling constant γN for fixed values of the other parameters of (155). Over a large range of the ratio $x = \gamma N/\alpha$ the width is proportional to the spin-rotation coupling constant. The effect of a distribution of N is to lower the predicted ratio of ΔH to γN by about 15%.

ACKNOWLEDGMENTS

This work was supported by the U.S. Air Force Office of Scientific Research under Grant No. AFOSR-81-0104-C.

[1]M. A. Bouchiat, T. R. Carver, and C. M. Varnum, Phys. Rev. Lett. 5, 373 (1960).
[2]R. L. Gamblin and T. R. Carver, Phys. Rev. 138, A946 (1965).
[3]F. D. Colegrove, L. D. Schearer, and G. K. Walters, Phys. Rev. 132, 2561 (1963).
[4]M. Leduc, F. Laloe, and J. Brossel, C. R. Acad. Sci. 271, 342 (1970).
[5]A. Noel, A. Leduc, and F. Laloe, C. R. Acad. Sci. 274, 77 (1972).
[6]B. C. Grover, Phys. Rev. Lett. 40, 391 (1978).
[7]C. H. Volk, T. M. Kwon, and J. G. Mark, Phys. Rev. A 21, 1549 (1980).
[8]N. D. Bhaskar, W. Happer, and T. McClelland, Phys. Rev. Lett. 49, 25 (1982).
[9]N. D. Bhaskar, W. Happer, M. Larsson, and X. Zeng, Phys. Rev. Lett. 50, 105 (1983).
[10]X. Zeng, E. Miron, W. A. van Wijngaarden, D. Schreiber, and W. Happer, Phys. Lett. 96A, 191 (1983).
[11]N. Ramsey, E. Miron, X. Zeng, and W. Happer, Chem. Phys. Lett. 102, 340 (1983).
[12]T. A. McClelland, Ph.D. thesis, Columbia University, 1981 (unpublished).
[13]C. C. Bouchiat, M. A. Bouchiat, and L. C. L. Pottier, Phys. Rev. 181, 144 (1969).
[14]M. A. Bouchiat, J. Brossel, and L. C. Pottier, J. Chem. Phys. 56, 3703 (1972).
[15]R. S. Frosch and H. M. Foley, Phys. Rev. 88, 1337 (1952).
[16]R. M. Herman, Phys. Rev. 137, A1062 (1965).
[17]W. J. Childs, D. R. Cok, and L. S. Goodman, J. Chem. Phys. 76, 3993 (1982).
[18]J. P. Barrat and C. Cohen Tannoudji, J. Phys. Radium 22, 329 (1961); 22, 443 (1961).
[19]W. Happer, Rev. Mod. Phys. 44, 169 (1972).
[20]U. Fano, Rev. Mod. Phys. 29, 74 (1957).
[21]M. Rose, *Elementary Theory of Angular Momentum* (Wiley, New York, 1957).
[22]L. W. Anderson, F. M. Pipkin, and J. C. Baird, Phys. Rev. 120, 1279 (1960).
[23]L. W. Anderson and A. T. Ramsey, Phys. Rev. 132, 712 (1963).
[24]F. A. Franz and A. Sieradzan, Phys. Rev. A 23, 2841 (1981).
[25]M. A. Bouchiat, J. Phys. (Paris) 24, 379 (1963); 24, 611 (1963).
[26]M. A. Bouchiat and F. Grossetete, J. Phys. (Paris) 27, 353 (1966).
[27]N. D. Bhaskar, J. Camparo, W. Happer, and A. Sharma, Phys. Rev. 23, 3048 (1981).
[28]J. S. Smart, *Effective Field Theories of Magnetism* (Saunders, Philadelphia, 1966).

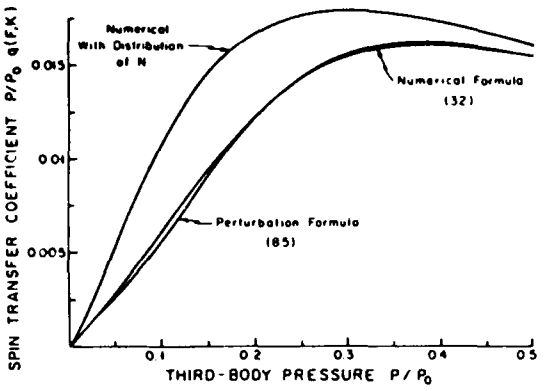

FIG. 14. Comparison between exact numerical evaluations and perturbative approximations of the spin-transfer coefficient $q(F,K)$. Effect of assuming a distribution in N is also shown.

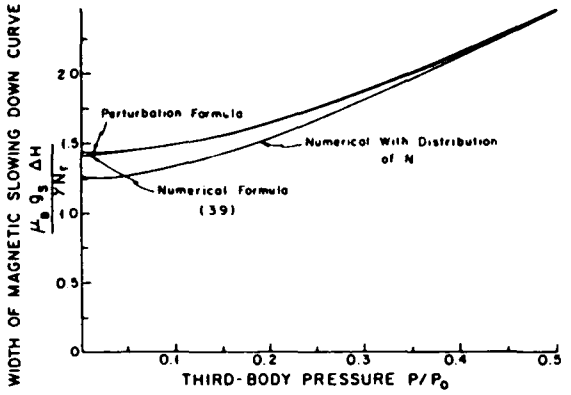

FIG. 16. Comparison between exact numerical evaluations and perturbative approximations to the width ΔH of the magnetic slowing-down curves. Effect of assuming a distribution of N is also shown.

and $P(N)=0$ for all other values of N. Here the constant N_r is the rms value of N defined by

$$N_r^2 = \int_0^\infty N^2 P(N) dN \ . \tag{165}$$

Since the perturbation formulas of Secs. VII and VIII are obtained as power-series expansions in N^{-1} we can expect difficulties if we naively average the formulas over the distribution (163), which has substantial contributions from small values of N where the expansion parameter $x^{-1}=\alpha/\gamma N$ exceeds unity. However, it is straightforward to average the numerical evaluations of (32), (34), and (39) over the distribution (163).

A comparison of the perturbation formula (82) with the numerical evaluations of (32) is shown in Fig. 12. There is good agreement over the whole range of relative pressures p/p_0 and the distribution of N makes little difference. A similar comparison of the perturbation formula (84) with the numerical evaluation of (32) is shown in Fig. 13. The distribution of N lowers the relaxation rate by about 10% near the peak of the curve. In Fig. 14 we compare the perturbation formula (85) to the numerical evaluation of (32). The distribution of N causes $q(F,K)$ to increase by nearly a factor of 2 for low third-body pressures. In Fig. 15 we compare the perturbation formula (86) for the frequency-shift coefficient $s(a,K)$ to the numerical evaluation of (34). There is good agreement even when the distribution of N is taken into account. From Figs. 12–15 we see that there is good agreement between perturbation formulas and the numerical evaluation of the coefficients in most cases, but the distribution of N can have a very large effect on the spin-transfer coefficient $q(F,K)$ for small third-body pressures. The overall agreement is best for the coefficient $q(K,K)$.

Studies of the slowing down of the spin-relaxation rates in a large external magnetic field, as illustrated in Fig. 6, have played an important role in determining the magnitudes of the coupling constants in the Hamiltonian (1). We will define the width of a magnetic slowing-down curve like one of those in Fig. 6 as the magnetic field ΔH at which the relaxation rate has decreased to half of its peak value. The width ΔH_0 at very low third-body pressures is a fairly direct gauge of the spin-rotation interaction constant γN. In Fig. 16 we show a comparison of the width determined from numerical evaluation of (39)

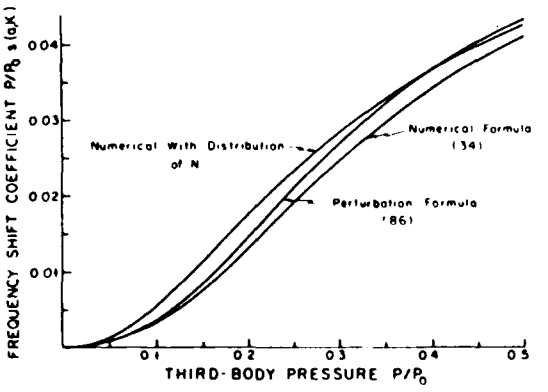

FIG. 15. Comparison between exact numerical evaluations and perturbative approximations of the frequency-shift coefficient $s(a,K)$. Effect of assuming a distribution in N is also shown.

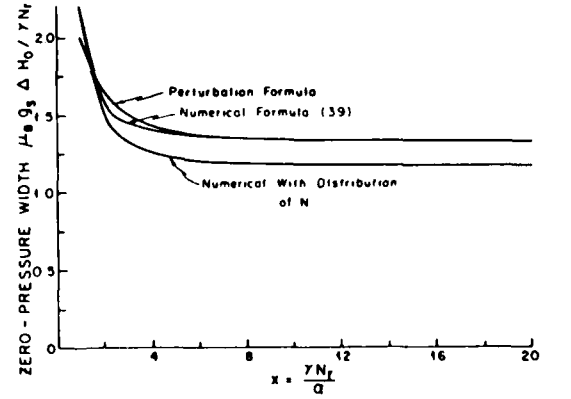

FIG. 17. Comparison between exact numerical evaluations and perturbative approximations to the zero-pressure width ΔH_0 of the magnetic slowing-down curves. Effect of assuming a distribution of N is also shown.

VIII and exact numerical evaluations of (32), (34), and (39) with a computer. To carry out the numerical evaluation, the matrix elements of the Hamiltonian (9) were evaluated in terms of the basis states $|f,m_f,m_K\rangle$ discussed in connection with Eq. (60). By dropping the very small terms proportional to g_I and g_K we obtained a matrix which was block diagonal, with each block corresponding to a total azimuthal quantum number m_f+m_K about the ζ axis of Fig. 8. The blocks were diagonalized and the eigenvectors were used to calculate the matrix elements in the numerators of (32), (34), and (39), while the eigenvalues were used to calculate the resonant denominators. We used the following parameters, which are representative of the $^{87}Rb^{129}Xe$ molecule:

$$I=\tfrac{3}{2},\quad K=\tfrac{1}{2},\quad \gamma N=4,\quad \alpha=1,\quad A=118\ . \tag{155}$$

The molecular lifetime τ of (30) was expressed in terms of the ratio p/p_0 of the third-body pressure to a characteristic pressure p_0

$$\tau=\frac{\hbar}{\gamma N}\frac{p_0}{p}\ . \tag{156}$$

That is, p_0 is that third-body pressure for which the molecular lifetime τ is equal to the spin rotational period $\hbar(\gamma N)^{-1}$. Ramsey *et al.*[11] have shown that the characteristic pressures p_0 for N_2 and He are 81 and 133 Torr, respectively.

We note that the spin-transfer rates are the product of a molecular formation rate $T^{-1}(J)$ and a spin-transfer coefficient $q(J,L)$ as shown in (26). We have therefore plotted as a function of p/p_0 the quantities $(p/p_0)q(J,L)$ which are proportional to $\{1/T(J)\}q(J,L)$, as one can see from the following arguments.

In chemical equilibrium the breakup rate of molecules per unit volume must equal the formation rate per unit volume and we must therefore have

$$[\mathrm{RbXe}]\tau^{-1}=\frac{[\mathrm{Xe}]}{T_K}=\frac{[\mathrm{Rb}]}{T_F}\ . \tag{157}$$

Thus, we may rewrite (157) as

$$\frac{1}{T_F}=[\mathrm{Xe}]\kappa\tau^{-1}=\frac{\gamma N}{\hbar}\kappa[\mathrm{Xe}]\frac{p}{p_0} \tag{158}$$

or

$$\frac{1}{T_K}=[\mathrm{Rb}]\kappa\tau^{-1}=\frac{\gamma N}{\hbar}\kappa[\mathrm{Rb}]\frac{p}{p_0}\ , \tag{159}$$

where the chemical equilibrium constant is

$$\kappa=\frac{[\mathrm{RbXe}]}{[\mathrm{Rb}][\mathrm{Xe}]} \tag{160}$$

thus

$$\frac{1}{T_F}q(f,K)=\frac{\gamma N}{\hbar}\kappa[\mathrm{Xe}]\frac{p}{p_0}q(f,K) \tag{161}$$

and

$$\frac{1}{T_K}q(K,f)=\frac{\gamma N}{\hbar}\kappa[\mathrm{Rb}]\frac{p}{p_0}q(K,f)\ . \tag{162}$$

We note that the parameters γN and α will depend on the vibrational and rotational state of the van der Waals molecule. If γ/α is approximately independent of the quantum state the important ratio $x=\gamma N/\alpha$ will depend on the distribution of the rotational quantum number N. All of the formulas of the preceding sections have implicitly assumed a fixed value of N. For the short-lifetime regimes described in Secs. IX and X, we are only concerned with the mean-squared value of N and the form of the probability distribution is unimportant. However, for the longer molecular lifetimes discussed in Secs. VII and VIII the rms value of N is not sufficient to determine the average-coupling constants. Bouchiat *et al.*[13] suggested that the following simple distribution of N is a reasonable approximation for heavy van der Waals molecules:

$$P(N)=\frac{9N}{10N_r^2}\left[2-\left[\frac{6}{5}\right]^{1/2}\frac{N}{N_r}\right] \tag{163}$$

for

$$0\le N\le 2\left[\frac{5}{6}\right]^{1/2}N_r \tag{164}$$

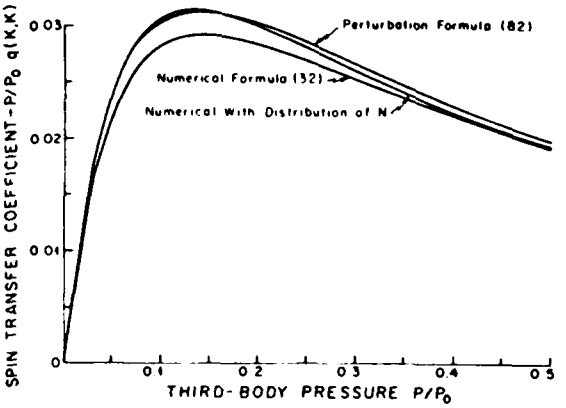

FIG. 12. Comparison between exact numerical evaluations and perturbative approximations of the spin-transfer coefficient $q(K,K)$. Effect of assuming a distribution in the rotational quantum number N is also shown.

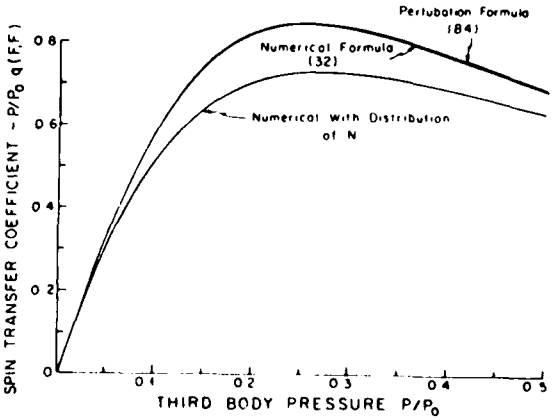

FIG. 13. Comparison between exact numerical evaluations and perturbative approximations of the spin-transfer coefficient $q(F,F)$. Effect of assuming a distribution in the rotational quantum number N is also shown.

That is, the optical admittance is just half the number of photons absorbed per second by the alkali-metal atoms in the sample cell.

We note that the capacitances C_{Rb} and C_{Xe} are proportional to factors $\langle \hat{F}^2 - F_z^2 \rangle$ and $\langle \hat{K}^2 - K_z^2 \rangle$ which depend on the spin polarization, except for the special case of spin $\frac{1}{2}$. For $S = \frac{1}{2}$ we have, independent of polarization,

$$\langle \hat{S}^2 - S_z^2 \rangle = \tfrac{1}{2} .$$

For spins greater than $\frac{1}{2}$, factors like $\langle \hat{K}^2 - K_z^2 \rangle$ are always larger than $\frac{1}{2}$ and they reflect the fact that more angular momentum can be stored in a large-spin atom than in an atom with the minimum spin $\frac{1}{2}$. Thus we may think of a minimum-spin atom (i.e., a spin-$\frac{1}{2}$ atom) as the equivalent of an "air-gap" capacitor for angular momentum, while an atom with spin greater than $\frac{1}{2}$ is like a capacitor with dielectric material between its plates. This suggests that we define a "paramagnetic constant" for a spin-K atom by

$$\epsilon(K,\beta) = 2\langle \hat{K}^2 - K_z^2 \rangle = 2\left\{ K(K+1) - \frac{1}{Z}\frac{d^2 Z}{d\beta^2} \right\} , \quad (148)$$

where

$$Z = \sum_{m_K=-K}^{+K} \exp(\beta m_K) \quad (149)$$

then the capacitance (144) can be written as

$$C_{Xe} = \Omega[\mathrm{Xe}]\tfrac{1}{2}\epsilon(K,\beta) , \quad (150)$$

where $\frac{1}{2}$ is the capacitance per atom for a spin-$\frac{1}{2}$ atom, the ideal air-gap capacitance, and $\epsilon(K,\beta)$ is the paramagnetic constant which corrects for the fact that the spin K may be larger than $\frac{1}{2}$.

For $K > \frac{1}{2}$ the paramagnetic constant will depend on the degree of polarization and the capacitance (150) will therefore be voltage dependent in somewhat the same way as the capacitance of a back-biased *pn* junction. We note that the paramagnetic constant decreases with increasing polarization and saturates at a minimum value

$$\epsilon(K,\infty) = 2K \quad (151)$$

for a fully polarized nucleus with $V_{Xe} = 1$ and all atoms in the state with maximum azimuthal angular momentum K. This ensures that the charge of a fully polarized nucleus of spin K is K. We also note that for very weak polarization the paramagnetic constant reaches its maximum value which is

$$\epsilon(K,0) = \tfrac{4}{3}K(K+1) . \quad (152)$$

Paramagnetic constants for a few selected examples are shown in Fig. 11 as a function of the voltage, $\tanh(\beta/2)$, of (137).

For an alkali-metal atom in spin-temperature equilibrium the paramagnetic constant is

$$\epsilon(F,\beta) = 2\langle \hat{F}^2 - F_z^2 \rangle = 2\langle \hat{S}^2 - S_z^2 \rangle + 2\langle \hat{I}^2 - I_z^2 \rangle$$
$$= 1 + \epsilon(I,\beta) , \quad (153)$$

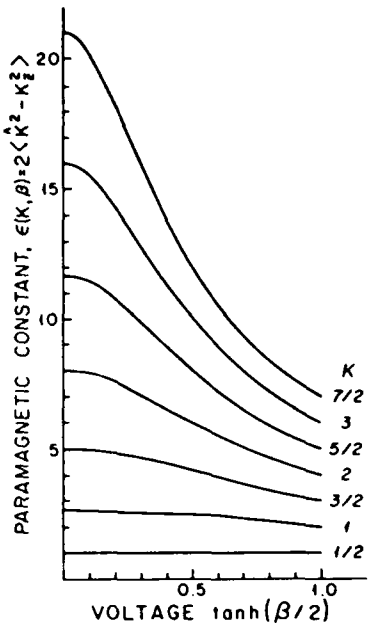

FIG. 11. Paramagnetic constants of a spin system are a measure of the amount of angular momentum which can be stored in a spin system.

where $\epsilon(I,\beta)$ is defined by (148). One may therefore obtain the paramagnetic constant for an alkali-metal atom of nuclear spin $I = K$ by adding one unit to the appropriate curves of Fig. 11. We note that the paramagnetic constants (148) are related as follows to the Brillouin functions $B_K(x)$ defined by Smart:[28]

$$\epsilon(K,\beta) = \frac{2KB_K(K\beta)}{B_{1/2}(\beta/2)} . \quad (154)$$

We note that in a typical experiment with stable heavy noble gases where the relaxation of both the alkali-metal and noble-gas spins is dominated by molecular formation, the number density (and therefore the capacitance C_{Xe}) of the noble-gas atoms is orders of magnitude larger than the number density (and therefore the capacitance C_{Rb}) of the alkali-metal atoms. Consequently, the RC time constant for charging or discharging the noble-gas capacitor with angular momentum will be orders of magnitude longer than the RC time constant for the alkali-metal capacitor. Representative time constants for the alkali-metal capacitor are a few milliseconds while representative time constants for the noble-gas capacitor are minutes to nearly one hour in our own work. We note that the effects on the alkali-metal atoms of other spin-destroying mechanisms like diffusion have been omitted from Fig. 10. These additional spin-relaxation mechanisms can be represented by resistor in parallel with R_{sr}.

XIII. COMPARISON OF PERTURBATION FORMULAS WITH EXACT NUMERICAL SOLUTIONS

We conclude this paper with a comparison between the relatively simple perturbation formulas of Secs. VII and

ized alkali-metal atoms. For example, (124) becomes

$$\frac{d}{dt}\langle F_z\rangle = R\left[\frac{s_z}{2}-\langle S_z\rangle\right]. \tag{130}$$

Since the details of optical pumping are not a central part of this paper we refer the reader to Ref. 27 for additional discussions of broad-line optical pumping with conservation of the nuclear spin in the optical-pumping cycle.

XII. *RC* NETWORK MODEL

Some insight into the behavior of the systems under consideration here can be gained by representing the system with the electrical circuit model shown in Fig. 10 and discussed in detail below. For simplicity we have limited our discussion to the high-pressure regime of Sec. IX. The collection of alkali-metal atoms in the sample cell is represented by the capacitor C_{Rb} and the noble-gas atoms are represented by the capacitor C_{Xe}. The total spin angular momentum of the alkali-metal atoms is equivalent to the charge stored on the capacitor:

$$Q_{\mathrm{Rb}}=\Omega[\mathrm{Rb}]\langle F_z\rangle , \tag{131}$$

where Ω is the volume of the cell and $\langle F_z\rangle$ is the volume averaged angular momentum per alkali-metal atom. In a like manner the total spin angular momentum of the noble-gas atoms is

$$Q_{\mathrm{Xe}}=\Omega[\mathrm{Xe}]\langle K_z\rangle . \tag{132}$$

If we sum (108) over the two possible values of f to obtain a formula for $(d/dt)\langle F_z\rangle$ and multiply the resulting equation by $\Omega[\mathrm{Rb}]$ we obtain

$$\frac{d}{dt}Q_{\mathrm{Rb}}=-\frac{V_{\mathrm{Rb}}}{R_{sr}}+\frac{1}{R_{ex}}(V_{\mathrm{Xe}}-V_{\mathrm{Rb}}) , \tag{133}$$

where the "voltages" V_{Rb} and V_{Xe} are

$$V_{\mathrm{Rb}}=\frac{\langle F_z\rangle}{\langle \hat{F}^2-F_z^2\rangle} , \tag{134}$$

$$V_{\mathrm{Xe}}=\frac{\langle K_z\rangle}{\langle \hat{K}^2-K_z^2\rangle} . \tag{135}$$

In the following discussion we shall assume that the spin systems are described by the spin-temperature distribution

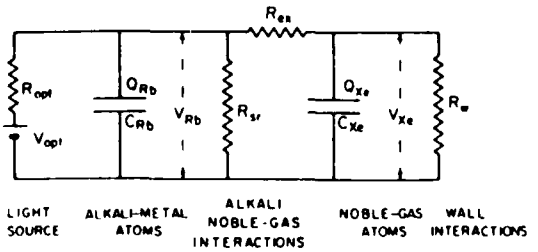

FIG. 10. Process of spin-exchange optical pumping is well described by an *RC* network model. Angular momentum is analogous to electrical charge which is stored on capacitors which represent the alkali-metal and noble-gas atoms. Spin polarization, $\tanh(\beta/2)$, is analogous to voltage. The resistors are related to various terms in the Hamiltonian (1).

(43). Then one can show that

$$V_{\mathrm{Rb}}=\frac{\langle F_z\rangle}{\langle \hat{F}^2-F_z^2\rangle}=\frac{\langle I_z\rangle}{\langle \hat{I}^2-I_z^2\rangle}=2\langle S_z\rangle=\tanh\frac{\beta(\mathrm{Rb})}{2} , \tag{136}$$

where $\beta(\mathrm{Rb})$ is the spin-temperature parameter of the alkali-metal atoms. Similarly, we assume that

$$V_{\mathrm{Xe}}=\frac{\langle K_z\rangle}{\langle \hat{K}^2-K_z^2\rangle}=\tanh\left[\frac{\beta(\mathrm{Xe})}{2}\right] , \tag{137}$$

where we expect, in general, that $\beta(\mathrm{Xe})\neq\beta(\mathrm{Rb})$. The magnitudes of the voltage are always less than one and angular momentum will flow from a "high-voltage" spin system to a "low-voltage" spin system just as ordinary charge flows under the influence of ordinary voltage.

The spin-rotation admittance is given by

$$\frac{1}{R_{sr}}=\frac{1}{T_0}\frac{2}{3}\left[\frac{\gamma N\tau}{[I]\hbar}\right]^2\langle \hat{F}^2-F_z^2\rangle , \tag{138}$$

where

$$\frac{1}{T_0}=\frac{\Omega[\mathrm{Rb}]}{T_F}=\frac{\Omega[\mathrm{Xe}]}{T_K} \tag{139}$$

is the total rate of formation of molecules in the sample cell.

The spin-exchange admittance is given by

$$\frac{1}{R_{ex}}=\frac{1}{T_0}\left[\frac{\alpha\tau}{[I]\hbar}\right]^2\langle \hat{F}^2-F_z^2\rangle\langle \hat{K}^2-K_z^2\rangle , \tag{140}$$

In a like manner, if we multiply (109) by $\Omega[\mathrm{Xe}]$ we see that it can be written as

$$\frac{d}{dt}Q_{\mathrm{Xe}}=\frac{1}{R_{ex}}(V_{\mathrm{Rb}}-V_{\mathrm{Xe}})-\frac{1}{R_w}V_{\mathrm{Xe}} , \tag{141}$$

where the wall admittance is given by

$$\frac{1}{R_w}=\frac{C_{\mathrm{Xe}}}{T_w} . \tag{142}$$

The capacitors are defined as the ratios of charge to voltage for the two types of atoms, i.e.,

$$C_{\mathrm{Rb}}=\frac{Q_{\mathrm{Rb}}}{V_{\mathrm{Rb}}}=\Omega[\mathrm{Rb}]\langle \hat{F}^2-F_z^2\rangle , \tag{143}$$

$$C_{\mathrm{Xe}}=\frac{Q_{\mathrm{Xe}}}{V_{\mathrm{Xe}}}=\Omega[\mathrm{Xe}]\langle \hat{K}^2-K_z^2\rangle . \tag{144}$$

If we multiply (131) by $\Omega[\mathrm{Rb}]$ we find

$$\frac{d}{dt}Q_{\mathrm{Rb}}=\frac{1}{R_{\mathrm{opt}}}(V_{\mathrm{opt}}-V_{\mathrm{Rb}}) , \tag{145}$$

where the optical emf is equal to the mean photon spin

$$V_{\mathrm{opt}}=s_z \tag{146}$$

and the optical admittance is given by

$$\frac{1}{R_{\mathrm{opt}}}=\frac{\Omega[\mathrm{Rb}]R}{2} . \tag{147}$$

$$\frac{d}{dt}\langle K_z\rangle=\frac{1}{T_K}\left[\frac{\alpha\tau}{\hbar}\right]^2[\langle\hat{K}^2-K_z^2\rangle\langle S_z\rangle-\tfrac{1}{2}\langle K_z\rangle]\ . \quad (123)$$

In the practically important case of spin-exchange equilibrium (see Sec. V) one can ignore the complicated coupled equations (118) and (119) and consider their sum which is simply

$$\frac{d}{dt}\langle F_z\rangle=-\frac{1}{T_F}\left\{\frac{2}{3}\left[\frac{\gamma N\tau}{\hbar}\right]^2+\left[\frac{\alpha\tau}{\hbar}\right]^2\langle\hat{K}^2-K_z^2\rangle\right\}\langle S_z\rangle+\frac{1}{2T_F}\left[\frac{\alpha\tau}{\hbar}\right]^2\langle K_z\rangle\ . \quad (124)$$

The frequency-shift formulas (110)–(112) remain valid for the conditions of this section as well as those of Sec. IX.

XI. OPTICAL PUMPING

For completeness we briefly discuss the primary source of angular momentum for the system considered here; of course this is the beam of circularly polarized light which is absorbed by the alkali-metal atoms. One of the simplest situations to analyze and also a situation which frequently is closely approximated in practice is broad-line pumping with circularly polarized D_1 light in the presence of an appropriate buffer gas.[26] As discussed in Ref. 26 broad-line pumping refers to a situation where the spectral profile of the exciting light is such that equal light intensities are available to drive transitions from any of the two ground-state multiplets $f_g=I\pm\frac{1}{2}$ to any of the excited-state multiplets $f_e=I\pm\frac{1}{2}$. As the name "broad-line" implies, this will usually be true if a pressure-broadened resonance lamp or a multimode laser is used as the pumping source. It will also be true for a single-mode laser if the Doppler and collisional broadening of the absorption line are much bigger than the hyperfine splitting.

It is well known that the details of optical pumping depend on the fate of the excited $P_{1/2}$ atoms which are produced when a photon is absorbed. Here we consider an especially simple situation which is nearly realized in many of the experiments on spin-exchange optical pumping of noble-gas nuclei.[8] We shall assume that the electronic angular momentum J of the excited $P_{1/2}$ atom is completely randomized before the excited atom decays either by spontaneous emission or, more likely, by a quenching collision with a N_2 molecule. We shall also assume that the hyperfine coupling in the excited state is so weak and the J-randomization time is so short that there is negligible depolarization of the nuclear spin I in the excited state. Under these conditions one can show that optical pumping is completely equivalent to spin exchange with a pseudo spin-$\frac{1}{2}$ particle.

The equivalence of optical pumping to spin exchange for the optical-pumping conditions mentioned above can be proved with the methods outlined in Ref. 27. However, we will give a physical plausibility argument here. In a binary spin-exchange collision the collision duration is so short compared to the hyperfine period of the alkali-metal atom that the nucleus has no time to evolve during the collision and the nuclear polarization is conserved. For broad-line optical pumping the duration of a "collision" between an alkali-metal atom and a photon can be thought of as the inverse of the optical frequency linewidth of the light source or the inverse of the optical absorption linewidth of the alkali-metal atoms, whichever is shorter. We are considering a situation where the photon collision duration is very short compared to the hyperfine period so the nucleus is unable to evolve during the time of a photon-atom collision. If the atoms are rapidly deexcited before the nuclear polarization can evolve under the influence of hyperfine interactions in the excited state, the collision with a photon will have no effect on the nuclear polarization. With respect to the electron spin, we know that an alkali-metal atom with a spin-down electron can undergo a binary spin-exchange collision with a spin-up collision partner. There will be no interaction if the electron spin of the alkali-metal atom is parallel to that of its collision partner. Similarly, an alkali-metal atom with a spin-down electron can absorb a σ_+ photon of D_1 light but no light will be absorbed if σ_- photons impinge on alkali-metal atoms with spin-down electrons or σ_+ photons impinge on alkali-metal atoms with spin-up electrons. After a spin-exchange collision between an alkali-metal atom with a spin-down electron and a spin-up collision partner the mean electron spin of the alkali-metal atom will be zero, so $\frac{1}{2}$ a unit of angular momentum will have been added to the alkali-metal atom. In a like manner, after a collision between a spin-down alkali-metal atom and a σ_+ photon the mean electron spin of the alkali-metal atom will be zero and $\frac{1}{2}$ a unit of angular momentum will have been added to the alkali-metal atom. The nuclear polarization of the alkali-metal atom is changed by ground-state hyperfine interactions in the relatively long intervals between spin-exchange or photon collisions.

Because of the equivalence of broad-line optical pumping with conservation of the nuclear spin polarization to spin-exchange collisions, the evolution of the observables $\langle a_z\rangle$ and $\langle b_z\rangle$ is given by Eqs. (118), (119), and (124) of Sec. X, with the following replacements:

$$\langle K_z\rangle\to\frac{s_z}{2}\ , \quad (125)$$

where s_z is the mean spin of the pumping photons,

$$\langle\hat{K}^2-K_z^2\rangle\to\tfrac{1}{2}\ , \quad (126)$$

$$\langle K_z^2-\tfrac{1}{3}\hat{K}^2\rangle\to 0\ . \quad (127)$$

Equations (126), (127), and (128) are all consequences of the fact that the photons behave like spin-$\frac{1}{2}$ particles as far as angular momentum transfer is concerned. To make use of (118), (119), and (124) we must also set

$$\gamma N=0\ , \quad (128)$$

and

$$\frac{1}{2T_F}\left[\frac{\alpha\tau}{\hbar}\right]^2\to R\ , \quad (129)$$

where R is the mean photon absorption rate for unpolar-

tion theory of Secs. VI–VIII. One can verify that the perturbation formulas of Sec. VII reduce to the formulas of this section when the criteria (91)–(93) are satisfied and when the factors $\langle \hat{f}^2 - f_z^2 \rangle$ and $\langle \hat{K}^2 - K_z^2 \rangle$ are replaced by their low-polarization limits $f(f+1)[f]/3[I]$ and $\frac{2}{3}K(K+1)$, respectively.

X. VERY SHORT MOLECULAR LIFETIMES, BINARY COLLISIONS, AND RELAXATION AND SPIN TRANSFER WITH $\Delta f = 0, \pm 1$

We consider finally the limit of very short molecular lifetimes where in addition to the criteria (91) and (92) we have

$$\left| \frac{[I] A \tau}{2\hbar} \right| \ll 1 . \tag{114}$$

The criterion (114) will always obtain for binary collisions between alkali-metal atoms and noble-gas atoms where the encounter duration is on the order of 10^{-12} sec. It will also hold for van der Waals molecules in the case of third-body pressures of a few atmospheres or greater as is indicated in Fig. 7. In view of (114) we may to good approximation write (102) as

$$\Delta \tilde{H} \simeq \Delta H \tag{115}$$

during the encounter between an alkali-metal atom and a noble-gas atom. Then the evolution operator is

$$U_n^{-1} U \simeq \exp\left[\frac{-i \Delta H t}{\hbar} \right] = 1 - \frac{i \Delta H t}{\hbar} - \frac{1}{2}\left[\frac{\Delta H t}{\hbar} \right]^2 + \cdots \tag{116}$$

and the evolved operator (17) becomes

$$M_{ev} = M + \frac{it}{\hbar}[\Delta H, M] - \frac{1}{2}\left[\frac{t}{\hbar} \right]^2 [\Delta H, [\Delta H, M]] + \cdots . \tag{117}$$

The commutators in (117) can be evaluated in a straightforward way. If we assume purely longitudinal polarization and average according to (30) over all times t and over all directions of $\vec{N}$ we find from (16)

$$\frac{d}{dt}\langle a_z \rangle = -\frac{1}{T_F}\left\{ \frac{2}{3}\left[\frac{\gamma N \tau}{\hbar} \right]^2 + \left[\frac{\alpha \tau}{\hbar} \right]^2 \langle \hat{K}^2 - K_z^2 \rangle \right\} \{ (1 - B_{aa}) \langle a_z \rangle - B_{ab} \langle b_z \rangle \}$$
$$- \frac{1}{T_F}\left[\frac{\alpha \tau}{\hbar} \right]^2 \left\langle K_z^2 - \frac{\hat{K}^2}{3} \right\rangle \left\{ \frac{3[I]}{4} \langle S_z \rangle - \frac{3}{[I]^2} (\langle a_z^3 \rangle - \langle b_z^3 \rangle) \right\}$$
$$+ \frac{1}{T_F}\left[\frac{\alpha \tau}{\hbar} \right]^2 \frac{\langle K_z \rangle}{[I]^2} \left\{ ([I]-2)\langle a_z^2 \rangle + \langle \hat{a}^2 \rangle + \frac{[I]+2}{[I]-2}\langle \hat{b}^2 \rangle + ([I]+2)\langle b_z^2 \rangle \right\}, \tag{118}$$

$$\frac{d}{dt}\langle b_z \rangle = -\frac{1}{T_F}\left\{ \frac{2}{3}\left[\frac{\gamma N \tau}{\hbar} \right]^2 + \left[\frac{\alpha \tau}{\hbar} \right]^2 \langle \hat{K}^2 - K_z^2 \rangle \right\} \{ -B_{ba} \langle a_z \rangle + (1 - B_{bb}) \langle b_z \rangle \}$$
$$+ \frac{1}{T_F}\left[\frac{\alpha \tau}{\hbar} \right]^2 \left\langle K_z^2 - \frac{\hat{K}^2}{3} \right\rangle \left\{ \frac{3[I]}{4} \langle S_z \rangle - \frac{3}{[I]^2} (\langle a_z^3 \rangle - \langle b_z^3 \rangle) \right\}$$
$$+ \frac{1}{T_F}\left[\frac{\alpha \tau}{\hbar} \right]^2 \frac{\langle K_z \rangle}{[I]^2} \left\{ -([I]+2)\langle b_z^2 \rangle + \langle \hat{b}^2 \rangle + \frac{[I]-2}{[I]+2}\langle \hat{a}^2 \rangle - ([I]-2)\langle a_z^2 \rangle \right\}, \tag{119}$$

where the coupling matrix is

$$B_{ff'} = \frac{1}{2[I]^2}\{[I] + 2(-1)^{a-f}\}\{[I] - (-1)^{a-f}\} . \tag{120}$$

Physically, B'_{ff} is the fraction of the angular momentum $\langle f'_z \rangle$ originally in the multiplet f' which is transferred to the multiplet f after a collision which destroys the electron spin S of the alkali-metal atom but which does not affect the nuclear spin I. This is often called an electron randomizing collision, and it occurs for collisions of very short duration because the Hamiltonian ΔH of (101) does not contain I explicitly (except possibly in a term of the form $\Delta A \vec{I} \cdot \vec{S}$ which could contribute to the coupling of $\langle I_z \rangle$ and $\langle S_z \rangle$ at very large magnetic fields).[24] As was first pointed out by Bouchiat,[26] the eigensolutions of (118) and (119) in the absence of noble-gas polarization correspond to two different time constants

$$\frac{1}{T_e} = \frac{1}{T_F}\left\{ \frac{2}{3}\left[\frac{\gamma N \tau}{\hbar} \right]^2 + \frac{1}{2}\left[\frac{\alpha \tau}{\hbar} \right]^2 \right\} \tag{121}$$

and

$$\frac{1}{T_n} = \frac{2}{[I]^2}\frac{1}{T_e} . \tag{122}$$

These time constants correspond to an observable which Bouchiat denotes by Q_e which is similar but not identical to the electron spin and to a slowly relaxing observable $\langle I_z \rangle$ which is identical to the longitudinal nuclear spin. We refer the reader to the literature[19,25] for a more detailed discussion of relaxation by electron randomization. The relaxation equation for $\langle K_z \rangle$ is much simpler and is

$$-q(F,F)=\frac{\mathcal{A}^2+1+\frac{4}{3x_1^2}K(K+1)}{4\mathcal{A}^2}+\frac{\frac{4}{3x_1^2}K(K+1)-\mathcal{A}^2+1}{16\mathcal{A}^3}\times(\mathcal{A}^2-1)\ln\left|\frac{\mathcal{A}+1}{\mathcal{A}-1}\right|^2. \quad (99)$$

IX. SHORT MOLECULAR LIFETIMES: RELAXATION AND SPIN TRANSFER WITH $\Delta f=0$

All of the spin coupling equations (26), (47), and (48) become much simpler when the criteria (91)–(93) are satisfied. We note that the compound unitary operator of (14) and (17) satisfies the Schrödinger equation

$$i\hbar\frac{d}{dt}U_n^{-1}U=\Delta\tilde{H}\,U_n^{-1}U\,, \quad (100)$$

where

$$\Delta H=H-H_n \quad (101)$$

and

$$\Delta\tilde{H}=U_n^{-1}\Delta H\,U_n\,. \quad (102)$$

If we write out the matrix elements of $\Delta\tilde{H}$ in terms of the eigenstates of H_n we notice that the terms which are off diagonal in f oscillate many times during the molecular lifetime because of the criterion (93). The matrix elements which are diagonal in f are time independent if the external magnetic field B is zero, or they oscillate a small fraction of a cycle if

$$B\ll\frac{\hbar}{\mu_B\tau} \quad (103)$$

we shall assume that the smallness criterion (103) for B is satisfied along with (91)–(93). Then the rapidly oscillating parts of $\Delta\tilde{H}$ will have negligible effect on the Schrödinger equation (100) and we may therefore drop the rapidly oscillating terms from $\Delta\tilde{H}$, ignore, because of (103), the slow oscillations due to B, and replace $\Delta\tilde{H}$ by its secular part

$$\Delta\bar{H}=\sum_f\Delta H(f)\,, \quad (104)$$

where the projections within the multiplets f are

$$\Delta H(f)=p(f)\,\Delta H\,p(f)\,. \quad (105)$$

The evolution operator is therefore

$$U_n^{-1}U=\exp\left[-\frac{i\,\Delta\bar{H}\,t}{\hbar}\right]=\sum_f\left[1-\frac{i\,\Delta H(f)t}{\hbar}-\frac{1}{2}\left|\frac{\Delta H(f)t}{\hbar}\right|^2+\cdots\right]p(f) \quad (106)$$

and the evolved operator (17) becomes

$$M_{ev}=M+\frac{it}{\hbar}\sum_f[\Delta H(f),M]-\frac{1}{2}\left|\frac{t}{\hbar}\right|^2\sum_f[\Delta H(f),[\Delta H(f),M]]+\cdots\,. \quad (107)$$

The commutators in (107) can be readily evaluated. If we assume that purely longitudinal polarization exists we find from (16), after averaging according to (30) over t and over all directions of $\vec{N}$,

$$\frac{d}{dt}\langle f_z\rangle=-\frac{1}{T_F}\frac{2}{3}\left|\frac{\gamma N\tau}{[I]\hbar}\right|^2\langle f_z\rangle+\frac{1}{T_F}\left|\frac{\alpha\tau}{[I]\hbar}\right|^2\times[\langle\hat{f}^2-f_z^2\rangle\langle K_z\rangle-\langle\hat{K}^2-K_z^2\rangle\langle f_z\rangle]\,, \quad (108)$$

$$\frac{d}{dt}\langle K_z\rangle=\frac{1}{T_K}\left|\frac{\alpha\tau}{[I]\hbar}\right|^2[\langle\hat{K}^2-K_z^2\rangle\langle F_z\rangle-\langle\hat{F}^2-F_z^2\rangle\langle K_z\rangle]\,. \quad (109)$$

The significance of the factors $\langle\hat{K}^2-K_z^2\rangle$ and $\langle\hat{F}^2-F_z^2\rangle$ is discussed in Sec. XII.

In the event that transverse polarization exists, e.g., during a magnetic resonance experiment or after a $\frac{1}{2}\pi$ pulse, the terms linear in τ from (107) lead to frequency-shift terms of the form

$$\frac{d}{dt}\langle f_x\pm if_y\rangle=\pm i\frac{s(f,K)\langle K_z\rangle}{T_F}\langle f_x\pm if_y\rangle+\cdots\,, \quad (110)$$

$$\frac{d}{dt}\langle K_x\pm iK_y\rangle=\pm i\frac{s(K,S)\langle S_z\rangle}{T_K}\langle K_x\pm iK_y\rangle+\cdots\,, \quad (111)$$

where the frequency-shift coefficients are

$$s(a,K)=-s(b,K)=\frac{s(K,S)}{[I]}=\frac{\alpha\tau}{\hbar[I]} \quad (112)$$

and where the electron spin (in the absence of coherence between the multiplets a and b) is

$$\vec{S}=\frac{1}{[I]}(\vec{a}-\vec{b})\,. \quad (113)$$

We note that the restriction to low spin polarization which was implicit in the use of the multipole expansions (20) and (22) does not apply to (108) and (109), which remain valid for arbitrarily large spin polarization. We also note that the expressions (108) and (109) are valid for arbitrary values of the ratio $x=\gamma N/\alpha$ and one can therefore analyze experiments at high buffer gas pressures, where (108) and (109) are valid, to determine the internal field parameter x, which plays a key role in the perturba-

VIII. PERTURBATION FORMULAS FOR SPIN-TRANSFER COEFFICIENTS WHEN $B \gtrsim \gamma N/\mu_B$

All magnetic decoupling experiments done so far have been concerned with the slowing down of the relaxation of the longitudinal noble-gas spin $\langle K_z \rangle$ or the longitudinal alkali-metal spin $\langle F_z \rangle$ in a large magnetic field B which defines the z axis of the laboratory coordinate system. The transverse spin polarization is negligible in such experiments. The relaxation processes of the alkali-metal and the noble-gas spins are therefore described by the longitudinal components of the spin coupling coefficients $q(F,F)$ and $q(K,K)$, and we shall therefore limit our discussion to them.

By substituting the perturbed energies and operators of Sec. VI into (39) we find

$$-q(K,K)=\tfrac{1}{2}\int \sin\psi\, d\psi \left\{ \frac{1}{6x^2}(4I^2+4I+3)\frac{\left[\frac{\phi}{[I]}\right]^2}{1+\left[\frac{\phi}{[I]}\right]^2}(1-\tfrac{1}{2}\sin^2\beta)+\frac{\sin^2\beta}{2[I]}\sum_{f,m_f}\left[1-\frac{1}{2x^2}[f(f+1)-m_f^2]\right] \right.$$
$$\left. \times\left[\frac{\left[\frac{\phi m_f}{[I]x}\right]^2}{1+\left[\frac{\phi m_f}{[I]x}\right]^2}+\delta_{m_f 0}\frac{\left[\frac{\phi f(f+1)}{2[I]x^2}\right]^2}{1+\left[\frac{\phi f(f+1)}{2[I]x^2}\right]^2}\right]\right\}. \tag{88}$$

Here both ϕ and x depend on the angle ψ since they are defined as

$$\phi=\omega\tau\,, \tag{89}$$

$$x=\frac{\hbar\omega}{\alpha}\,, \tag{90}$$

and ω depends on ψ as shown in Fig. 8.

Although the integrals over ψ in (88) can be evaluated in closed form, the general result is so cumbersome that we shall only present two limiting cases here, the situations with very long and very short molecular lifetimes τ. For very short molecular lifetimes such that

$$\left|\frac{\gamma N\tau}{\hbar}\right|\ll 1\,, \tag{91}$$

$$\left|\frac{\alpha\tau}{\hbar}\right|\ll 1\,, \tag{92}$$

but also for lifetimes sufficiently long that I and S can couple to F during a molecular lifetime, i.e.,

$$\left|\frac{[I]A\tau}{2\hbar}\right|\gg 1\,, \tag{93}$$

the limiting value of (88) can be verified to be

$$-q(K,K)=\tfrac{2}{3}[I(I+1)+\tfrac{3}{4}]\frac{\left[\frac{\alpha\tau}{[I]\hbar}\right]^2}{1+\left[\frac{\omega_0\tau}{[I]}\right]^2}\,. \tag{94}$$

In a similar way we may show that the short-lifetime limit for $q(F,F)$ is

$$-q(F,F)=\frac{2}{3}\left[\left[\frac{\gamma N\tau}{[I]\hbar}\right]^2+K(K+1)\left[\frac{\alpha\tau}{[I]\hbar}\right]^2\right]\times\frac{1}{1+\left[\frac{\omega_0\tau}{[I]}\right]^2}\,. \tag{95}$$

For $^{87}Rb^{129}Xe$ the range of validity of the criteria (91)–(93) is indicated in Fig. 7.

For the limit of very long molecular lifetimes where

$$\left|\frac{\alpha\tau}{[I]\hbar}\right|\gg 1\,. \tag{96}$$

The limiting value of (88) can be shown to be

$$-q(K,K)=\frac{\mathcal{A}^2+1+\frac{4}{3x_1^2}[I(I+1)+\frac{1}{4}]}{4\mathcal{A}^2}+\frac{\frac{4}{3x_1^2}[I(I+1)+\frac{3}{4}]-\mathcal{A}^2+1}{16\mathcal{A}^3}\times(\mathcal{A}^2-1)\ln\left[\frac{\mathcal{A}+1}{\mathcal{A}-1}\right]^2, \tag{97}$$

where the dimensionless field parameter is

$$\mathcal{A}=\frac{\omega_0}{\omega_1}=\frac{g_S\mu_B B}{\gamma N} \tag{98}$$

and in a like manner we can show that

$$-q(K,K)=\frac{1}{9x^2}[4I^2+4I+3]\frac{\left[\frac{\phi}{[I]}\right]^2}{1+\left[\frac{\phi}{[I]}\right]^2}$$

$$+\frac{1}{3[I]}\sum_{f,m_f}\left\{1-\frac{1}{2x^2}[f(f+1)-m_f^2]\right\}\left\{\frac{\left[\frac{\phi m_f}{[I]x}\right]^2}{1+\left[\frac{\phi m_f}{[I]x}\right]^2}+\delta_{m_f0}\frac{\left[\frac{\phi f(f+1)}{2[I]x^2}\right]^2}{1+\left[\frac{\phi f(f+1)}{2[I]x^2}\right]^2}\right\}. \tag{82}$$

Here the phase is

$$\phi=\omega\tau\simeq\frac{\gamma N\tau}{\hbar}. \tag{83}$$

In (82) the terms involving m_F come from matrix elements between states $|i\rangle$ and $|j\rangle$ with $\Delta m_K\pm1$, $\Delta m_f=0$. The first term in (82) came from matrix elements with $\Delta m_f=\pm1$, $\Delta m_K=0$ and $\Delta m_f=\pm1$, $\Delta m_K=\mp1$.

In a like manner we find the self-transfer coefficient $q(F,F)$ to be

$$-q(F,F)=\frac{2}{3}\frac{\left[\frac{\phi}{[I]}\right]^2}{1+\left[\frac{\phi}{[I]}\right]^2}+\frac{2K(K+1)}{9x^2}\frac{\left[3-\left[\frac{\phi}{[I]}\right]^2\right]}{\left[1+\left[\frac{\phi}{[I]}\right]^2\right]^3}\left[\frac{\phi}{[I]}\right]^2+\frac{2K(K+1)}{3x^2 2[I]\{I(I+1)+\frac{3}{4}\}}\sum_{f,m_f}\frac{m_f^2\left[\frac{\phi m_f}{x[I]}\right]^2}{1+\left[\frac{\phi m_f}{x[I]}\right]^2}. \tag{84}$$

In (84) the first term, which is independent of x, comes from matrix elements with $\Delta m_f=1$, $\Delta m_K=0$. The second term which is proportional to $[1+(\phi/[I])^2]^{-3}$ arises from the same class of matrix elements, but it is due to the dependence of the energy factor $(\omega_{ij}\tau)^2[1+(\omega_{ij}\tau)^2]^{-1}$ on x. The last term comes from matrix elements with $\Delta m_K=1$, $\Delta m_f=0$.

The transfer coefficient between F and K is

$$q(K,F)=\frac{2K(K+1)}{9x^2}\left[\frac{\phi}{[I]}\right]^2\frac{\left[3+\left[\frac{\phi}{[I]}\right]^2\right]}{\left[1+\left[\frac{\phi}{[I]}\right]^2\right]^2}$$

$$-\frac{K(K+1)}{6x^2[I]\{I(I+1)+\frac{3}{4}\}}\sum_{f,m_f}[3m_f^2-f(f+1)]\left\{\frac{\left[\frac{\phi m_f}{x[I]}\right]^2}{1+\left[\frac{\phi m_f}{x[I]}\right]^2}+\delta_{m_f0}\frac{\left[\frac{\phi f(f+1)}{2[I]x^2}\right]^2}{1+\left[\frac{\phi f(f+1)}{2[I]x^2}\right]^2}\right\}. \tag{85}$$

We may use (49) to obtain $q(F,K)$ from (85).

Finally, the scalar frequency-shift coefficients (34) are, to order x^{-1},

$$s(f,K)=\pm\frac{1}{3x}\frac{\phi}{[I]}\frac{3+\left[\frac{\phi}{[I]}\right]^2}{\left[1+\left[\frac{\phi}{[I]}\right]^2\right]^2}, \tag{86}$$

$$s(K,f)=\pm\frac{\phi}{x[I]}\left[\frac{2}{3}\frac{1}{1+\left[\frac{\phi}{[I]}\right]^2}+\frac{1}{f(f+1)[f]}\sum_{m_f}\frac{(m_f)^2}{1+\left[\frac{\phi m_f}{x[I]}\right]^2}\right], \tag{87}$$

where the $\pm$ signs are associated with $f=I\pm\frac{1}{2}$.

(39) by replacing the true operators, e.g., K_ζ, by perturbed operators $\tilde{K}_\zeta$ which give the correct matrix elements when inserted between the pure states, i.e.,

$$\langle i \mid K_\zeta \mid j \rangle = (i \mid \tilde{K}_\zeta \mid j) , \tag{65}$$

where, to order x^{-2},

$$\tilde{K}_\zeta = R^{-1} K_\zeta R = K_\zeta - [u, K_\zeta] + \tfrac{1}{2}[u, [u, K_\zeta]] - [v, K_\zeta] + \cdots . \tag{66}$$

We note that the spin-transfer coefficients, e.g., (32), contain squares of matrix elements of $\vec{K}$ or $\vec{F}$ or they may contain the product of a matrix element of $\vec{K}$ with a matrix element of $\vec{F}$. We may therefore ignore any components of $\tilde{K}_\zeta$, etc., which upon squaring, or being paired as a matrix element with a corresponding matrix element of $\tilde{F}_\zeta$, will give a term of order higher than $1/x^2$. Because each term in (32) and in analogous expressions contains one or more factors of ω_{ij} in the numerator we may ignore all components of $\tilde{K}_\zeta$ or $\tilde{F}_\zeta$ which contribute to diagonal matrix elements. Thus the components of the perturbed operators needed for our calculations are

$$\tilde{K}_\zeta = \frac{1}{2x}(K_+ F_- + K_- F_+) + \cdots , \tag{67}$$

$$\tilde{F}_\zeta = \frac{-1}{2x}(K_+ F_- + K_- F_+) + \cdots . \tag{68}$$

These operators cause transitions of the type denoted by iii in Fig. 9. The raising and lowering operators $\tilde{K}_\pm$ and $\tilde{F}_\pm$ [cf. (64)] each have two classes of terms which we denote by the subscripts 1 and 2:

$$\tilde{K}_+ = (\tilde{K}_+)_1 + (\tilde{K}_+)_2 . \tag{69}$$

The terms with the selection rules $\Delta m_J = 0$, $\Delta m_K = 1$ are

$$(\tilde{K}_+)_1 = K_+ - \frac{1}{8x^2}(\{F_+, F_-\}K_+ + 2\{K_+, K_\zeta\}F_\zeta) . \tag{70}$$

They cause transitions of the type denoted by i in Fig. 9. The terms with the selection rules $\Delta m_J = 1$, $\Delta m_K = 0$ are

$$(\tilde{K}_+)_2 = -\frac{1}{x}K_\zeta F_+ - \frac{1}{2x^2}(\{F_+, F_\zeta\}K_\zeta - [3K_\zeta^2 - \hat{K}^2]F_+) . \tag{71}$$

They cause transitions of the type denoted by ii in Fig. 9. The curly brackets denote an anticommutator, i.e.,

$$\{K_+, K_-\} = K_+ K_- + K_- K_+ \tag{72}$$

and the notation $\hat{K}^2$ indicates the squared angular momentum *operator* with eigenvalue $K(K+1)$. The corresponding terms for F_+ are

$$\tilde{F}_+ = (\tilde{F}_+)_1 + (\tilde{F}_+)_2 , \tag{73}$$

where

$$(\tilde{F}_+)_1 = \frac{K_+ F_\zeta}{x} + \frac{K_+}{2x^2}[3F_\zeta^2 - \hat{F}^2] - \frac{F_\zeta}{2x^2}\{K_+, K_\zeta\} \tag{74}$$

and

$$(\tilde{F}_+)_2 = F_+ \left[1 - \frac{1}{8x^2}\{K_-, K_+\}\right] - \frac{K_\zeta}{4x^2}\{F_\zeta, F_+\} . \tag{75}$$

We shall only evaluate the frequency-shift coefficients (34) to order $1/x$. The components of the cross product

$$\vec{F} \times \vec{K} = \vec{G} \tag{76}$$

needed for calculation of the shift coefficients are then

$$\tilde{G}_\zeta = \frac{i}{2}(F_+ K_- - F_- K_+) + \cdots , \tag{77}$$

$$\tilde{G}_+ = (\tilde{G}_+)_1 + (\tilde{G}_+)_2 , \tag{78}$$

$$(\tilde{G}_+)_1 = iK_+ F_\zeta - \frac{i}{4x}K_+\{F_+, F_-\} - \frac{i}{2x}\{K_+, K_\zeta\}F_\zeta + \cdots , \tag{79}$$

$$(G_+)_2 = -iF_+ K_\zeta - \frac{i}{4x}F_+\{K_+, K_-\} - \frac{i}{2x}\{F_+, F_\zeta\}K_\zeta + \cdots . \tag{80}$$

VII. PERTURBATION FORMULAS FOR SPIN-TRANSFER COEFFICIENTS WHEN $B \ll \gamma N/\mu_B$

We may now evaluate the spin-transfer coefficients (32) and the frequency-shift coefficients (34) with the perturbed energies and perturbed operators discussed in Sec. VI. Since we are considering the situation of a magnetic field which satisfies the smallness criterion (31) we may set

$$x \simeq x_1 = \frac{\gamma N}{\alpha} \tag{81}$$

and we may neglect the dependence of the eigenvalues and eigenvectors on the orientation of $\vec{N}$. Then the coefficient $q(K,K)$ is found to be

VI. PERTURBATIC: SOLUTION

It is possible to evaluate the spin-transfer coefficients directly by numerical diagonalization of the Hamiltonian (1) to obtain eigenvalues and eigenvectors for evaluation of the energy denominators and matrix elements. In Sec. XIII we shall discuss the results of numerical calculations. However, extensive experimental studies of van der Waals molecules of alkali-metal atoms (K, Rb, and Cs) with ^{129}Xe and ^{131}Xe have shown that at least for these systems there is a convenient hierarchy of magnitudes

$$A^2 \gg (\gamma N)^2 \gg \alpha^2 \tag{51}$$

in the Hamiltonian (1). For example, for ^{87}Rb^{129}Xe, $A/h \simeq 3400$ MHz, $\gamma N/h \simeq 116$ MHz, and $\alpha/h \simeq 37$ MHz. We shall develop the perturbation theory of this section with the assumption that (51) is valid. The Hamiltonians (1) or (9) will be written as

$$H = H_0 + V_0 + V_1 \, . \tag{52}$$

The unperturbed Hamiltonian is

$$H_0 = A\vec{I}\cdot\vec{S} + \frac{\hbar\omega}{[I]}(a_\zeta - b_\zeta) \, . \tag{53}$$

The eigenstates of (53) will form the basis states for our perturbation expansion.

The most important perturbation is

$$V_0 = \frac{\hbar\omega}{x[I]}(\vec{a} - \vec{b})\cdot\vec{K} \, . \tag{54}$$

This is the projection of $\alpha\vec{S}\cdot\vec{K}$ within the multiplets $f = I + \frac{1}{2} = a$ and $f = I - \frac{1}{2} = b$. The parameter x is the Breit-Rabi field parameter

$$x = \frac{\hbar\omega}{\alpha} \, . \tag{55}$$

In view of (51) we see that

$$x^{-2} \ll 1 \, , \tag{56}$$

so x^{-1} is an appropriate expansion parameter for perturbation calculations. The perturbation V_1 is

$$V_1 = \hbar \sum_{\substack{f,f' \\ f \neq f'}} p(f)\{\omega S_\zeta + (\omega/x)\vec{S}\cdot\vec{K}\}p(f') \, . \tag{57}$$

This perturbation causes transitions between the two hyperfine multiplets a and b. Such transitions can occur only if the molecular lifetime τ is comparable to or less than the hyperfine period divided by 2π. Experiments show that the molecular lifetime is on the order of 10^{-7} sec at 1 Torr of gas pressure. Consequently we can neglect V_1 for pressures below an atmosphere, with the possible exception of systems containing isotopes like ^{41}K which have unusually small hyperfine structure. With this caveat we shall ignore V_1 for all perturbation calculations.

The energy eigenvalues of $H_0 + V_0$, correct to order x^{-2}, are

$$E(f,m_f m_K) = E_f \pm \frac{\hbar\omega}{[I]}\left[m_f + \frac{1}{x} m_f m_K + \frac{1}{2x^2} m_f \{K(K+1) - m_K^2\} - \frac{1}{2x^2} m_K \{f(f+1) - m_f^2\} \right] , \tag{58}$$

where the "center of mass" of the multiplet f is

$$E_f = \tfrac{1}{4} A \{ f(f+1) - I(I+1) - \tfrac{3}{4} \} \, . \tag{59}$$

The energies are sketched in Fig. 9.

The perturbed states $|f,m_f,m_K\rangle$, i.e., the approximate eigenstates of $H_0 + V_0$, can be labeled by the same quantum numbers as the eigenstates $|f,m_f,m_K\rangle$ of H_0. The two sets of states are related to each other by the unitary transformation

$$|f,m_f,m_K\rangle = R\,|f,m_f,m_K\rangle \, , \tag{60}$$

where the unitary operator R, correct to order x^{-2}, is

$$R = 1 + u + \tfrac{1}{2}u^2 + v \, . \tag{61}$$

The anti-Hermitian operators u and v are

$$u = \frac{1}{2x}(F_- K_+ - F_+ K_-) \tag{62}$$

and

$$v = \frac{1}{2x^2}[F_\zeta K_\zeta, (F_+ K_- + F_- K_+)] \tag{63}$$

and as usual the subscripts $\pm$ denote

$$K_\pm = K_\xi \pm i K_\eta \, . \tag{64}$$

Then we may evaluate the matrix elements of (32), (34), or

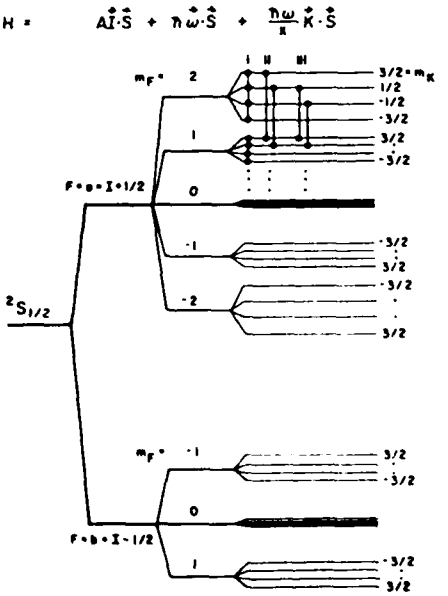

FIG. 9. Energy levels of the Hamiltonian $H_0 + V_0$ of Eq. (52).

iltonian (1), and the circular frequencies ω_{ij} are related to the energy eigenvalues E_i and E_j of (1) by the Bohr condition

$$\hbar\omega_{ij}=E_i-E_j\ . \tag{35}$$

IV. FORMAL AVERAGE OVER THE DIRECTION OF $\vec{N}$ FOR MAGNETIC FIELDS $B \gtrsim N/\mu_B$

We now consider the situation where the Larmor frequency ω_0 of (7) is comparable to the internal Larmor frequency ω_1 of (6); i.e.,

$$\omega_0 \gtrsim \omega_1\ . \tag{36}$$

For RbXe this regime occurs for fields greater than a few gauss. The average over the azimuthal direction of $\vec{N}$ (see Fig. 8) reduces the spin-transfer coefficients to a form which is diagonal in the spherical laboratory basis system,[21] i.e.,

$$q(J,L)=\sum_{\mu=-1}^{+1} q_{\mu\mu}(J,L)\hat{x}_\mu\hat{x}_\mu^*\ , \tag{37}$$

where

$$\hat{x}_{\pm1}=\frac{\hat{x}\pm i\hat{y}}{\mp\sqrt{2}}\ ,\qquad \hat{x}_0=\hat{z}\ . \tag{38}$$

The longitudinal component of $q(J,L)$ is

$$q_{00}(J,L)=\frac{3}{2[I][K]L(L+1)W(L)}\int_0^\pi \sin\psi\, d\psi \sum_{i,j,\rho}\frac{-(\omega_{ij}\tau)^2\langle j|J_\rho|i\rangle\langle i|L_{-\rho}|j\rangle(-1)^\rho|d^1_{\rho0}|^2}{1+(\omega_{ij}\tau)^2}\ , \tag{39}$$

where the Wigner functions are

$$d^1_{\pm1,0}=\mp\frac{\sin\beta}{\sqrt{2}}\ ,\qquad d^1_{00}=\cos\beta\ . \tag{40}$$

We note that the basis states $|i\rangle$ and $|j\rangle$ of (39) are *eigenstates of the Hamiltonian* (9). *They are axially symmetric about the axis* ζ and they depend on the colatitude angle ψ of Fig. 8.

The subscript ρ in (39) refers to one of the spherical unit vectors $\hat{\xi}_\rho$ in the (ζ,η,ξ) coordinate system:

$$\hat{\xi}_{\pm1}=\frac{\hat{\xi}\pm i\hat{\eta}}{\mp\sqrt{2}}\ ,\qquad \hat{\xi}_0=\hat{\zeta}\ , \tag{41}$$

we have

$$J_\rho=\hat{\xi}_\rho\cdot\vec{J}\ . \tag{42}$$

The transverse spin-transfer coefficients $q_{11}(J,L)$ and $q_{-1-1}(J,L)$ are given by formulas analogous to (39). They have imaginary as well as real parts and they account for field-dependent frequency shifts of the magnetic resonance spectrum. Since the transverse spin-transfer coefficients at high fields have not yet been needed for the interpretation of experimental data we shall not discuss them further here.

V. THE SPIN-TEMPERATURE LIMIT

Under many experimental conditions, including most of those considered here, the alkali-metal atoms are well described by a spin temperature,[22,23] i.e., the density matrix of the alkali-metal atom can be written as

$$\rho_{Rb}=Z^{-1}e^{\vec{\beta}\cdot\vec{F}}\ , \tag{43}$$

where the sum on states is

$$Z=\mathrm{Tr}\,e^{\vec{\beta}\cdot\vec{F}}\ . \tag{44}$$

We may think of β^{-1} as a spin temperature.

Under the conditions of interest for the work described here, the parameter β is small compared to unity and we may therefore write (23) as

$$\rho_{Rb}=\frac{1}{2[I]}(1+\vec{\beta}\cdot\vec{F}+\cdots)\ , \tag{45}$$

where we have neglected higher-order terms in β. When (45) is valid we may write

$$\langle\vec{f}\rangle=\frac{[f]f(f+1)}{2[I]\{I(I+1)+\frac{3}{4}\}}\langle\vec{F}\rangle+\cdots\ . \tag{46}$$

The spin polarization of the alkali-metal atoms is described by the single vector $\langle\vec{F}\rangle$ rather than by $\langle\vec{a}\rangle$, $\langle\vec{b}\rangle$, and the higher multipole moments which characterize an arbitrary state of polarization when spin-temperature equilibrium does not prevail. It will therefore be convenient to use (46) to reduce the spin-transfer equation (26) to the coupled pair

$$\frac{d}{dt}\langle\vec{K}\rangle=\frac{1}{T_K}\{q(K,K)\langle\vec{K}\rangle+q(K,F)\langle\vec{F}\rangle\}\ , \tag{47}$$

$$\frac{d}{dt}\langle\vec{F}\rangle=\frac{1}{T_F}\{q(F,K)\langle\vec{K}\rangle+q(F,F)\langle\vec{F}\rangle\}\ . \tag{48}$$

We have ignored the frequency-shift terms for simplicity. The transfer coefficients $q(K,K)$, $q(F,F)$, and

$$q(F,K)=\frac{I(I+1)+\frac{3}{4}}{K(K+1)}q(K,F) \tag{49}$$

are given by (32) or (39) where the labels J and L can each take on the two possible symbols F and K, and the weight factors $W(F)$ which occur are to be defined by

$$F(F+1)W(F)=I(I+1)+\tfrac{3}{4}\ . \tag{50}$$

That is, by measuring spin-transfer coefficients one cannot distinguish between a weak Hamiltonian acting for a long molecular lifetime and a strong Hamiltonian acting for a short molecular lifetime. Experiments have shown that the simplest spin Hamiltonian consistent with presently known experimental data is[6]

$$H = A\vec{I}\cdot\vec{S} + \gamma\vec{N}\cdot\vec{S} + \alpha\vec{K}\cdot\vec{S}\,, \tag{3}$$

where $A\vec{I}\cdot\vec{S}$, the isotropic magnetic dipole interaction between the nuclear spin $\vec{I}$ and the electron spin $\vec{S}$ of the alkali atom, is similar in magnitude to that of a free alkali-metal atom. The spin-rotation interaction $\gamma\vec{N}\cdot\vec{S}$ is the primary cause of the spin relaxation of alkali-metal atoms in heavy noble gases, and it has been measured for alkali–noble-gas systems in elegant experiments by Bouchiat *et al.*[7] Finally, the isotropic magnetic dipole interaction $\alpha\vec{K}\cdot\vec{S}$ between the nuclear spin $\vec{K}$ of the noble gas and the electron spin $\vec{S}$ of the alkali-metal atom is responsible for spin exchange between the alkali-metal and noble-gas atoms, and theoretical estimates of the magnitude of α have been given by Herman.[2]

The interaction $A\vec{I}\cdot\vec{S}$ is so large compared to the other terms in the Hamiltonian or compared to the natural width $h\tau^{-1}$ of the energy levels under ordinary experimental conditions that $A\vec{I}\cdot\vec{S}$ has no influence on the spin-transfer coefficients and serves only to make $\vec{F}=\vec{I}+\vec{S}$ a good quantum number of the molecule. The spin-tranfer coefficients therefore depend only on the two parameters $\gamma N\tau$ and $\alpha\tau$. We shall find it more convenient to choose the related dimensionless parameters

$$x = \frac{\gamma N}{\alpha} \tag{4}$$

and

$$\phi = \frac{\gamma N\tau}{\hbar} \tag{5}$$

as the independent variables of the spin-transfer coefficients.

The parameter $x=\gamma N/\alpha$ plays the same role in the Hamiltonian (3) as the Breit-Rabi field parameter for the hyperfine structure of the hydrogen atom.[8] Our experiments show that $x^2 \gg 1$ in all alkali–noble-gas systems studied thus far, and it is therefore possible to use x^{-2} as a perturbation expansion parameter in closed-form theoretical expressions for the spin-transfer coefficients. The phase angle ϕ can be thought of as the angle by which the alkali spin $\vec{S}$ would precess about $\vec{N}$ during a molecular lifetime if there were no nuclear spin I to slow down the precession frequency. Since the molecular lifetime is limited by collisions of van der Waals molecules with the gas in the cell, we expect that ϕ will be inversely proportional to the gas pressure p, i.e.,

$$\phi = \frac{p_0}{p}\,, \tag{6}$$

TABLE I. Summary of results of measuring parameters x, p_0, and Z.

Parameter (unit)	Description	Comment	$^{39}K^{129}Xe$	$^{85}Rb^{129}Xe$	$^{87}Rb^{129}Xe$	$^{133}Cs^{129}Xe$
I	Nuclear spin of alkali-metal atom	Slower optical pumping or alkali-metal relaxation rates for large I	$\frac{3}{2}$	$\frac{5}{2}$	$\frac{3}{2}$	$\frac{7}{2}$
K	Nuclear spin of noble-gas atom		$\frac{1}{2}$	$\frac{1}{2}$	$\frac{1}{2}$	$\frac{1}{2}$
x	Breit-Rabi field parameter $x=\frac{\gamma N}{\alpha}$	Determines fractions of alkali-metal atom spin S which are transferred to rotational angular momentum N and noble-gas nuclear spin K	3.5± 0.3	3.2± 0.3	3.2± 0.3	2.9± 0.3
p_0 (Torr)	Characteristic pressure $p_0=p\frac{\gamma N\tau}{h}$	Sets scale for dependence of spin-transfer rates on third-body pressure	105 ±20	103 ± 10	103 ±10	130 ±40
Z (10^{-32} cm^6 sec^{-1})	$Z[M][Xe][N_2]$ molecular formation rate per unit volume	Sets magnitude of spin-transfer rates	5.7± 0.5	5.0± 0.5	5.2± 0.5	5.3±1

where p_0 is a characteristic pressure.

In the experiments described below the sample cells contain 0.5—1 Torr of Xe gas, about 10^{-5} Torr of alkali-metal-atom vapor and 10—100 Torr of N_2 gas. The molecular breakup will almost always be due to a collision with a N_2 molecule and we may therefore identify p in (6) as the third-body (N_2) pressure.

The characteristic pressure will depend on the chemical nature of the van der Waals molecule (i.e., p_0 will not be the same for KXe and RbXe) and we also expect p_0 to depend on the nature of the gas responsible for collisional breakups of the molecule (e.g., we know that p_0 is different for N_2 and He gas).[9] However, we expect p_0 to be the same for van der Waals molecules which differ only in their isotopic composition (i.e., p_0 should be the same for $^{129}Xe^{87}Rb$ and $^{131}Xe^{85}Rb$). In contrast, we expect the Breit-Rabi parameter x to be independent of the gas which causes the collisional breakup of the molecule. We also expect x to be the same for van der Waals molecules containing different isotopes of the alkali-metal atom (i.e., x will be the same for $^{129}Xe^{87}Rb$ and $^{129}Xe^{85}Rb$). However, we expect x to be different for van der Waals molecules containing different isotopes of the noble gas (i.e., we expect different values of x for $^{129}Xe^{85}Rb$ and $^{131}Xe^{85}Rb$, but the values of x should be proportional to the Larmor frequencies of the nuclei of ^{129}Xe and ^{131}Xe).

The molecular formation rates $(T_F)^{-1}$ and $(T_K)^{-1}$ per alkali-metal atom M and per noble-gas atom should be related to the respective number densities $[M]$ and [Xe] by

$$\frac{[M]}{T_F}=\frac{[Xe]}{T_K}=Z[M][Xe][N_2], \tag{7}$$

where $[N_2]$ is the number density of nitrogen molecules which, as we mentioned above, are almost always the third body involved in the formation of van der Waal molecules. We must therefore know the rate constant Z for three-body formation of van der Waals molecules as well as the parameters x and p_e to fully describe the spin-transfer process (1) and (2). All three of these parameters have been measured by methods to be described below, and the results are summarized in Table I.

II. CELL PREPARATION

The sample cells for our experiments are Pyrex glass spheres with an outer diameter of about 30 mm and a wall thickness of about 1 mm. The cells are prepared with a constricted glass stem, and a silicone coating[10] is applied to the interior of the cells by injecting about 2 ml of a 10% solution of "Surfrasil" in cyclohexane into the cell and shaking the cell vigorously. The solution is then removed and the cell interior is rinsed one or two times with pure cyclohexane. The cells are allowed to dry in air for about one day, and they are then sealed onto a 13-mm Pyrex manifold. The seal is made carefully to avoid heating and possible damage to the silicone coating within the sphere, and the completed manifold is not annealed for the same reason. The manifold is attached to a vacuum system as sketched in Fig. 2. A Pyrex U tube with a 1 g ampoule of K metal is inserted between the cells and the pump to serve as a getter for any impurities in the commercial gases used to fill the cell and to limit any contamination due to back streaming from the silicone oil diffusion pump. An open stopcock C is placed between the getter and the cells. Pure alkali metal from a glass ampoule, or alkali chloride salt and calcium metal chips, are placed in a glass retort sealed to the extreme end of the cell manifold. The cells are baked under a vacuum of 10^{-6} Torr at 150°C for 12 h. This seems to do no harm to the silicone coatings. While the cells are cooling down to room temperature the potassium metal getter is flashed with a hand torch so that some 15 cm of the U tube is coated with potassium metal. The alkali metal of interest is then distilled into the cells and the alkali retort is pulled off at the constriction D. The cells are then isolated from the pump by closing the valve V, and the desired amount (usually 1 Torr) of isotopically enriched Xe (69 wt. % ^{129}Xe) (Ref. 11) is admitted to the cells from the stainless-steel lecture bottle B. The gas pressure is read at ~20°C with mechanical billows gauges made by the Wallace Tiernan Company, one with a range of 0—20 Torr and one with a range of 0—800 Torr. The stopcock C is then closed and the xenon gas to the left of the stopcock is frozen back into steel bottle B by immersing the bottle in

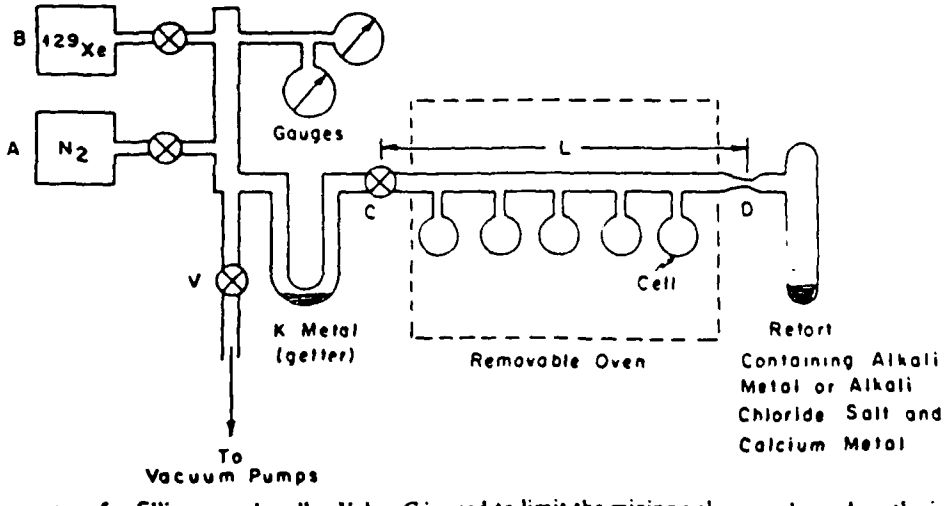

FIG. 2. Vacuum system for filling sample cells. Valve C is used to limit the mixing volume and speed up the interdiffusion of Xe

liquid nitrogen. Nitrogen gas is now admitted to the system from a glass bottle A and the desired pressure is obtained by pumping out any excess gas if necessary. The nitrogen pressure is always much larger than the pressure of the Xe to the right of stopcock C. Stopcock C is opened for about one-half second, and nitrogen gas rushes in to equalize the pressure on both sides of stopcock C. Owing to the rapid inflow of N_2 gas, a negligible amount of xenon flows to the left side of stopcock C during the brief time it is open. The glassware to the right of stopcock C now contains the same amount of Xe as before, and it contains the same total pressure, determined from the gauges, as the gas to the left of the closed stopcock C. Ample time must be allowed for the nitrogen and xenon to mix by diffusion, since convective mixing is probably negligible after the initial turbulence of the inflowing N_2 gas has decayed. Before pulling off the cells we allow the elapse of at least five characteristic time intervals

$$\frac{L^2 p(N_2)}{4\pi^2 D_0(760\ \text{Torr})},$$

where $D_0 \cong 0.1\ \text{cm}^2\text{sec}^{-1}$ is the diffusion constant of Xe in N_2 gas at a pressure of 760 Torr (one atmosphere) and L is the length of the cell manifold (see Fig. 2).

The cells are wrapped in wet asbestos paper to avoid overheating the silicone-coated interior of the glass sphere during the melting of the glass neck to pull the cells from the manifold. The average cell temperature does not deviate much from room temperature during the sealoff operation.

Before using the cells we are careful to leave about 0.5 cm^2 of alkali metal exposed near the tip of the cell. The interior of the cell also contains minute droplets of alkali metal spread across the surface. These small droplets do not interfere with the optical pumping and they help to ensure that the alkali-metal-atom vapor pressure is close to the saturated vapor pressure at the cell temperature. We have found that the alkali-metal-atom vapor pressure is below the saturated vapor pressure limit if the alkali metal is confined to an extended neck of the cell, or if the cells are not "cured" by being baked at 85 °C for at least three days before use.

III. MEASUREMENT AND ANALYSIS OF SPIN-RELAXATION TRANSIENTS OF ALKALI-METAL ATOMS

In this section we describe our experimental method to measure the spin-relaxation transients of alkali-metal atoms, and we show that the slowest decay rate γ_1 of spin-polarized alkali-metal atoms is mainly due to spin relaxation in alkali-metal—noble-gas van der Waals molecules, i.e.,

$$\gamma_1 = \frac{1}{T_F} |q(F,F)| + \cdots , \tag{8}$$

where $1/T_F$ is the molecular formation rate per alkali-metal atom and $|q(F,F)|$ is the probability that the total angular momentum $\langle F_z \rangle$ of the alkali-metal atom is destroyed during the lifetime of the van der Waals molecule. Relatively small contributions to γ_1 from optical pumping, spatial diffusion, binary collisions, and alkali-metal-atom—alkali-metal-atom spin-exchange collisions are denoted by the centered ellipsis in (8).

The spin relaxation of alkali-metal atoms is substantially more complicated than the nuclear spin relaxation of ^{129}Xe. This is because the number of potentially different longitudinal relaxation times is one less than the number of sublevels for the spin system of interest.[12] Thus, for the spin-$\frac{1}{2}$ nucleus of ^{129}Xe only one longitudinal relaxation time is expected, and indeed our experiments have shown that the spin-relaxation transient of ^{129}Xe is always very well described by a single exponential function of time. On the other hand, experimental studies of spin relaxation in alkali-metal-atom vapors almost always reveal more than one exponential decay. Since there are $2(2I+1)$ spin sublevels of an alkali-metal atom we could have to deal with $4I+1$ different decay rates or 15 decay rates in the case of ^{133}Cs with $I=\frac{7}{2}$. This large number of relaxation times can occur even if the spin Hamiltonian which is responsible for the relaxation is very simple and contains only one interaction, for example, a spin-rotation interaction $\gamma \vec{N}\cdot\vec{S}$. Fortunately, the experimental situation is simplified by two factors. First, no more than five of the $4I+1$ relaxation times can contribute to the optical signal at low magnetic fields.[13,14] Second, under the conditions of our experiments, in particular the occurrence of rapid alkali-metal-atom—alkali-metal-atom spin-exchange collisions, one of the relaxation rates, γ_1, is substantially slower than all of the rest. Our experiments are designed to measure the slowest relaxation rate, and we make no attempt to quantitatively measure any of the faster rates.

As was first shown by Bouchiat *et al.*,[13] five observables can contribute to the polarization-dependent attenuation of D_1 or D_2 light by spin-polarized alkali-metal-atom vapors in weak magnetic fields. There is one monopole observable $\langle \vec{I}\cdot\vec{S} \rangle$, the population imbalance between the Zeeman multiplets a and b; two dipole observables $\langle a_z \rangle$ and $\langle b_z \rangle$; and also two quadrupole observables $\langle 3a_z^2 - a(a+1) \rangle$ and $\langle 3b_z^2 - b(b+1) \rangle$. Because the relaxation processes have an isotropic character at low magnetic fields, the observable $\langle \vec{I}\cdot\vec{S} \rangle$ relaxes with a single exponential decay rate γ_0. The two observables $\langle a_z \rangle$ and $\langle b_z \rangle$ can be coupled to each other by the relaxation process so that their relaxation is characterized by two exponential decay rates γ_1 and γ_1'. Under the conditions of our experiments the rate γ_1 is the slowest of the five observable rates. Similarly, two rates γ_2 and γ_2' contribute to the relaxation of the quadrupole observables.

The apparatus used to measure the alkali-metal-atom spin-relaxation transients is sketched in Fig. 3. A more detailed description of the main components of the apparatus is given in Sec. IV. All of the sample cells contained 1 Torr Xe (69 wt. % ^{129}Xe), alkali metal, and various amounts of N_2 gas. The method is similar to that of Franz,[15] since we observe the time-dependent increase in intensity of circularly polarized light as it passes through an initially unpolarized alkali-metal-atom vapor while the spin polarization is being built up by optical pumping. An example of such an optical-pumping transient is shown in Fig. 4. Before the transient begins, the longitudinal polarizations $\langle a_z \rangle$ and $\langle b_z \rangle$ are maintained equal to zero by a radio-frequency magnetic field which oscillates at the Zeeman resonance frequency, $(2I+1)^{-1}2.8$

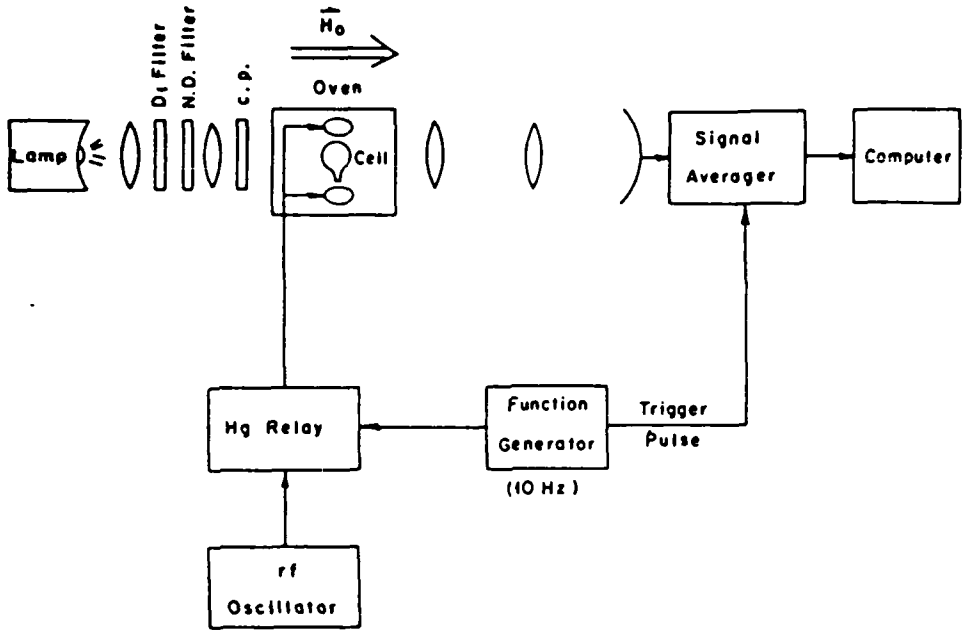

FIG. 3. Apparatus to measure the optical-pumping transients of alkali-metal-atom vapors. The sudden removal of the saturating rf field allows the transparency of the vapor to build up to its steady-state value with several different exponential time constants.

MHz/G of the alkali-metal atoms. The static magnetic field of ~ 6 G is so low that the strong rf field drives the Zeeman transitions in both the upper and lower multiplets to saturation. The transient response of Fig. 4 begins when the rf field is suddenly turned off with the Hg relay. The transients are repetitively generated at a 10 Hz rate and added in a signal averager to build up good signal-to-noise ratios. The longitudinal polarizations build up exponentially to their steady-state, optically pumped values. For example, as a function of time t after the rf is turned off, the dipole polarization evolves according to

$$\langle f_z \rangle = W_{1f}(1-e^{-\gamma_1 t}) + W'_{1f}(1-e^{-\gamma'_1 t}) . \tag{9}$$

Here $f = I \pm \frac{1}{2}$ (a or b) and both $\langle a_z \rangle$ and $\langle b_z \rangle$ evolve with the same decay rates, a slow rate γ_1 and a faster rate γ'_1. The weights W_{1f} and W'_{1f} depend on the details of the relaxation process but W_{1f} will ordinarily be larger than W'_{1f}. Equations similar to (9) hold for the two quadrupole observables and for $\langle \vec{I} \cdot \vec{S} \rangle$, except that only one exponential occurs for $\langle \vec{I} \cdot \vec{S} \rangle$ and the observables may not be zero at $t=0$ since neither $\langle \vec{I} \cdot \vec{S} \rangle$ nor the quadrupole observables are necessarily destroyed by a resonant rf field.

The intensity J of the transmitted light will be related to the intensity J_0 of the light incident on the sample cell by

$$J = J_0 A , \tag{10}$$

where A is the attenuation of the vapor. We expect A to depend on the spectral profile and polarization of the light, the alkali-metal-atom vapor density, and the five observables $\langle \vec{I} \cdot \vec{S} \rangle$, $\langle a_z \rangle$, $\langle b_z \rangle$, ..., which determine the photon absorption cross section of the alkali-metal atoms. For sufficiently small spin polarization we can always write for $\sigma_\pm$ light

$$A_\pm(\langle a_z \rangle, \langle b_z \rangle, \ldots) = A_0 \pm \langle a_z \rangle \frac{\partial A}{\partial \langle a_z \rangle} \pm \langle b_z \rangle \frac{\partial A}{\partial \langle b_z \rangle} + \cdots . \tag{11}$$

The partial derivatives $\partial A / \partial \langle a_z \rangle$ are to be evaluated at $\langle a_z \rangle = 0$, $\langle b_z \rangle = 0$, etc. They can be calculated in terms of the spectral profile and polarization of the incident light and in terms of the polarization-dependent cross section of the alkali-metal atoms for light absorption.[16] In view of (9) we can write (11) as

$$A = A_0 \pm A_1(1-e^{-\gamma_1 t}) \pm A'_1(1-e^{-\gamma'_1 t}) + \cdots , \tag{12}$$

where the coefficients A_1 and A'_1 can be easily evaluated in terms of the weights W_{1f}, W'_{1f} and the coefficients $\partial A / \partial \langle f_z \rangle$. The difference between the limiting attenuation A_∞ at long times after the start of the transient and the attenuation [illegible]

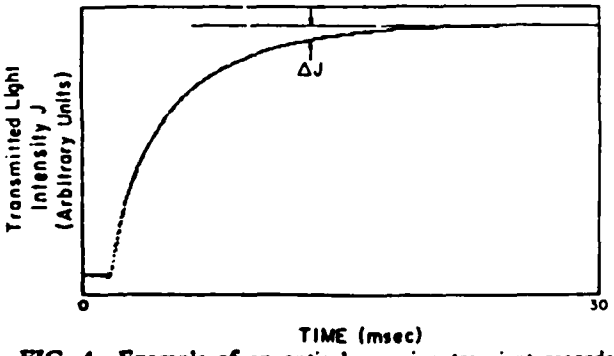

FIG. 4. Example of an optical-pumping transient recorded with the apparatus of Fig. 3. The intensity of the transmitted light increases with time because of the buildup of spin polarization in the vapor as a result of optical pumping

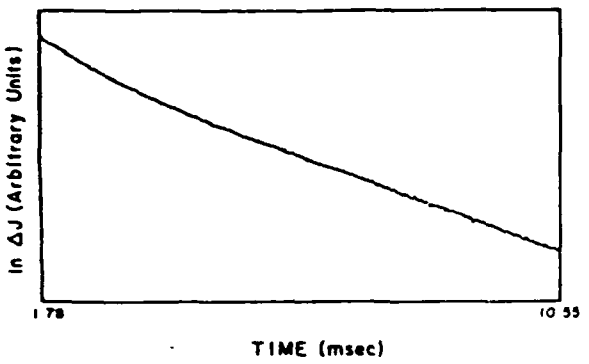

FIG. 5. The difference $\Delta J = J_\infty - J$ between the steady-state light intensity J_∞ and the transient light intensity J decays with several exponentials; the slowest exponential has a particularly simple significance.

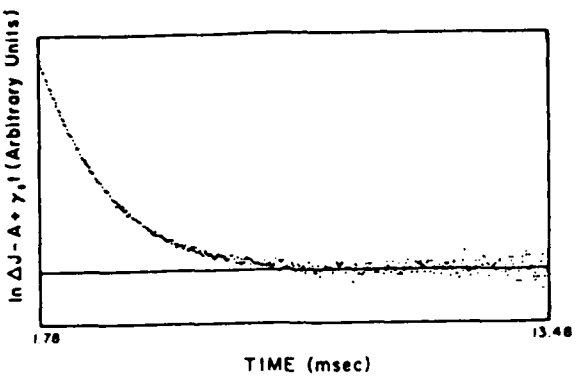

FIG. 6. Residuals for a fit to the slowest exponential of data like those of Fig. 5.

$$\Delta A = A_\infty - A = A_1 e^{-\gamma_1 t} + A_1' e^{-\gamma_1' t} + \cdots . \tag{13}$$

For times longer than a few units of $(\gamma_1' - \gamma_1)^{-1}$ we may ignore all but the slowest transient in (13) and use (10) to write the observed transient as

$$\Delta J \simeq J_0 A_1 e^{-\gamma_1 t} \quad \text{for } t \gg (\gamma_1' - \gamma_1)^{-1} . \tag{14}$$

Thus in our experiments we measure ΔJ as a function of time and we identify the limiting slope of $\ln \Delta J$ at large times as the slow decay constant $-\gamma_1$. An example of a measured value of $\ln \Delta J$ versus t is shown in Fig. 5. In Fig. 6 we show the residuals for linear fit to the data of Fig. 5. From Fig. 6 we see that there is negligible contribution of the faster exponentials to the decay transient after about 6 msec.

Both experimental measurements and theory show that γ_1 is an increasing function of the pumping-light intensity J. For sufficiently weak light we expect to find a linear dependence on J,

$$\gamma_1(J) = \gamma_{10} + J \left[\frac{\partial \gamma}{\partial J} \right] + \cdots , \tag{15}$$

with the partial derivative evaluated at $J = 0$. In Fig. 7 we show an example of an experimental measurement of γ_1 versus J. The effect of the pumping light is relatively small and we may obtain γ_{10}, the slowest relaxation rate in the dark, by extrapolating γ_1 back to zero light intensity.

Using formulas from Ref. 17, Hou *et al.*[18] have shown that the decay rate of the slowest transient is expected to be

$$\gamma_{10} = r_1 + \frac{(2I+1)^2+2}{2(2I+1)^2} r_2 + \frac{1}{3T_{ex}} \frac{(2I+1)^2+2}{(2I+1)^2} - \frac{1}{2} \left[\left\{ \frac{2}{3T_{ex}} \frac{[(2I+1)^2+2]}{(2I+1)^2} \right\}^2 + \frac{4r_2}{3T_{ex}} \left\{ \frac{(2I+1)^4 - 2(2I+1)^2 + 4}{(2I+1)^4} \right\} + \left\{ r_2 \frac{(2I+1)^2-2}{(2I+1)^2} \right\}^2 \right]^{1/2} . \tag{16}$$

There are three characteristic rates in (16). The fastest, the alkali-metal-atom–alkali-metal-atom spin-exchange rate, is expected to be on the order of[19,20]

$$\frac{1}{T_{ex}} \sim 10^{-9} [M] \text{ cm}^3 \text{ sec}^{-1} , \tag{17}$$

where $[M]$ is the alkali-metal number density. Representative values of $[M]$ in our work are 5×10^{11} cm^{-3}, so we expect to find values of $1/T_{ex}$ on the order of 500 sec^{-1}. It is interesting to note that (16) becomes independent of $1/T_{ex}$ in the limit $1/T_{ex} \to \infty$. The second characteristic rate is r_2, the electron randomization rate. This refers to a relaxation process which destroys the electron-spin polarization $\langle S_z \rangle$ without affecting the nuclear-spin polarization $\langle I_z \rangle$. In our work we expect electron randomization to be associated with sudden binary collisions between alkali-metal atoms and Xe atoms or N_2 molecules. Alkali-metal-atom–alkali-metal-atom collisions also lead to electron randomization at a rate which has been measured in Cs vapor to be about 1% of the spin-exchange rate.[21] Thus, for Cs-Cs collisions we expect a contribution to r_2 on the order of 5 sec^{-1}, a negligible amount. It is reasonable to expect negligible contributions to r_2 from alkali-metal-atom–alkali-metal-atom collisions in Rb and K vapors also. The contribution of Rb-N_2 collisions to r_2 has been measured by Franz[22] to be 0.145 sec^{-1} per Torr of N_2 gas. Thus, even at the highest N_2 pressure (100 Torr) used in our experiments the contribution Rb-N_2 collisions make to r_2 will only be approximately 14.5 sec^{-1}, a negligible amount. It is reasonable to expect a negligible contribution to r_2 from similar N_2 pressures for Cs and K spin relaxation also.

The electron randomization rate due to binary collisions of alkali-metal atoms with Xe gas is expected to be given

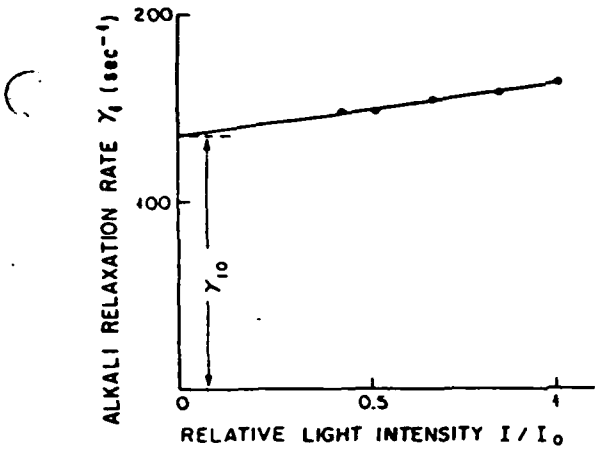

FIG. 7. Dependence of the slowest decay rate γ_1 on the intensity of the pumping light. The light-independent decay rate γ_{10} is obtained by extrapolating the rate to the limit of zero light intensity.

by the formula[6]

$$r_2=\frac{1}{T_{FB}}\left[\frac{2}{3}\left[\frac{\gamma N\tau_B}{\hbar}\right]^2+\frac{2}{3}K(K+1)\left[\frac{\alpha\tau_B}{\hbar}\right]^2 f\right], \quad (18)$$

where T_{FB}^{-1} is the rate of binary collisions per alkali-metal atom, and τ_B is an appropriately defined duration of a binary collision. The fraction of ^{129}Xe atoms in the isotopically enriched sample is f, and we may ignore the interaction of ^{131}Xe, the other isotope with nonzero nuclear spin, because it is much less abundant in our gas samples and because the term in (18) proportional to α^2 is about a factor of 2 smaller for ^{131}Xe than for ^{129}Xe for equal isotopic fractions as a result of the different spins and nuclear moments of the two isotopes.

The electron randomization rate due to binary collisions of alkali-metal atoms with Xe gas has been measured in two instances. For RbXe Bouchiat *et al.*[7] report

$$r_2(\text{RbXe})=185\ \text{sec}^{-1}\,\text{Torr}^{-1}\,p(\text{Xe}), \quad (19)$$

while for NaXe Bhaskar *et al.*[23] report

$$r_2(\text{NaXe})=266\ \text{sec}^{-1}\,\text{Torr}^{-1}\,p(\text{Xe}). \quad (20)$$

Unfortunately, there seem to be no measurements of the corresponding rates for KXe and CsXe.

The contribution of r_2 to γ_{10} depends on the relative size of r_2 and the spin-exchange rate $1/T_{ex}$ as demonstrated by Hou *et al.*[18] In the limit $1/r_2T_{ex}\to\infty$, Eq. (16) reduces to

$$\gamma_{10}=r_1+\frac{3r_2}{(2I+1)^2+2}, \quad (21)$$

while in the opposite extreme $1/r_2T_{ex}\to 0$, Eq. (16) becomes

$$\gamma_{10}=r_1+\frac{2r_2}{(2I+1)^2}. \quad (22)$$

In both cases there is a substantial slowing-down factor due to the nuclear spin I which is not destroyed in the electron randomizing collision and which therefore regenerates much of the electron-spin polarization after the collision is over. We note that in the limit $1/T_{ex}\to 0$ the eigenobservable associated with γ_{10} was shown by Bouchiat *et al.*[13] to be I_z (or more precisely the sum of the projections of I_z in the upper and lower Zeeman multiplets). In the other limit, where $1/T_{ex}\to\infty$ the eigenobservable[12] is simply F_z, the total spin angular momentum of the alkali-metal-atom vapor. Our experiments on spin relaxation in the alkali-metal-atom vapors are ordinarily done at an alkali-metal number density which corresponds to $1/r_2T_{ex}\gtrsim 3$. This leads to a slowing-down factor which is closer to (21) than (22), and for simplicity we shall use (21) to correct our data. In the case of ^{87}Rb the numerical value of the correction is $r_2/8\simeq 23\ \text{sec}^{-1}$ if we use formula (22) and $r_2/6\simeq 30\ \text{sec}^{-1}$ if we use formula (21). Since both corrections are comparable to the error in the experimental measurements there is little to be gained from choosing a more precise intermediate value. We shall also make the simplifying assumption that the electron ran-

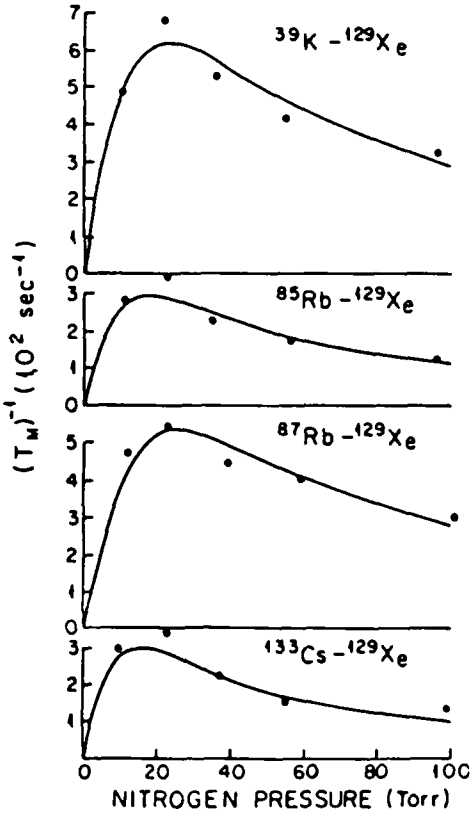

FIG. 8. Summary of the experimentally determined molecular contribution $(T_M)^{-1}$ to the slowest decay rate γ_1 of alkali-metal-atom spins. All cells contained 1 Torr of Xe gas (60 wt. % ^{129}Xe). Small contributions to γ_1 from the pumping light, diffusion to the cell walls, and electron-randomizing binary collisions have been subtracted from γ_1 to obtain $(T_M)^{-1}$ [see Eq. (28)]. Solid curves are $|q(F,F)|T_F^{-1}$ with a distribution of the rotational angular momentum N taken into account. Note that the nuclear spin of the alkali-metal atom causes a substantial slowing down of the alkali-metal decay rates so that the decay rates of ^{85}Rb and ^{87}Rb differ by nearly a factor of 2. These data are used to determine the parameters $(T_F)^{-1}$ and p_0.

domization rates of K and Cs atoms in xenon are the same as for Rb in xenon.

Since the contributions of electron randomization r_2 and spin exchange $1/T_{ex}$ to (16) are small compared to the measured magnitude of γ_{10} (see Fig. 8), we conclude that the dominant contribution to γ_{10} comes from r_1, the third and simplest characteristic rate in (16). The rate r_1 describes those relaxation processes which cause $\langle a_z \rangle$ and $\langle b_z \rangle$ to decay at the rate r_1 with no coupling of $\langle a_z \rangle$ to $\langle b_z \rangle$, i.e.,

$$\frac{d}{dt}\langle f_z \rangle = -r_1 \langle f_z \rangle , \tag{23}$$

where $f = a$ or b. An obvious contributor to r_1 is the diffusion of spin polarized alkali-metal atoms to the cell walls. The silicone coatings which are so effective in slowing down the spin relaxation of ^{129}Xe nuclei cause no measurable slowing down of the alkali-metal-atom spin relaxation, probably because we leave the inner walls of the cells coated with many small droplets of alkali metal to try to ensure that the equilibrium saturated vapor pressure of alkali-metal atoms prevails within the cell at a given temperature. The lowest diffusion mode of a sphere of radius R with disorienting walls has a relaxation rate[24]

$$\gamma_D = \frac{\pi^2 D_0}{R^2}\frac{760}{p} , \tag{24}$$

where p is the pressure in Torr of the gas (N_2) through which the alkali-metal atoms diffuse and D_0 is the diffusion constant of the gas at one atmosphere (760 Torr). We have measured D_0 for Rb in N_2 and we find

$$D_0(\mathrm{RbN_2}) = 0.20\ \mathrm{cm^2\,sec^{-1}} \tag{25}$$

at 70°C. This is in satisfactory agreement with the value D_0 ($\mathrm{RbN_2}$) = 0.16 $\mathrm{cm^2\,sec^{-1}}$ at 32°C measured by Franz.[22] For our cells, which have radii of about 13 mm, the diffusion rates γ_D for cells with the lowest N_2 pressures (~10 Torr) do not exceed 50 $\mathrm{sec^{-1}}$, a relatively small contribution to γ_{10}.

The most important contribution to r_1 and to γ_{10} is relaxation due to the formation of alkali-metal–noble-gas van der Waals molecules. As we already mentioned in connection with (1) and (2) the molecule-induced rate is the product of a formation rate per alkali-metal atom T_F^{-1} and a spin destruction probability $|q(F,F)|$ per molecular lifetime. At high N_2 pressures where $\phi/(2I+1) \ll 1$ one can show that[6]

$$|q(F,F)| = \frac{2}{3}\left[\frac{\phi}{2I+1}\right]^2\left[1+\frac{K(K+1)}{x^2}f\right] \tag{26}$$

where f is the isotopic fraction of ^{129}Xe. There is no restriction on the magnitude of the Breit-Rabi parameter x in (26). For lower N_2 pressures where $\phi/(2I+1) \gtrsim 1$, we may write $|q(F,F)|$ as a power series in x^{-2} and find[6]

$$|q(F,F)| = \frac{2}{3}\frac{\left[\frac{\phi}{2I+1}\right]^2}{1+\left[\frac{\phi}{2I+1}\right]^2} + \frac{2K(K+1)f}{9x^2}\frac{\left[3-\left[\frac{\phi}{2I+1}\right]^2\right]}{\left[1+\left[\frac{\phi}{2I+1}\right]^2\right]^3}\left[\frac{\phi}{2I+1}\right]^2$$
$$+\frac{K(K+1)f}{3x^2(2I+1)[I(I+1)+\frac{3}{4}]}\sum_{m_f}\frac{m_f^2\left[\frac{\phi m_f}{x(2I+1)}\right]^2}{1+\left[\frac{\phi m_f}{x(2I+1)}\right]^2} . \tag{27}$$

Formula (27) is valid only if $x^2 \gg 1$.

We studied the effects of cell temperature on the slowest decay rate γ_{10} described above and we found that in the case of ^{87}Rb, γ_{10} was independent of cell temperatures in the range of 50 to 80°C to within the ~10% accuracy of the measurements. The main effect of increasing the cell temperature was to increase the weights of the faster relaxation transients shown in Figs. 5 and 6 and to increase the influence of the pumping light on the slowest decay rate; i.e., the slope of the plots like those of Fig. 7 were less at higher cell temperatures, These observations suggest that neither alkali-metal-atom–alkali-metal-atom spin-exchange collisions nor higher-order spatial diffusion modes had any significant effects on the measured value of the slowest relaxation rate γ_1.

In summary, we attribute most of the measured slow decay rate γ_1 to relaxation in alkali-metal–noble-gas van der Waals molecules. To extract the best estimate of the molecular contribution, we make three relatively small corrections to the raw data.

(1) We extrapolate the measured slowest decay rate γ_1 to zero probing light intensity, as shown in Fig. 7, to obtain slowest decay rate γ_{10} for relaxation in the dark.

(2) We subtract from γ_{10} an estimate (24) of the contribution of spatial diffusion of spin polarized alkali-metal atoms to the depolarizing walls of the cell.

(3) We also subtract an estimate of the contribution of electron randomizing collisions between spin polarized alkali-metal atoms and Xe atoms. Since the electron randomization rate has only been measured for Rb and N_2 we approximate the rates for K and Cs by the rate (19) for Rb.

Our best estimate for the contribution of van der Waals molecules to the slowest spin-relaxation rate of alkali-

metal atoms is thus

$$\frac{1}{T_M}=\gamma_{10}-\frac{\pi^2 D_0}{R^2}\frac{760}{p}-\frac{3r_2}{(2I+1)^2+2}. \quad (28)$$

In Fig. 8 we summarize measured spin-relaxation rates of alkali-metal atoms in 1 Torr of Xe gas (69 wt.% ^{129}Xe), corrected for diffusion and binary collisions according to the right-hand side of Eq. (28). The solid curves are the theoretical value $|q(F,F)|\,T_F^{-1}$ for the relaxation due to van der Waals molecules. Theoretical curves were fit to the data by using the molecular formation rate T_F^{-1} per alkali-metal atom and the characteristic pressure p_0 of (6) as free parameters. The curves are not very sensitive to the Breit-Rabi parameter x and the value of x was not a free parameter in the fits of Fig. 8, but x was instead determined, as described in Sec. V, from the ratio of the ^{129}Xe and alkali-metal-atom spin relaxation rates at higher third-body pressures. The values of $q(F,F)$ used to fit the data of Fig. 8 are about 12% smaller than the value given by Eq. (27) because we averaged the spin-transfer coefficient over a distribution of rotational angular momenta N as described in Ref. 6.

IV. MEASUREMENT AND ANALYSIS OF SPIN-RELAXATION TRANSIENTS OF ^{129}Xe NUCLEI

The relaxation of ^{129}Xe nuclei is relatively simple compared to the spin relaxation of alkali-metal atoms discussed in Sec. III. Since the nuclear spin of ^{129}Xe is $K=\frac{1}{2}$ there can only be one longitudinal relaxation time and our experiments show that the ^{129}Xe transients are well described by a single exponential decay curve instead of a superposition of several exponential decay curves as is observed for spin relaxation of the alkali-metal atoms.

The experimental apparatus for observing the relaxation of the ^{129}Xe spins is shown in Fig. 9. A dc magnetic field ($H_0\approx 5$ G) which is produced by large coils (not shown in Fig. 9) defines the Larmor frequencies of alkali-metal atoms and ^{129}Xe nuclei and lessens the sensitivity of the system to stray magnetic fields. The cell is heated by a stream of hot air and the gas mixture in it is optically pumped by an alkali-metal-atom vapor resonance lamp using a circular polarizer (CP) and a filter which transmits the $D1$ line. During the probe phase of the experiment the circular polarizer is removed and the small amount of elliptical polarization introduced in the unpolarized light by the polarized alkali-metal atoms is detected with a photoelastic modulator. The signal is proportional to the number density of the spin polarized ^{129}Xe nuclei since the short-lived (≈ 1 msec) polarized ^{87}Rb atoms are produced by spin exchange with the xenon. Small amounts of stray elliptical polarization caused by the lamp itself and by the optical components are initially compensated by a rotatable $\lambda/4$ plate. The stray components of the elliptical polarization are temperature sensitive. This leads to a slow, unpredictable drift in the elliptical background polarization during the long ($\approx\frac{1}{2}$ h) relaxation time. To compensate for the slow drift we perform adiabatic rapid passage, i.e., we periodically invert the ^{129}Xe nuclear polarization with a chirped audio-frequency magnetic field which is applied to the small coils. The frequency is swept from 3 to 7 kHz through the ^{129}Xe magnetic resonance of 5 kHz. The xenon polarization is determined by subtracting the average signals during the 5-sec intervals before and after an inversion. This procedure is equivalent to transforming the signal power to higher frequencies and it substantially attenuates noise components with periods longer than 10 sec. An Apple II + computer controls the inversion rates and performs on-line data processing. The signal amplitude is given by $A(t)=A(0)(\epsilon-1)^n\exp(-\tau/\theta)$, where ϵ is the decay per inversion, n is the number of inversions which have occurred by time t, and θ is the ^{129}Xe relaxation time. Variation of the interval betweeen consecutive inversions permits the determination of both θ and ϵ from the decay curve. Independent measurements of θ under the same conditions have a variance from their mean of $\approx 5\%$. Typical decay curves of ^{129}Xe in ^{39}K, ^{85}Rb, and ^{133}Cs alkali-metal-atom vapors are shown in Fig. 10. The decay rate of the ^{129}Xe nuclear polarization θ^{-1} results from the combined effects of the alkali-metal-induced rate

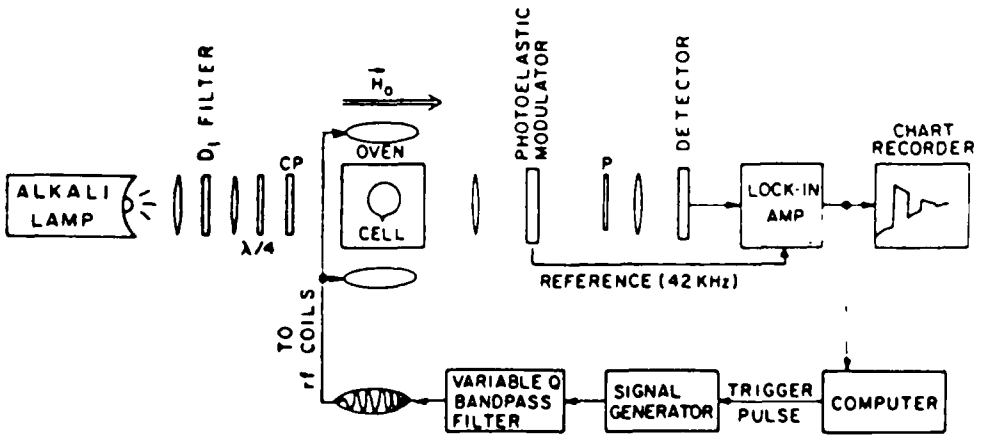

FIG. 9. Apparatus to measure the nuclear-spin relaxation transients of ^{129}Xe in various alkali-metal-atom vapors and in the presence of various amounts of N_2 gas. The ^{129}Xe nuclear polarization is inverted with a chirped audio-frequency pulse from time to time to eliminate slow drifts from the recording system.

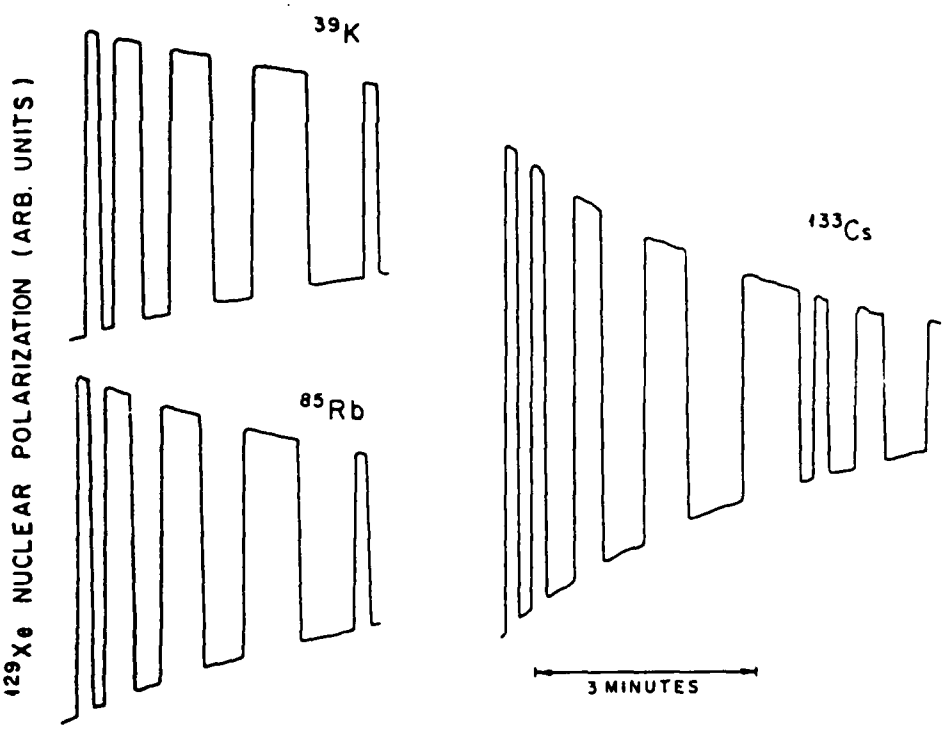

FIG. 10. Representative ^{129}Xe nuclear-spin relaxation transients in ^{39}K, ^{85}Rb, and ^{133}Cs alkali-metal-atom vapors as observed with the apparatus of Fig. 9.

θ_0^{-1} and wall relaxation rate T_w^{-1},

$$\theta^{-1}=\theta_0^{-1}+T_w^{-1}=C[\mathrm{Rb}]+T_w^{-1}, \tag{29}$$

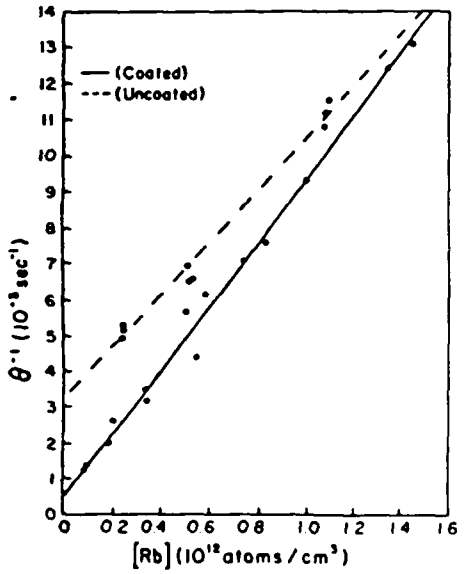

FIG. 11. Dependence of the ^{129}Xe spin-relaxation rate on the ^{87}Rb number density in an uncoated Pyrex cell containing 21 Torr of N^2 gas and in a silicone-coated Pyrex cell containing 14.9 Torr of N_2. Both cells contain 0.5 Torr of Xe, enriched to 69 *wt. % isotopic fraction of* ^{129}Xe. The wall-induced relaxation rate is the intercept at [Rb]=0. Silicone-coated cells have much longer wall-relaxation times for ^{129}Xe than uncoated cells. The Rb-induced contribution to the ^{129}Xe relaxation rate depends on the third-body (i.e., N_2) gas pressure.

where C and T_w^{-1} are temperature-independent constants. The quantities C and T_w^{-1} are determined by measuring θ^{-1} at various temperatures as shown in Fig. 11. The alkali-metal density is deduced from the measurement of the cell temperature with a nonmagnetic thermocouple and by using empirical saturated vapor-pressure curves for the alkali metals. We should mention that several pieces of evidence have convinced us that the Rb vapor-pressure curve given by Smithells[25] and used by us[5,9,10,30] and by the group at Litton Industries[3,4] to interpret spin-relaxation measurements of xenon isotopes in Rb vapor is incorrect and gives a vapor pressure which is more than a factor of 2 smaller than the true vapor pressure. Bouchiat and Brossel[26] have already commented on this discrepancy. The best data for Rb seem to be those of Killian,[27] whose empirical formula for the saturated vapor pressure of Rb metal, in dyn/cm^2, is

$$\log_{10}p=10.55-4132/T\ . \tag{30}$$

Faraday rotation measurements in our laboratory have shown that the K vapor pressure in our cells for the temperature range 70 to 110 °C is adequately represented by a variant of Killian's[27] formula

$$\log_{10}p=11.57-4964/T\ . \tag{31}$$

Here T is the absolute temperature in Kelvin. For Cs we used the formula tabulated by Nesmeyanov[28] for the saturated vapor pressure in Torr (1 Torr = 1333. dyn/cm^2):

$$\log_{10}p=11.0531-1.35\log_{10}T-4041/T\ . \tag{32}$$

There is good evidence[29] that the wall-induced rate is a

decreasing function of the cell temperature in the case of ^{131}Xe. In our experiments with ^{129}Xe, the wall-induced rate is so small compared to the alkali-metal-induced rate that any temperature dependence of $1/T_w$ will introduce a negligible error in our inferred values of the alkali-metal-induced rate $C[M]$. We believe that there are two contributions to the alkali-metal-induced rate:

$$C[M]=\frac{1}{\theta_0}=\frac{1}{T_K}|q(K,K)|+\frac{1}{T_{KB}}\frac{1}{2}\left[\frac{\alpha\tau_B}{\hbar}\right]^2. \quad (33)$$

The relaxation due to alkali-metal—noble-gas van der Waals molecules is the product of a molecular formation rate T_K^{-1} per noble-gas atom and a probability $|q(K,K)|$ that the nuclear spin is destroyed during the molecular lifetime. The last term in (33) describes the relaxation due to binary alkali-metal—noble-gas collisions where T_{KB}^{-1} is the rate of binary collisions per noble-gas atom and τ_B is an appropriately defined mean duration of the binary collision.

Several pieces of evidence show that the contribution from binary collisions is small compared to the contribution from van der Waals molecules. First, the binary contribution should be independent of the third-body (nitrogen) pressure, but all of our data show a strong dependence of the ^{129}Xe relaxation rates on the nitrogen pressure. Second, the binary rate should be independent of magnetic fields less than 10^6 G. Measurements by Bhaskar *et al.*[31] have shown that the relaxation rate of ^{129}Xe in Rb is nearly eliminated by an external magnetic field of 200 G.

We may estimate the contribution of binary collisions to the nuclear-spin relaxation of ^{129}Xe by noting that the binary-collision rate T_{KB}^{-1} of (33) is related to the binary-collision rate per alkali-metal atom T_{FB}^{-1} of (18) by

$$\frac{[M]}{T_{FB}}=\frac{[\mathrm{Xe}]}{T_{KB}}. \quad (34)$$

Substituting (18) and (34) into (33) we find that we may write the binary contribution as

$$\frac{1}{\theta_B}=\frac{1}{T_{KB}}\frac{1}{2}\left[\frac{\alpha\tau_B}{\hbar}\right]^2=r_2\frac{[M]}{[\mathrm{Xe}]}\frac{1}{\frac{4}{3}x^2+f}. \quad (35)$$

Thus for Rb in Xe where r_2 was given by (19) and $x\simeq 3.1$, we find

$$\frac{1}{\theta_B}=4.1\times10^{-16}\,\mathrm{sec}^{-1}\,\mathrm{cm}^3[\mathrm{Rb}]. \quad (36)$$

At a representative number density of $[\mathrm{Rb}]=10^{12}\,\mathrm{cm}^{-3}$ we expect a binary contribution to the relaxation of ^{129}Xe, $\theta_B^{-1}=0.4\times10^{-3}\,\mathrm{sec}^{-1}$, about 5% of the peak rate at 17 Torr of N_2 but about 13% of the total rate at 100 Torr of N_2 (see Fig. 12). Unfortunately, the electron randomization rates r_2 for K and Cs in xenon gas have not been measured but it is reasonable to guess that they are comparable to the rate for Rb or Na, as discussed in Sec. III, and we shall therefore assume that the contribution of binary collisions to the relaxation of ^{129}Xe in K and Cs vapor is small compared to the relaxation due to van der Waals molecules.

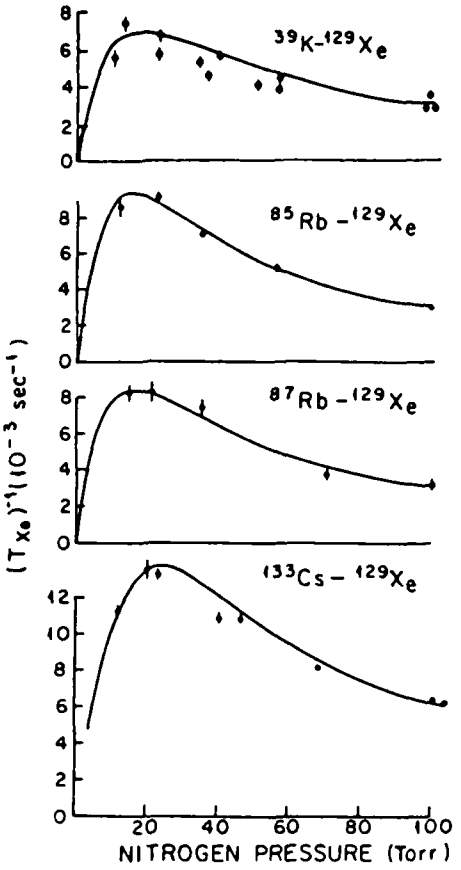

FIG. 12. Summary of the experimentally determined molecular contribution $(T_{Xe})^{-1}$ to the nuclear-spin relaxation rate of ^{129}Xe in cells containing alkali-metal-atom vapors at a number density of $10^{12}\,\mathrm{cm}^{-3}$, as deduced from the empirical formulas (30)—(32) and the cell temperatures. Small contributions to $(T_{Xe})^{-1}$ from wall relaxation and electron-randomizing binary collisions have been subtracted to obtain $(T_{Xe})^{-1}$ [see Eq. (39)]. Solid curves are $|q(K,K)|T_K^{-1}$ with $q(K,K)$ given by Eq. (38). Note that the alkali-metal nuclear spin has very little effect on the relaxation of ^{129}Xe, as is evidenced by the data for ^{85}Rb and ^{87}Rb. These data are used to determine the parameters T_K^{-1} and p_0.

For sufficiently high N_2 pressures where $\phi/(2I+1)\ll 1$, one can show that the nuclear-spin destruction probability for ^{129}Xe is

$$|q(K,K)|=\frac{2}{3}\left[\frac{\phi}{(2I+1)x}\right]^2\left[I(I+1)+\tfrac{1}{4}\right] \quad (37)$$

for unpolarized alkali-metal atoms but with no restriction on whether x is larger or small than unity. For smaller N_2 pressures where $\phi/(2I+1)\gtrsim 1$ we can express $|q(K,K)|$ as a power series in x^{-2} and we find

$$|q(K,K)| = \frac{1}{9x^2}(4I^2+4I+3)\frac{\left[\frac{\phi}{2I+1}\right]^2}{1+\left[\frac{\phi}{(2I+1)}\right]^2} + \frac{1}{3(2I+1)}\sum_{fm_f}\left[1-\frac{1}{2x^2}[f(f+1)-m_f^2]\right]\left[\frac{\left[\frac{\phi m_f}{(2I+1)x}\right]^2}{1+\left[\frac{\phi m_f}{(2I+1)x}\right]^2}+\delta m_{f0}\frac{\left[\frac{\phi f(f+1)}{2(2I+1)x^2}\right]^2}{1+\left[\frac{\phi f(f+1)}{2(2I+1)x^2}\right]^2}\right]. \quad (38)$$

Formula (38) is valid only for small values of the expansion parameter x^{-2}.

In summary, we attribute most of the alkali-metal dependent decay rate θ_0^{-1} of ^{129}Xe to relaxation due to van der Waals molecules. A relatively small contribution to θ_0^{-1} from binary alkali-metal–noble-gas collisions is subtracted to obtain the best estimate of the molecule-induced relaxation

$$\frac{1}{T_{Xe}} = \theta^{-1} - r_2\frac{[M]}{[Xe]}\frac{1}{\frac{4}{3}x^2+f} - \frac{1}{T_w}, \quad (39)$$

where as before we approximate the electron randomization rate r_2 for K and Cs by the measured rate $r_2 = 185$ sec^{-1} for Rb.

In Fig. 12 we summarize the measured spin-relaxation rates of ^{129}Xe nuclear spins corrected for wall relaxation and for electron randomizing collisions according to Eq. (39). Alkali-metal-atom vapor densities of 10^{12} atoms/cm^3, as inferred from the empirical formulas (30)—(32), were assumed for Fig. 12. The solid curves in Fig. 12 are the theoretical value $|q(K,K)|T_K^{-1}$ for the relaxation due to van der Waals molecules. The theoretical curves are not very sensitive to the Breit-Rabi parameter x and the value of x was not taken to be a free parameter in the fits of Fig. 12, but x was inferred instead from the ratio of the ^{129}Xe and alkali-metal-atom spin-relaxation rates at high third-body pressures. The two free parameters in the fit were T_K^{-1}, the molecular formation rate per noble-gas atom, and p_0, the characteristic pressure. The value of $|q(K,K)|$, the probability that the ^{129}Xe nuclear spin is destroyed during the molecular lifetime, was taken from Eq. (38).

V. DETERMINATION OF THE BREIT-RABI PARAMETER x FROM THE RATIO OF THE SPIN-RELAXATION TIMES OF THE ALKALI-METAL ATOMS AND THE NOBLE-GAS ATOMS

Let us consider the ratio of the wall-corrected spin-relaxation rate $C[M]$ of the xenon atoms to the slowest spin-relaxation rate of the alkali-metal atoms M,

$$\frac{1}{T_{M,0}} = \gamma_{10} - \frac{\pi^2 D_0\, 760\ \text{Torr}}{R^2 P(N_2)} \quad (40)$$

after the effects of optical pumping and spatial diffusion have been eliminated. From (26), (33), and (37) we find that the expected ratio at high N_2 pressures is

$$\frac{\theta_0}{T_{M,0}} = \frac{[Xe]}{[M]}\frac{(x^2+3f/4)}{I(I+1)+\frac{3}{4}} \quad (41)$$

provided that we assume that the Breit-Rabi parameter x is the same for binary collisions as it is for van der Waals molecules and provided that we assume that the contribution of binary collisions to the relaxation of the alkali-metal atoms is given by (21), the value appropriate to the eigenobservable F_z of spin temperature equilibrium. Since we have already shown that the contribution of binary

TABLE II. Data used to determine x for ^{85}Rb^{129}Xe from Eq. (42). Cells all contained 1 Torr of xenon (69 wt. % ^{129}Xe) and the ^{129}Xe relaxation rates were determined at a number density of 10^{12} cm^{-3} according to formula (30). Small contributions of the cell walls to the alkali-metal-atom and noble-gas spin-relaxation rates have been subtracted in accordance with Eqs. (29) and (40).

N_2 pressure in cell	$T_{M,0}$ sec^{-1}	θ_0^{-1} sec^{-1}	$\frac{\theta_0}{T_{M,0}}$
23	346	9.06×10^{-3}	3.82×10^4
35	228	7.13×10^{-3}	3.20×10^4
56	178	5.25×10^{-3}	3.38×10^4
96	124	3.04×10^{-3}	4.06×10^4
Mean value of 56- and 96-Torr cells			3.72×10^4

FIG. 15. Comparison between exact numerical evaluations and perturbative approximations of the frequency-shift coefficient $s(a,K)$. Effect of assuming a distribution in N is also shown.

FIG. 17. Comparison between exact numerical evaluations and perturbative approximations to the zero-pressure width ΔH_0 of the magnetic slowing-down curves. Effect of assuming a distribution of N is also shown.

ollisions is small for both $T_{M,0}^{-1}$ and θ_0^{-1}, any modest parture of the alkali-metal eigenobservable from F_z or the binary value of x from the molecular value will use a negligible error in our results. We may therefore e (41) to evaluate x^2 from the measured values of θ_0, $_{M,0}$ and [Xe] and from the alkali-metal number density M] which we infer from the cell temperature and the turated vapor-pressure formulas (30)–(32). The explicit pression is

$$x^2=\frac{[M]}{[\mathrm{Xe}]}\frac{\theta_0}{T_{M,0}}[I(I+1)+\tfrac{1}{4}]-\frac{3f}{4}. \tag{42}$$

epresentative data for $^{85}Rb^{129}Xe$ are shown in Table II. ie values of x inferred for ^{129}Xe paired with ^{39}K, ^{85}Rb, Rb, and ^{133}Cs are summarized in Table I.

VI. RATIO OF REPOLARIZATION SIGNAL TO PUMPING SIGNAL

In our experiment we detect the nuclear-spin polarization of the noble gas indirectly by observing the "repolarization" signal, i.e., by observing the electronic-spin polarization induced in the alkali-metal atoms by collisions with e nuclear-spin-polarized noble-gas atoms. The magnitude of the repolarization signal depends on many parameters in addition to the magnitude of the nuclear-spin polarization of the noble gas. The intensity, circular polarization, and spectral profile of the probing light; the number densities of the alkali-metal atoms, the noble-gas atoms, and the third-body atoms or molecules; and the spin-relaxing properties of the cell walls can all influence the repolarization signals. The purpose of this section is to show that there is good agreement between the magnitude of the observed repolarization signals and the theoretically expected values.

We measured the repolarization signals with the apparatus sketched in Fig. 13. The cell was optically pumped for several spin-relaxation times of the noble-gas nuclei; a typical pumping time was about 15 min. The pumping light passed through a neutral density (ND) filter, a circular polarizer (CP), the sample cell, and a circular analyzer (CA). At the end of the pump phase the CP was removed from the optical train and a stopwatch was started simultaneously. A radio-frequency magnetic field, 100% square-wave modulated at 10 Hz, was applied to the sample cell at the resonance frequency, 700 KHz/G of the ^{87}Rb atoms. The electron-spin polarization $\langle F_z\rangle$ of the ^{87}Rb was thereby driven to zero for half of the 10-Hz cycle and it was allowed to recover to its repolarized value during the half cycle the rf was off. The recovery time was a few milliseconds and the saturation time in the rf field was even shorter, so the ^{87}Rb polarization was very nearly square-wave modulated also. The modulated ^{87}Rb polarization $\langle F_z\rangle$ modulated the attenuation A of the va-

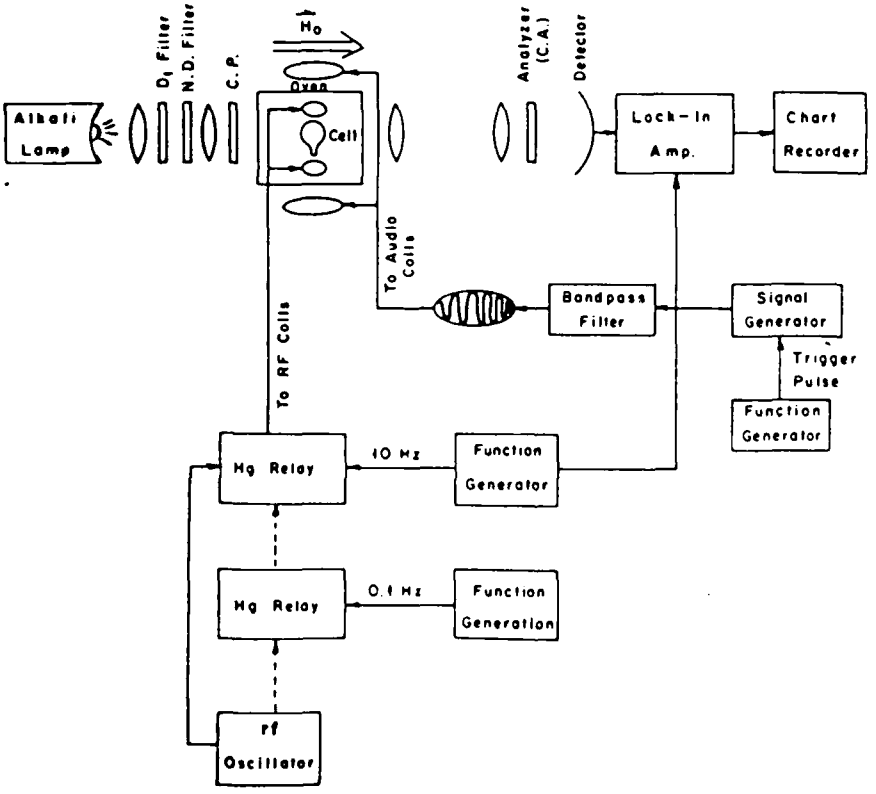

FIG. 13. Apparatus used to measure the ratio of the alkali-metal-atom spin polarization produced by collisions with nuclear-spin arized ^{129}Xe to the alkali-metal-atom spin polarization during the optical-pumping phase.

or, so the light reaching the detector was square-wave modulated by an amount proportional to the ^{87}Rb spin polarization. The 10-Hz optical signal was detected with a lock-in amplifier referenced to the same 10-Hz modulation frequency. This probe signal decayed slowly because of the relaxation of the ^{129}Xe nuclear polarization which was responsible for the repolarization. To eliminate drifts and offset signals the ^{129}Xe polarization was periodically inverted as described in Sec. IV and the time between the removal of the circular polarizer and the occurrence of the first adiabatic inversion was recorded with the stopwatch. The ^{129}Xe relaxation signal was recorded on chart paper, and by extrapolating the signal amplitude back to the time of removal of the circular polarizer, we were able to infer the initial repolarization signal S_{Xe}.

The circular polarizer was then replaced in the optical train and the much larger signal due to the optically pumped Rb atoms was recorded with exactly the same 10 Hz chopped rf. The rf was turned off completely several times to establish the baseline for the optical pumping signal S_{Rb}. During the recording of the optical pumping signal the adiabatic-inversion pulses were turned off, although we found that this made very little difference to the pumping signal. Data from a representative measurement are shown in Fig. 14.

The ND filter was then replaced by a filter with a different attenuation, the rf was turned off, the cell was pumped for another 15 minutes, and the measurement cycle was repeated as described above. All of the measurements were done at the same cell temperature.

The ratios S_{Xe}/S_{Rb} of the repolarization signal to the pump signal was then plotted as a function of the relative light intensity. A representative plot is shown in Fig. 15. It can be seen that the ratio decreases linearly from the zero-light-intensity intercept $(S_{Xe}/S_{Rb})_0$. Similar plots were made for other sample cells with different amounts of nitrogen buffer gas but with the same amount, 0.5 torr, of isotopically enriched Xe gas. We shall subsequently show that except for a correction factor of order unity which accounts for the attenuation of the circular polarizer, the signal ratio S_{Xe}/S_{Rb} is equal to the ratio $\langle F_z\rangle_{repol}/\langle F_z\rangle_{pump}$, where $\langle F_z\rangle_{pump}$ and $\langle F_z\rangle_{repol}$ are the expectation values of the alkali-metal angular momenta during the pump and probe phases, respectively.

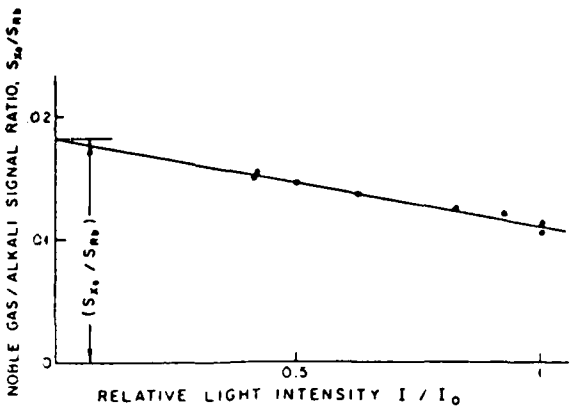

FIG. 15. Dependence of the signal ratio on the intensity of the optical-pumping light. Strong unpolarized light during the probe phase can substantially decrease the magnitude of the repolarization signal.

To interpret these experiments we recall that for weak polarization the attenuation A of the vapor was given by (11). For simplicity we shall neglect the contributions to A of $\langle\vec{I}\cdot\vec{S}\rangle$ and of the two quadrupole observables. This is a good approximation for ^{87}Rb cells probed with ^{87}Rb lamps, since the spectral profile of the lamp is then quasi-broadline and cannot produce $\langle\vec{I}\cdot\vec{S}\rangle$ or the quadrupole observables efficiently[13,16] Furthermore, the attenuation of the light will be relatively insensitive to $\langle\vec{I}\cdot\vec{S}\rangle$, i.e., we expect to find

$$\left|\frac{\partial A}{\partial\langle\vec{I}\cdot\vec{S}\rangle}\right| \ll \left|\frac{\partial A}{\partial\langle f_z\rangle}\right| . \tag{43}$$

Finally, as we mentioned in Sec. III, the relaxation of $\langle\vec{I}\cdot\vec{S}\rangle$ and the quadrupole observables is normally faster than that of $\langle a_z\rangle$ and $\langle b_z\rangle$, and this will further suppress the magnitudes of $\langle\vec{I}\cdot\vec{S}\rangle$ and of the two quadrupole observables relative to the magnitudes of $\langle a_z\rangle$ and $\langle b_z\rangle$. We shall further assume that $\langle a_z\rangle$ and $\langle b_z\rangle$ are well described by the spin temperature approximations,[6] i.e.,

$$\langle f_z\rangle = \frac{f(f+1)(2f+1)}{2(2I+1)[I(I+1)+\frac{1}{4}]}\langle F_z\rangle , \tag{44}$$

where $f = I \pm \frac{1}{2}$. Then (11) can be written as

$$A_\pm = A_0 \pm A_F\langle F_z\rangle , \tag{45}$$

where A_F is a linear combination of $\partial A/\partial\langle a_z\rangle$ and $\partial A/\partial\langle b_z\rangle$.

We will denote the number density of σ_+ photons entering the cell by n_+ and the number density of σ_- photons by n_-. The numbers of σ_+ and σ_- photons emerging from the cell will be $n_+(A_0+A_F\langle F_z\rangle)$ and $n_-(A_0-A_F\langle F_z\rangle)$, respectively. These photon currents

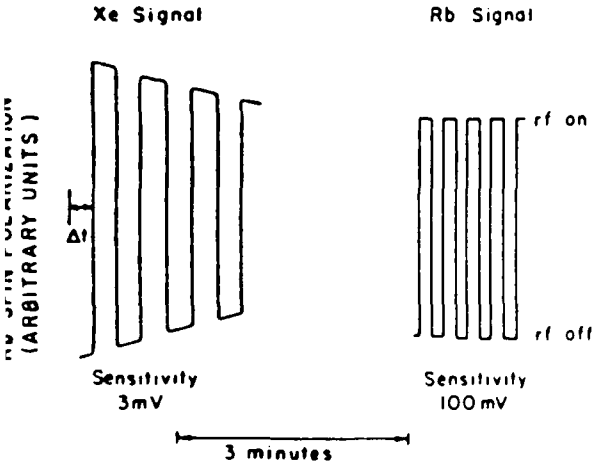

FIG. 14. Sample data (the noise is too small to reproduce) of the repolarization signal and the optical-pumping signal. The initial envelope of the Xe signal is $2S_{Xe}$ (the factor of 2 comes from the adiabatic inversion) and the envelope of the Rb signal S_{Rb}.

be attenuated further by factors of a_+ and a_-, ctively, when they pass through the CA. The num- ensity of photons reaching the detector is therefore

$$n_+a_+(A_0+A_F\langle F_z\rangle)+n_-a_-(A_0-A_F\langle F_z\rangle) \quad (46)$$

he signal detected by the lock-in amplifier of Fig. 13 be proportional to

$$\Delta S=(n_+a_+-n_-a_-)A_F\langle F_z\rangle . \quad (47)$$

ng the repolarization phase of the measurement the lar polarizer is removed and we will therefore have $n_-=n_0/2$, where n_0 is the number density of pho- in the beam of unpolarized light from the lamp.

$$\Delta S_{\rm repol}=\frac{n_0}{2}(a_+-a_-)A_F\langle F_z\rangle_{\rm repol} . \quad (48)$$

ng the pump-phase measurement we have $=(n_0/2)a_+$ and $n_-=(n_0/2)a_-$. This is so because olarizer and analyzer are nearly identical and are cut the same sheet of laminated plastic circular- izer material. Thus the pump-phase signal is

$$\Delta S_{\rm pump}=\frac{n_0}{2}(a_+^2-a_-^2)A_F\langle F_z\rangle_{\rm pump} . \quad (49)$$

ratio of the signals is

$$\frac{\text{repol}}{\text{amp}}=\frac{1}{a_++a_-}\frac{\langle F_z\rangle_{\rm probe}}{\langle F_z\rangle_{\rm pump}}=\frac{1}{2\bar a}\frac{\langle F_z\rangle_{\rm probe}}{\langle F_z\rangle_{\rm pump}} . \quad (50)$$

can easily verify that the fractional attenuation of un- ized light by the polarizer is

$$\bar r=\frac{a_++a_-}{2} . \quad (51)$$

a good polarizer the fractional attenuation is very y $\frac{1}{2}$, and for our polarizers we measure

$$\bar r=0.44 , \quad (52)$$

e correction factor is $2\bar a=0.88$ for our experiments. ie evolution of the noble-gas spin polarization during ump phase is given by

$$\frac{d}{dt}\langle K_z\rangle=-\frac{1}{T_w}\langle K_z\rangle+\frac{1}{T_K}[q(K,K)\langle K_z\rangle+q(K,F)\langle F_z\rangle] \quad (53)$$

h has the steady-state solution

$$\langle K_z\rangle_0=\frac{q(K,F)\langle F_z\rangle_{\rm pump}}{\frac{T_K}{T_w}+|q(K,K)|} \quad (54)$$

$q(K,K)<0$.

we ignore the effects of spatial diffusion and other relaxation mechanisms (but not spin exchange, has no effect on $\langle F_z\rangle$) we may describe the evolu- f the alkali-metal-atom spin polarization by

$$\frac{d}{dt}\langle F_z\rangle=-\frac{1}{T_{\rm opt}}\langle F_z\rangle+\frac{1}{T_F}[q(F,F)\langle F_z\rangle+fq(F,K)\langle K_z\rangle] , \quad (55)$$

where $(T_{\rm opt})^{-1}$ is the spin-depolarization rate due to the unpolarized probe light. The value of $\langle K_z\rangle$ decreases very slowly with time compared to the characteristic time $T_F\simeq10^{-3}$ sec, so we may write the quasi-steady-state solution to (55) as

$$\langle F_z\rangle_{\rm repol}=\frac{fq(F,K)\langle K_z\rangle}{\frac{T_F}{T_{\rm opt}}+|q(F,F)|} \quad (56)$$

since $q(F,F)<0$.

Thus, we expect the ratio of the alkali-metal-atom spin polarization at the beginning of the repolarization measurement to the pump-phase polarization to be

$$\frac{\langle F_z\rangle_{\rm repol}}{\langle F_z\rangle_{\rm pump}}=\frac{fq(F,K)q(K,F)}{\left[\frac{T_F}{T_{\rm opt}}+|q(F,F)|\right]\left[\frac{T_K}{T_w}+|q(K,K)|\right]} . \quad (57)$$

In the limit of low light intensity, $T_{\rm opt}\to\infty$, and we may rewrite (57) as

$$r=\frac{fq(F,K)q(K,F)}{q(F,F)q(K,K)}=\frac{\frac{1}{T_w}+\frac{1}{T_K}|q(K,K)|}{\frac{1}{T_K}|q(K,K)|}\left[\frac{\langle F_z\rangle_{\rm repol}}{\langle F_z\rangle_{\rm pump}}\right]_0 . \quad (58)$$

The correction factor

$$\frac{\frac{1}{T_w}+\frac{1}{T_K}|q(K,K)|}{\frac{1}{T_K}|q(K,K)|}=\frac{\frac{1}{T_w}+C[\mathrm{Rb}]}{C[\mathrm{Rb}]} \quad (59)$$

can be determined experimentally from data like those of Fig. 11, and in view of (50) we expect to find

$$r=\frac{fq(F,K)q(K,F)}{q(F,F)q(K,K)}=\frac{\frac{1}{T_w}+C[\mathrm{Rb}]}{C[\mathrm{Rb}]}2\bar a\left[\frac{\Delta S_{\rm repol}}{\Delta S_{\rm pump}}\right]_0 . \quad (60)$$

Equation (60) gives two expressions for the repolarization ratio r: a purely theoretical formula in the middle involving the spin-transfer coefficients $q(F,K)$, etc., and on the right-hand side, an experimental ratio corrected for the effects of ^{129}Xe wall relaxation (a factor slightly larger than 1) and for the polarizer attenuation ($2\bar a=0.88$, a factor slightly less than 1). The experimental and theoretical values of r are compared in Fig. 16. Note that there are no adjustable parameters in Fig. 16. The Breit-Rabi parameter x and the characteristic pressure p_0 which go into the evolution of the spin-transfer coefficients [e.g., see (38)

Spin exchange collisions between gaseous atoms first attracted attention n the 1950's when V. Weisskopf and N. Ramsey[3,4] first suggested in a Harvard eminar that the collisional transfer of population between the hyprfine sub-evels of H atoms in a gas would be dominated by the spin exchange interac-ion. The cause of the exchange is illustrated in Fig. 1 which shows the owest singlet and triplet potentials of a pair of H atoms. These potentials an be represented by a spin-dependent potential

$$V = V_1(R) + V_2(R)\ \vec{S}_1 \cdot \vec{S}_2 \qquad (1)$$

here $\vec{S}_1$ and $\vec{S}_2$ are the spin operators of the two H atoms and $V_1(R)$ and $V_2(R)$ re spin-independent functions of the internuclear separation R. The poten-ial (1) cause $\vec{S}_1$ and $\vec{S}_2$ to rotate about each other or exchange at a fre-uency $\frac{V_2(R)}{h}$, i.e. at the difference frequency of the singlet and triplet otential curves. This rate is so large that the spins can exchange many imes even for collision impact parameters of several atomic diameters where egligible momentum transfer occurs.

Following the suggestion of Weisskopf and Ramsey, the details of spin change collisions were worked out by two groups in 1956. Purcell and eld[3] were interested in the thermalization mechanism for the hyperfine iblevels of H atoms which produce the famous 21 cm line of radio astronomy, d they carried out a semiclassical analysis of spin exchange collisions. cke and Wittke[4] were interested in the effects of spin exchange collisions the line widths of the magnetic resonance curves of atomic hydrogen, which ey were investigating by microwave spectroscopy. They used partial waves analyze the effects of spin exchange on the line widths.

Spin Exchange, Past, Present and Future

"Paper presented at the Alfred Kastler Symposium
École Normale Supérieure, January 1985"

W. Happer

Department of Physics

Princeton University

Princeton, NJ 08544

U.S.A.

Spin exchange provides a means to transfer the spin angular momentum of atoms which have been optically pumped by Kastler's[1] methods to other atoms which cannot be optically pumped directly. Such experiments often use alkali atoms as the optically pumped species because the strong adsorption lines of alkali atoms lie in the visible or near infrared region of the spectrum where efficient lasers and lamps are available. We may think of the alkali atoms and the light source as a kind of prime mover of angular momentum which provides spin for various secondary spin systems.

The basic physics of spin exchange was first recognized in the singlet-triplet spectrum of the helium atom. As Heisenberg[2] first pointed out, the singlet-triplet splitting, or the exchange frequency, is of an electrostatic nature and is due to the Pauli principle and not, as one might naively suppose, to the magnetic interaction between the spins. Spin exchange interactions are ubiquitous in physics and are an important aspect of ferromagnetism, of chemical bonds, and of course of the topic of this paper, spin exchange collisions between atoms, molecules, electrons and ions in a gas.

References

1. F.A. Franz and A. Sieradzan, Phys. Rev. A29, 1599 (1984).

2. M.A. Bouchiat, J. Physique 24, 379 (1963); 24, 611 (1966).

3. M.A. Bouchiat, J. Brossel and L.C. Pottier, J. Chem. Phys. 56, 3703 (1972).

$$\frac{[NaNe]}{[Na]} = K[Ne] \qquad (8)$$

where K is an equilibrium constant which may be chosen to describe the quasi-bound molecular concentration in the particular vibrational and rotational states which are supposed to be responsible for the spin relaxation. Thus, the assumptions of Ref. 1 imply a violation of the law of mass action.

In conclusion, the authors of Ref. 1 do not adequately justify their omission of the million-fold suppression factor from their basic equation (1), and the assumption that quasibound molecules form in predominantly resonant binary collisions but are broken up predominantly by collisions with other atoms is inconsistent with detailed balance.

This work was supported by the U.S. Air Force Office of Scientific Research under Grant No. AFOSR-81-0104-C.

would show chaotic collisions with an occasional encounter in which a quasi-bound NaNe molecule is formed in resonant binary collision. The number of NaNe molecules formed in three body collisions involving a Na atom and two Ne atoms would be negligible. The molecules would be observed to live for a short time before being broken up by a collision with another Ne atom. Spontaneous breakup of NaNe molecules would be negligible. If the "motion picture" were run in reverse quite a different scenario would unfold. Molecules would be formed predominantly in three body collisions, the inverse of collisional breakup, and moleucles would break up predominantly by spontaneous decay, the inverse of resonant binary collisions. Thus, the arguments involved in Ref. 1 are not invariant to time reversal. This time asymmetry has nothing to do with the spin polarization, since the spins are assumed to have no influence on the formation and breakup rates.

As one more example of the difficulties which follow from the assumptions of Ref. 1 consider the equality of the molecular formation and breakup rates which must obtain in thermal equilibrium. We have

$$[\mathrm{Na}]\,\frac{1}{T_f} = [\mathrm{NaNe}]\,\frac{1}{\tau_{el}} \tag{6}$$

or

$$\frac{[\mathrm{NaNe}]}{[\mathrm{Na}]} = \frac{\tau_{el}}{T_f} = \text{neon-independent ratio} \tag{7}$$

since T_f^{-1} and τ_{el}^{-1} are both assumed to be proportional to the neon pressure in Ref. 1. However, according to the law of mass action

δa I.S.

The authors of Ref. 1 state in connection with their Eq. 2 "In fitting Eq. (1) to the R* data we found no significant distinction between τ_{e1} and τ_{e2}; we take

$$\tau_{e1}^{-1} = \tau_{e2}^{-1} = \tau_0^{-1} + n_0\sigma_B v_{rel} p/p_0, \tag{4}$$

where n_0 is Loschmidt's number, σ_B is the breakup cross section for the quasi bound complexes, v_{rel} is the mean relative velocity of Na atoms and Ne atoms, p is the Ne pressure , and p_0 is atmospheric pressure. Fits also indicate that the average natural lifetime τ_0 of the quasibound complex is sufficiently long that both τ_{e1}^{-1} and τ_{e2}^{-1} are determined solely by the collisional breakup rate. The best fit to the data, indicated by the solid line in Fig. 2, yields

$$\sigma_B\ 3.2\times10^{-13}\text{cm}^2,\ \langle\delta a^2\rangle T_f^{-1} = 7.2\times10^{18}\text{psec}^{-3}. \tag{5}$$

This cross section is about an order of magnitude larger than the cross section for the breakup of truly bound van der Waals molecules. If we assume that the shift in "a" in a quasibound state can be as much as 10% of a, that implies a formation rate 900 psec^{-1}, not an unreasonable number based on the known NaNe potentials."

The arguments above are inconsistent with the principle of detailed balance or microreversibility since they assume that the molecular formation rate T_f^{-1}, per Na atom is dominated by resonant binary collisions but the breakup rate is dominated by collisions of NaNe molecules with other Ne atoms. For example a "motion picture" of the Na and Ne atoms in the cell

$$\left(\frac{\mu_B H}{h\Delta W}\right)^2 \simeq 10^{-6} \qquad (3)$$

for relaxation in low magnetic fields. This problem is alluded to in the last paragraph of Ref. 1 which states: "Of several questions which remain, one is why R* is not affected by a scale factor dependent upon magnetic field. It is this factor which allows the $\delta a(\vec{S}\cdot\vec{I})$ interaction in sudden binary collisions (the origin of the well-known pressure shift of the hyperfine interaction) to yield negligible relaxation in low H_0 but substantial relaxation at high H_0.[13] Our data and analyses suggest that R* behaves as if a strong effective local magnetic field is present in the molecular state. For present purposes we have taken the scale factor to be 1, but more substantial consideration of this assumption clearly is warranted."

In our opinion this statement is insufficient to alert the average reader that the scale factor is not 1 but is forced by the laws of quantum mechanics to be on the order of 10^{-6}. While the authors are not too clear about what they meany by a "strong effective magnetic field", it is hard to understand how such a field could fail to contribute to the relaxation rate Z_1, and the authors offer no suggestions for a physical mechanism to produce the field.

The authors of Ref. 1 refer to the magnetic slowing down data of their Fig. 3 as "a conclusive test of the molecular origin of R*". In fact, if the anomalous relaxation is due to the interaction $\delta a\ \vec{I}\cdot\vec{S}$ as claimed by the authors of Ref. 1, the relaxation rate would <u>increase</u> with magnetic field as the authors themselves mention in their last paragraph. Thus, the magnetic field dependence of Ref. 1 has the wrong sign if it is due to the interaction

peak at a neon pressure of about 17 Torr and to decrease for both lower and higher pressures.

The authors of Ref. 1 attribute the anomalous relaxation to an interaction $\delta a\, \vec{I}\cdot\vec{S}$ which acts during the lifetime of quasibound Na Ne van der Waals molecules. According to the authors of Ref. 1; "If the attribution of R* to $\delta a(\vec{S}\cdot\vec{I})$ relaxation in NaNe van der Waals molecules is correct, the following theoretical description should apply.[14,18]

$$R^* = \frac{8\pi^2}{3}\,\frac{\langle\delta a\rangle^2\tau_{e1}\tau_{e2}I(I+1)T_f^{-1}}{1+\tau_{e2}^2\Delta W^2} \qquad (1)$$

where τ_{e2} is the correlation time for the perturbation, τ_{e1} is the duration of the perturbation, $\langle\delta a\rangle$ is the average shift in the Na hyperfine constant a per perturbation, I is the nuclear spin, ΔW is 2π times the separation between hyperfine states, and T_f^{-1} is the formation rate of complexes".

Eq. 1 cannot give a correct description of spin relaxation due to the interaction $\delta a\, \vec{I}\cdot\vec{S}$. At low magnetic fields where Eq. 1 is supposed to be valid the off-diagonal matrix elements of $\delta a\, \vec{I}\cdot\vec{S}$ between the Zeeman basis states of the Na atom are very nearly zero; the sole non-zero matrix elements are

$$\langle 2m \mid \delta a\, \vec{I}\cdot\vec{S} \mid 1m\rangle \sim \frac{\mu_B H}{h\Delta W}\,\delta a \qquad (2)$$

between states of the same azimuthal quantum number m but different total angular momentum quantum numbers, 2 and 1. Formula (1) should therefore be multiplied by a factor on the order of

Franz and Sieradzan[1] have recently presented experimental data and theoretical arguments which are said to show that quasibound van der Waals NaNe molecules make an important contribution to the spin relaxation of Na atoms in neon buffer gas. Here we point out certain problems with the arguments of that paper.

In Ref. 1 exponential decay time constants for the spin polarization of optically pumped Na atoms in neon buffer gas are measured at various pressures and in the presence of strong and weak magnetic fields. As Bouchiat[2] first pointed out, the observed spin relaxation transients of optically pumped alkali atoms are normally the sum of several exponential decay curves. The rate of the slowest exponential is denoted by Z_1 in Ref. 1, and it is apparently thought to be due to the combined effects of the lowest-order mode for the spatial diffusion of spin polarized Na atoms to the depolarizing walls of the cell and the bulk-phase relaxation of spin polarized Na atoms due to the spin rotation interaction[3] $\gamma\vec{N}\cdot\vec{S}$ which acts during sudden, binary NaNe collisions. Here $\vec{N}$ is the rotational angular momentum of the Na and Ne atoms about each other during a collision, γ is the spin rotation coupling constant and $\vec{S}$ is the electron spin of the Na atom. We find no fault with this interpretation of Z_1, whose dependence on the neon pressure is shown in Fig. 1 of Ref. 1.

In Ref. 1 it is claimed that the initial fast transient is characterized by a single exponential with a rate constant Z_2 and that Z_2 is larger than one would infer from the rate Z_1 of the slow transient. The authors of Ref. 1 assign this discrepancy to an "anomalous mode of relaxation" R*. The anomalous relaxation is shown in Fig. 2 of Ref. 1. It is said to exhibit a

Comment on "Binary formation of Na Ne quasibound molecules observed in spin relaxation of Na"

"Accepted for publication in the Physical Review"

W. Happer
Department of Physics
Princeton University
Princeton, NJ 08544

A factor of about 10^{-6} has been omitted without adequate justification from a key formula of the recent paper "Binary Formation of Na Ne quasibound molecules observed in spin relaxation of Na". The arguments of the paper are also inconsistent with the principle of detailed balance.

[1]M. A. Bouchiat, T. R. Carver, and C. M. Varnum, Phys. Rev. Lett. 5, 373 (1960); R. L. Gamblin and T. R. Carver, Phys. Rev. 138, A946 (1965).
[2]R. M. Herman, Phys. Rev. 137, A1062 (1965).
[3]B. C. Grover, Phys. Rev. Lett. 40, 391 (1978).
[4]C. H.Volk, T. M. Kwon, and J. G. Mark, Phys. Rev. A 21, 1549 (1980).
[5]N. D. Bhaskar, W. Happer, and T. McClelland, Phys. Rev. Lett. 49, 25 (1982).
[6]W. Happer, E. Miron, S. Schaefer, D. Schreiber, W. A. van Wijngaarden, and X. Zeng, Phys. Rev. A 29, 3092 (1984).
[7]M. A. Bouchiat, J. Brossel, and L. C. Pottier, J. Chem. Phys. 56, 3703 (1972); C. C. Bouchiat, M. A. Bouchiat, and L. C. L. Pottier, Phys. Rev. 181, 144 (1969).
[8]H. Kopferman, *Nuclear Moments* (Academic, New York, 1968).
[9]N. Ramsey, E. Miron, X. Zeng, and W. Happer, Chem. Phys. Lett. 102, 340 (1983).
[10]X. Zeng, E. Miron, W. A. van Wijngaarden, D. Schreiber, and W. Happer, Phys. Lett. 96A, 191 (1983).
[11]The isotopically enriched sample of Xe gas used in this work was purchased from the Isotec Corporation of Centerville, Ohio.
[12]W. Happer, Rev. Mod. Phys. 44, 169 (1972).
[13]M. A. Bouchiat, J. Phys. (Paris) 24, 379 (1963); 24, 611 (1963).
[14]M. A. Bouchiat and F. Grossetete, J. Phys. (Paris) 27, 353 (1966).
[15]F. A. Franz and C. Volk, Phys. Rev. A 14, 1711 (1976).
[16]B. S. Mathur, H. Y. Tang, and W. Happer, Phys. Rev. A 2, 648 (1970).
[17]N. D. Bhaskar, J. Camparo, W. Happer, and A. Sharma, Phys. Rev. A 23, 3048 (1981).
[18]Mei-Yin Hou, Bing-Ying Cheng, and Rui Ju, Chin. Phys. Lett. 1, 57 (1984).
[19]K. Ernst and E. Strumia, Phys. Rev. 170, 48 (1968).
[20]H. M. Gibbs, and R. J. Hull, Phys. Rev. 153, 132 (1967).
[21]N. D. Bhaskar, J. Pietras, J. Camparo, and W. Happer, Phys. Rev. Lett. 44, 930 (1980).
[22]F. A. Franz and C. E. Sooriamoorthi, Phys. Rev. A 8, 2390 (1973).
[23]N. D. Bhaskar, M. Hou, M. Ligare, B. Suleman, and W. Happer, Phys. Rev. A 22, 2710 (1980).
[24]F. Masnou-Seeuws and M. A. Bouchiat, J. Phys. (Paris) 28, 406 (1967).
[25]C. Smithells, *Metals Reference Handbook* (Butterworths, London, 1962).
[26]M. A. Bouchiat and J. Brossel, Phys. Rev. 147, 41 (1966).
[27]T. Killian, Phys. Rev. 27, 578 (1926).
[28]A. N. Nesmeyanov, *Vapor Pressure of the Elements* (Academic, New York, 1963).
[29]C. H. Volk, T. M. Kwon, J. G. Mark, Y. B. Kim, and J. C. Woo, Phys. Rev. Lett. 44, 136 (1980).
[30]B. A. Andrianov, V. M. Lopatin, P. S. Ovcharenko, Yu. M. Petukhov, and E. M. Sychugov, Pis'ma Zh. Tekh. Fiz. 7, 848 (1981) [Sov. Tech. Phys. Lett. 7, 363 (1981)].
[31]N. D. Bhaskar, W. Happer, M. Larsson, and X. Zeng, Phys. Rev. Lett. 50, 105 (1983).

extrapolation of Fig. 15 is designed to eliminate the shunting effect of R_{opt} across R_{sr}.

Finally, we should note that the RC network of Fig. 17 is appropriate to high N_2 pressures where $\phi \ll 1$ and $q(K,K) = -q(K,F)$. Under these conditions very little spin transfer among F, N, and K occurs during each molecular lifetime. For lower N_2 pressures where $\phi \gtrsim 1$, very substantial changes of F and K can occur during each molecular lifetime, and much of the atomic and nuclear spin angular momentum is transferred to the rotational angular momentum N of the molecule. Then the RC network of Fig. 17 should be modified to include an additional shunt resistor across C_{Xe}. This new shunt resistor as well as the resistors R_{ex} and R_{sr} can be defined in a straightforward way in terms of the spin coupling coefficients of Eqs. (1) and (2).

VIII. CONCLUSIONS

The data of Fig. 10 demonstrate that excellent ^{129}Xe nuclear-spin polarization signals can be observed in K, Rb, and Cs alkali-metal-atom vapors. Adrianov[30] *et al.* have already reported that ^{133}Cs is comparable to the Rb isotopes as a spin-exchange partner for ^{129}Xe, but they reported no systematic studies of the dependence of the exchange rate on third-body pressure. The quantitative data of Table I, the main results of the work described in this paper, show that the parameters x, p_0, and Z are similar in magnitude for all three alkali metals.

We are unable to deduce absolute values for the spin-rotation constant γN and the spin-exchange constant α from the spin-relaxation data described in this paper. Independent magnetic-decoupling experiments[31] are low being carried out in our laboratory to establish the magnitude of γN.

The dependence of the relaxation rates on third-body (N_2) pressure (see Figs. 8 and 12) is characteristic of three-body processes where the relaxation rate is the product of a molecular-formation rate T_K^{-1} or T_F^{-1} and a spin-destruction probability $|q(K,K)|$ or $|q(F,F)|$, as indicated in Eq. (33) or (8). At low N_2 pressures the molecular lifetimes are so long that $|q(K,K)|$ and $|q(F,F)|$ are independent of pressure and equal to their saturated values, $\frac{2}{3}$, which is the probability that $\vec{N}$ will be perpendicular to the external magnetic field when a van der Waals molecule is formed. The relaxation rates are therefore proportional to the molecular-formation rates or the N_2 pressure.

For very high N_2 pressure the spin-destruction probabilities must be proportional to the square of the molecular lifetime or inversely proportional to the square of the N_2 pressure. The relaxation rate at high N_2 pressure must therefore be inversely proportional to the N_2 pressure. The noble-gas and alkali-metal-atom spin-relaxation rates attain their peak values at pressures on the order of $p_0/3x$ and $p_0/(2I+1)$, respectively.

The overall precision of these experiments is not very high, especially since we have relied on the saturated vapor-pressure formulas (30)–(32) to estimate the alkali-metal number density from the cell temperature. A temperature measurement error of 1°C corresponds to a vapor-density error of 5–10%. As we discussed in Sec. IV, published vapor-pressure curves for Rb differ by more than a factor of 2 in the temperature range of our experiments.

We also note that the value $x = 3.1$ given in Table I for Rb ^{129}Xe is substantially smaller than the value $x = 4.1$ estimated in earlier work from this laboratory.[31] The reason for this discrepancy is not clear although it may be at least partially due to inadequate mixing of the Xe, N_2, and He gases used in the sample cells of Ref. 31. Those cells were prepared without the stopcock C of Fig. 2 and therefore much longer times were required to ensure complete interdiffusion of the gases. In the analysis of the data of Ref. 31 a crucial assumption was that each absorbed σ_+ photon deposited $\hbar/2$ units of angular momentum in the vapor. The spin-transfer efficiency from photons to alkali-metal atoms needs more study. Finally, the NMR data of Ref. 29 were calibrated by comparison to a rather noisy signal from distilled water. We believe that the value of $x = 3.1$ obtained for RbXe in this experiment is more reliable than the earlier value $x = 4.1$ because the same value was measured for both ^{87}Rb and ^{85}Rb and because the ratio data of Sec. VI are in good agreement with the theory. The repolarization ratio is very sensitive to the value of x. The data for ^{133}Cs were less extensively checked.

From a practical point of view the data of Table I indicate that K vapor might be a more useful spin-exchange medium for noble gases than Rb or Cs vapor. This is because the 769.9-nm D_1 absorption line of K atoms is near the peak of the gain curves for oxazine or LD700 dyes. Dye-laser operation is less efficient at the 794.7- and 894.4-nm D_1 lines of Rb and Cs. The larger value of x for potassium compared to cesium or rubidium is a disadvantage since of the alkali-metal-atom spin angular momentum lost during a collison, a fraction, $3/4x^2$, goes into the nuclear spin K of the noble gas; the remainder is lost to the rotational angular momentum N. However, for laser pumping at high cell temperatures the alkali-metal-atom spins are destroyed mainly by alkali-metal-atom–alkali-metal-atom collisions[21] rather than by spin-rotation interactions in alkali-metal–noble-gas van der Waals molecules. The important physical quantity is therefore not the value of x but the relative size of the alkali-metal-atom–noble-gas spin-exchange rate and the alkali-metal-atom–alkali-metal-atom spin-destruction rate, a rate which has been measured[21] only for Cs. Because of the smaller value of the nuclear charge of K atoms compared to Cs atoms, the alkali-metal-atom–alkali-metal-atom spin-destruction rates, which can be traced back to spin-orbit interactions, may be much smaller for K atoms than for Cs atoms or Rb atoms.

ACKNOWLEDGMENTS

This work was supported by the U. S. Air Force Office of Scientific Research under Grant No. AFOSR-81-0104-C.

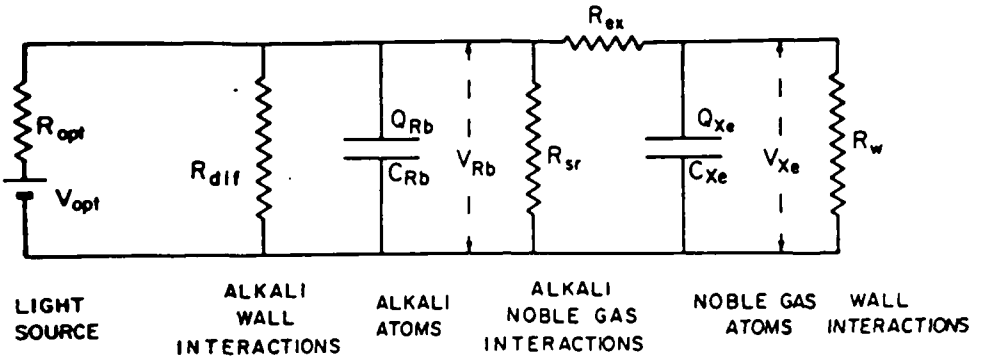

FIG. 17. *RC* network model for alkali-metal–noble-gas spin exchange. Angular momentum is analogous to electrical charge, and the alkali-metal and noble-gas atoms in which the angular momentum is stored are represented by capacitors. The optical-pumping light is equivalent to a battery whose emf is the mean spin of the pumping photons.

$$\frac{1}{T_0}=\frac{\Omega[M]}{T_F}=\frac{\Omega[\mathrm{Xe}]}{T_K}\ . \tag{70}$$

The capacitors C_M and C_{Xe} are coupled by the exchange resistor R_{ex} defined by

$$\frac{1}{R_{ex}}=\frac{f}{T_0}\left[\frac{\alpha\tau}{(2I+1)}\right]^2\langle F^2-F_z^2\rangle\langle K^2-K_z^2\rangle\ . \tag{71}$$

The xenon capacitor is shunted to ground through the wall resistor R_w, which is defined in terms of the empirically determined wall-relaxation time T_w by

$$\frac{1}{R_w}=\frac{C_{Xe}}{T_w}\ . \tag{72}$$

The alkali-metal capacitor is shunted to ground by an analogous diffusion resistor defined by

$$\frac{1}{R_{dif}}=C_{Xe}\gamma_D\ , \tag{73}$$

where the slowest diffusion rate γ_D was defined in (24). The voltages on the capacitors are

$$V_{Rb}=\frac{Q_M}{C_M}=\frac{\langle F_z\rangle}{\langle F^2-F_z^2\rangle} \tag{74}$$

and

$$V_{Xe}=\frac{Q_{Xe}}{C_{Xe}}=\frac{\langle K_z\rangle}{\langle K^2-K_z^2\rangle}\ . \tag{75}$$

Under the conditions of spin temperature equilibrium, described more fully in Ref. 6, the magnitudes of the voltages in (74) and (75) never exceed unity, the value corresponding to 100% positive or negative polarization.

From inspection of (48), (49), and the equations which follow from (11), it can be seen that most of our experiments are designed to detect $\langle F_z\rangle$ or in view of Eq. (63), the charge Q_M on the alkali-metal capacitor. We detect the charge Q_{Xe}, or equivalently the nuclear-spin polarization of the xenon atoms, indirectly through the charge induced on the alkali-metal capacitor by the voltage V_{Xe}.

The measurement of the slowest spin-relaxation transient of the alkali-metal atoms, which was described in Sec. III, can be thought of as an experiment to determine the *RC* time constant of the alkali-metal capacitor. This time constant is dominated by the leakage of charge off of C_M through the relatively small spin-rotation resistor R_{sr} to ground. Some shortening of the time constant is caused by discharge through the internal resistance R_{opt} of the battery, and this parasitic leakage is eliminated by the extrapolation to zero light intensity illustrated in Fig. 7. The leakage through the diffusion resistor R_{dif} is small at high nitrogen pressures and is accounted for in Eq. (28). The leakage through R_{ex} to ground is accounted for by the term proportional to x^{-2} in Eq. (26).

The measurement of the ^{129}Xe spin-relaxation transient described in Sec. IV can be thought of as an experiment to determine the *RC* time constant of the xenon capacitor C_{Xe}. The charge on C_{Xe} leaks to ground through the wall resistor R_w and through the series combination of the relatively large exchange resistor R_{ex} and the much smaller ($\lesssim 5\%$ R_{ex}) parallel combination of R_{sr}, R_{dif}, and R_{opt}. In analyzing the data of Secs. IV and V we have made the simplifying assumption that because of the low alkali-metal spin polarization during the ^{129}Xe relaxation transient the left side of R_{ex} in Fig. 17 is essentially at ground potential.

The ^{129}Xe nuclear spins relax about 10^5 times more slowly than the alkali-metal-atom spins according to Figs. 8 and 12. This is because the xenon capacitor C_{Xe} is about 10^4 times larger than the alkali-metal capacitor C_M due to the much larger ($\sim 3\times 10^4$) number of xenon atoms than alkali-metal atoms, and also because the leakage resistor for C_{Xe}, R_{ex} is about a factor of 10 larger than R_{sr}, the leakage resistor for C_M. However, C_M is increased relative to C_{Xe} because of the large contribution of the nuclear spin I of the alkali-metal atom to the paramagnetic constant of C_M. This can be clearly seen from Fig. 8, where the measured time constant for ^{85}Rb ($I=\frac{5}{2}$) relaxation is about a factor of 2 longer than the time constant for ^{87}Rb ($I=\frac{3}{2}$) relaxation.

The repolarization ratio measurements described in Sec. VI can be thought of as experiments to determine the magnitude of the "voltage divider" which consists of the resistors R_{ex} and R_{sr} connected in series between C_{Xe} and ground. The high-pressure asymptote $r\simeq 0.05$ shown in Fig. 16 is the voltage-divider ratio $R_{sr}/(R_{sr}+R_{ex})$. The

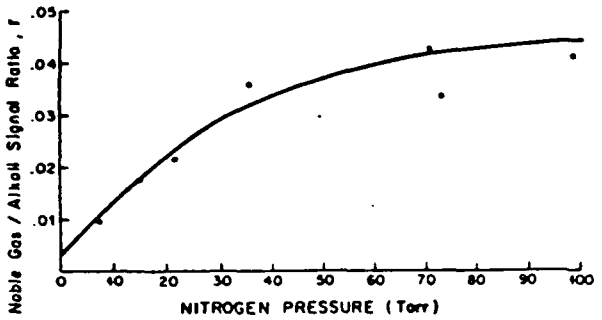

FIG. 16. Dependence of the measured ratio of the repolarization signal to the pump-phase signal on the third-body (N_2) pressure in the sample cells. The ratio was corrected for the attenuation of the polarizers in Fig. 13 and for the wall relaxation of the ^{129}Xe according to Eq. (60). The signal ratio is severely depressed at low nitrogen pressures. It is therefore difficult to observe repolarization signals at low nitrogen pressures. The solid curve is drawn according to Eq. (60) with a distribution of the rotational angular momentum N taken into account. There are no free parameters for the solid curve.

and (6)] were determined from the independent data of Secs. III–V. We should also mention that the number density of ^{129}Xe need not be known precisely for the ratio measurements since additional xenon decreases the pump and repolarization signals by the same factor. The ratio measurement is also not affected by any miscalibration of the Rb vapor-pressure curves versus temperature as long as the same curves are used to deduce the correction factor (59) for ^{129}Xe wall relaxation from data like those of Fig. 11.

We have not made quantitative measurements of the repolarization ratios for ^{85}Rb or ^{133}Cs because we do not feel that the ratio measurements are as effective a way to measure the parameters x and p_0 as the methods based on analyzing the spin-decay transients of the alkali-metal atoms and the xenon nuclei, which were discussed in Secs. III–V. One problem with the ratio measurements is the contribution of observables other than $\langle F_z \rangle$ to the attenuation of the light. The influence of these observables is nearly eliminated when we measure the slowest spin-relaxation transient of alkali-metal atoms as described in Sec. III. However, $\langle \vec{I} \cdot \vec{S} \rangle$, the quadrupole observables, and the more rapidly relaxing dipole observable all contribute somewhat to the optical pumping signal and repolarization signal described in this section. This is an especially annoying problem with ^{133}Cs, where quadrupole polarization is easily generated and observed because of the relatively large excited-state hyperfine structure of the ^{133}Cs atom. The large contribution of quadrupole observables to the optical pumping signals of ^{133}Cs was first pointed out by Bouchiat *et al.*[14] We can therefore expect to find somewhat poorer quantitative agreement between theoretically calculated and experimentally measured values of the repolarization ratio for ^{133}Cs than for the ^{87}Rb data shown in Fig. 16. The ratio measurements should be very reliable for ^{39}K, with its small hyperfine-structure intervals, and experimental measurements of the ratio for ^{39}K, similar to those described above for ^{87}Rb, are well fit by the parameters of Table I.

VII. *RC* NETWORK MODEL

The motivation for many of the experiments described in the earlier sections of this paper can be understood with the aid of the *RC* network model illustrated in Fig. 17. As was shown in Ref. 6, the spin-polarized alkali-metal atoms and noble-gas atoms can be thought of as two capacitors with values,

$$C_M = \Omega[M]\langle F^2 - F_z^2 \rangle \tag{61}$$

and

$$C_{Xe} = f\Omega[Xe]\langle K^2 - K_z^2 \rangle , \tag{62}$$

on which the angular momentum charges

$$Q_M = \Omega[M]\langle F_z \rangle \tag{63}$$

and

$$Q_{Xe} = f\Omega[Xe]\langle K_z \rangle \tag{64}$$

are stored. Here Ω is the volume of the cell, so $\Omega[M]$ and $\Omega[Xe]$ are the total number of alkali-metal and xenon atoms in the sample cell. The quantities

$$2\langle F^2 - F_z^2 \rangle = 1 + \tfrac{4}{3}I(I+1) + \cdots \tag{65}$$

and

$$2\langle K^2 - K_z^2 \rangle = \tfrac{4}{3}K(K+1) + \cdots \tag{66}$$

which occur in (61) and (62) play much the same role as dielectric constants for ordinary electrical capacitors. They account for the fact that atoms with high-spin quantum numbers can store more angular momentum than atoms with low spin quantum numbers. Corrections to the "paramagnetic constants" at high spin polarization are denoted by centered ellipses in (65) and (66) and are discussed in detail in Ref. 6.

The optical pumping lamp or laser is represented by a battery attached to the alkali-metal capacitor. The emf of the battery is

$$V_{opt} = s_z , \tag{67}$$

where s_z is the mean spin of the pumping photons ($s_z = \pm 1$ for $\sigma_\pm$ light). The internal resistance R_{opt} of the battery is defined by

$$\frac{1}{R_{opt}} = \frac{\Omega[M]R}{2} , \tag{68}$$

where R is the mean optical-pumping rate of the light source. That is, (68) implies that the optical admittance is one-half of the number of photons absorbed per second by the alkali-metal atoms in the cell. More details about the physical assumptions leading to (67) and (68) can be found in Ref. 6.

The capacitor C_M is shunted to ground by the spin-rotation resistor R_{sr} defined by

$$\frac{1}{R_{sr}} = \frac{1}{T_0}\frac{2}{3}\left[\frac{\gamma N \tau}{(2I+1)}\right]^2 \langle F^2 - F_z^2 \rangle , \tag{69}$$

where the global molecular-formation rate in the sample cell is given by

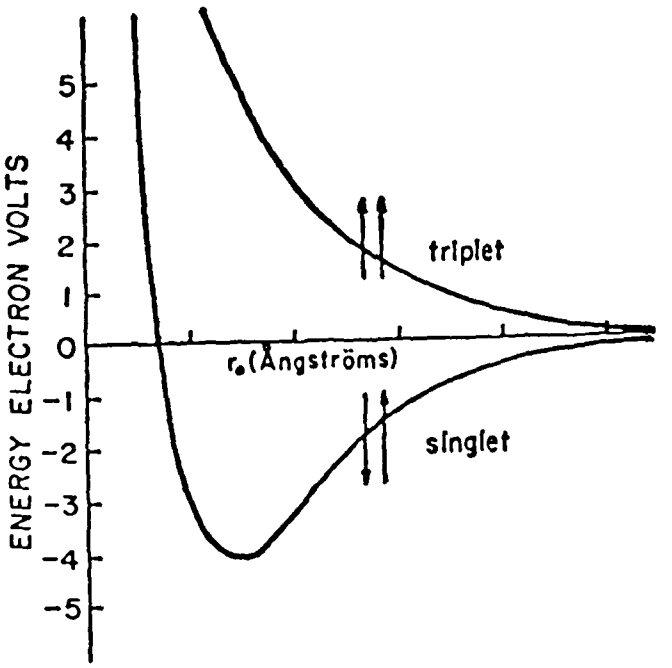

Fig. 1. Electron-electron spin exchange occurs at a rate proportional to the difference between the singlet and triplet potential curves of the interacting pair. The exchange is basically of an electrostatic nature. From T.R. Carver, Science 141, 598 (1963).

A very important property of spin exchange collisions which was first emphasized by Dehmelt[5] is the fact that spin exchange collisions cause no change in the total electronic spin $\vec{S}_1+\vec{S}_2$ of the colliding atoms. In fact one can easily verify that

$$[\vec{S}_1+\vec{S}_2,\ V] = 0 \qquad (2)$$

i.e. the commutator of the total spin with the interaction potential (1) is zero so $\vec{S}_1+\vec{S}_2$ is a constant of the motion. Later on we shall discuss much smaller terms in the interaction potential which were omitted from (1) but which do cause a transfer of spin angular momentum into the translational degrees of freedom of the gas.

It is hard to improve Dehmelt's own description of the first experiment on spin exchange spectroscopy[5] "The electrons were polarized by allowing them to undergo exchange collisions with oriented sodium atoms in which the total spin component with respect to the axis of orientation, a magnetic field H_0, is conserved and the orientation of the atoms is transferred to the initally unpolarized electrons by exchange of spin directions."

Spin exchange with optically pumped alkali vapors was soon used to polarize a number of interesting species, among them nitrogen[6] and phosphorous[7] atoms which have slowly relaxing $^4S_{3/2}$ ground states but which have optical absorption lines which are too far in the ultraviolet region of the spectrum to permit convenient optical pumping. The hyperfine structure of these atoms is quite interesting since both the magnetic and electric hyperfine interactions should be zero in lowest order because of the symmetry of the electronic state. Nevertheless, there is a substantial magnetic hyperfine interaction which arises from the polarization of the closed-shell cores

of these atoms. A representative magnetic resonance curve for spin exchange spectroscopy is shown in Fig. 2.

Grossetete[8] and her colleagues in Paris carried out careful measurements of the spin exchange rate constants for various alkali vapors, and they showed that the spin exchange rate R for an alkali atomic vapor of number density [A] was always on the order of

$$R \approx 10^{-9} \text{ cm}^3 \text{ sec}^{-1} [A] \tag{3}$$

Grossetete[9] also carried out a careful theoretical analysis of the effects of spin exchange on the spin relaxation of alkali vapors. Similar work was done at about the same time by Gibbs[10]. The analysis of spin exchange collisions is complicated because spin exchange is described by non-linear rate equations. The nonlinearity is essential if one is to account for the spin polarization of both atoms which are involved in the collision.

One of the most interesting theoretical aspects of spin exchange collisions was pointed out by Anderson, Pipkin and Baird.[11] They showed that spin exchange collisions lead to a spin temperature equilibrium such that the occupation probability of an atomic sublevel of azimuthal quantum number m is

$$\rho(m) = \frac{1}{Z} e^{\beta m} \tag{3}$$

where β is the spin temperature parameter and the sum on states is

$$Z = \sum_m e^{\beta m} \tag{4}$$

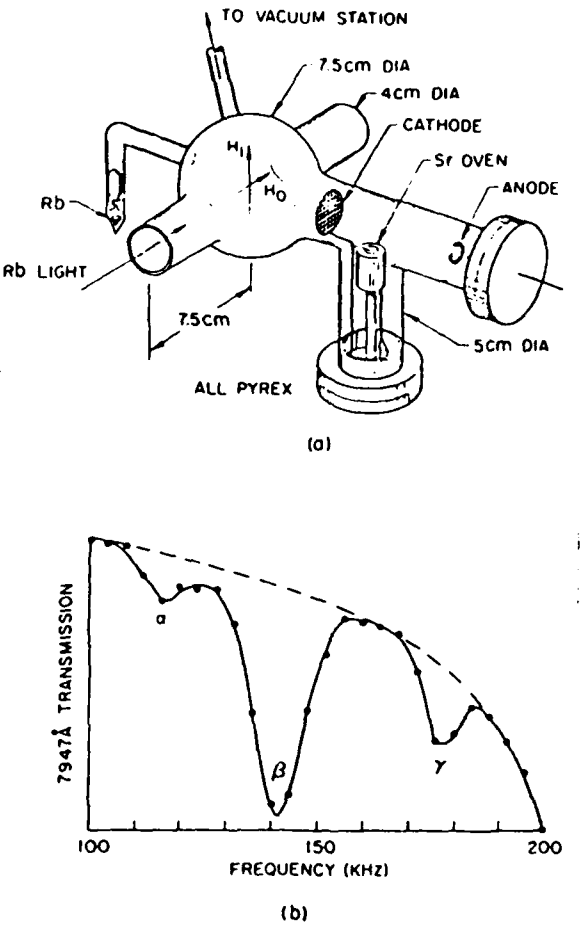

Fig. 2. A typical experiment with spin exchange spectroscopy. Strontium ions are polarized by spin exchange with optically pumped rubidium. Changes in the Sr^+ polarization produce corresponding changes in the Rb polarization which is detected by optical pumping methods. From H.M. Gibbs and G.C. Churchill, Phys. Rev. 3, 1617 (1971).

In contrast to a situation with arbitrary spin polarization where many parameters are needed to describe the population distribution, only one parameter β is required to characterize a sample of atoms in spin temperature equilibrium. Anderson and Ramsey[12] showed experimentally that the spin distribution (3) prevails in sufficiently dense alkali vapors. The spin distribution (3) is the state of maximum entropy for a fixed amount of internal spin angular momentum. As was pointed out by Tang et.al.[13], it is sometimes convenient to think of the distribution (3) as the diagonal element of the density operator

$$\rho = \frac{1}{Z} e^{\vec{\beta}\cdot\vec{F}} \tag{5}$$

where the vector spin temperature parameter $\vec{\beta}$ specifies both the magnitude of the spin temperature and the axis of quantization. The distribution (5) is especially useful in understanding magnetic resonance experiments.

It is natural to ask how well spin is really conserved in the collisions between atoms. If either atom has non-zero orbital angular momentum in its ground state, large amounts of spin angular momentum will be lost to translational angular momentum at each collision. Thus, the remarkable properties of spin exchange collisions are most dramatic for collisons between S-state atoms. If the interaction (1) were a complete and rigorous description of the interatomic potential there really would be no loss of spin angular momentum in spin exchange collisions. However, it is well known that there are additional small spin-dependent interactions which couple spin angular momentum into the translational angular momentum of the gas. For example, $^3\Sigma$ states are known to have a spin interaction of the form[14]

$$V = \frac{2}{3} \lambda \left[3S_\zeta S_\zeta - S(S+1)\right] \qquad (6)$$

This interaction is well studied for the O_2 molecule and it is due to a combination of the magnetic spin-spin interaction and the spin-orbit interaction. Bhaskar et. al.[15] have attributed the observed spin relaxation of Cs vapor at high spin exchange rates to the interaction (6). There appears to be very little information about the spin loss mechanism for collisions between alkali atoms other than Cs, but R. Knize reports that the spin loss rates for the lighter alkali atoms appear to be substantially slower than the rates for Cs, based on his very recent measurements at Princeton University.

The question of how much spin is lost in a spin exchange collision is important both in principle and in practice. For example, Kulsrud et al.[16] have suggested that the 50% enhancement of the thermonuclear fusion rate of spin polarized deuterium and tritium nuclei with respect to randomly polarized d and T nuclei would make it worthwhile to load tokomaks with spin polarized fuel. One way to produce polarized nuclei of d and T is to polarize these isotopes of hydrogen by spin exchange with alkali atoms as suggested by Cecchi, Knize and Happer[17]. If even a small amount of spin is lost during spin exchange collisions it would have an important influence on the design of a source of nuclear fuel which is to be polarized by spin exchange collisions.

In recent years the phenomenon of spin exchange between electrons and nuclei has attracted increasing attention. The first experiments on spin exchange between optically pumped alkali atoms and noble gas nuclei were carried out by Bouchiat Caraver and Varnum[18] in 1962 at Princeton. They

showed that it was possible to transfer some of the angular momentum of optically pumped Rb atoms to the nuclei of a ^{3}He buffer gas. The observed exchange rates were very slow, typically many hours, and this method of polarizing ^{3}He was soon abandoned in favor of the much more efficient process of metastability exchange with optically pumped $^3S_1$ metastable helium atoms, a method invented by Colegrove, Schearer and Walters[19]. The electron-nuclear spin exchange method was not forgotten, however, and in 1978 Grover[20] at Litton Industries showed that surprisingly efficient spin transfer could take place between Rb atoms and ^{129}Xe nuclei. The high efficiency of the spin transfer process turned out to be due to the formation of alkali-noble-gas van der Waals molecules in a process similar to that sketched in Fig. 3. The importance of alkali-noble gas van der Waals molecules for spin relaxation of optically pumped alkali atoms was first recognized by Bouchiat et al.[21] at Ecole Normale Supérieure. A sketch of the van der Waals potential curve for a RbKr molecule is shown in Fig. 4. Molecules are important because they permit the spin interactions to act coherently for a collisionally limited molecular lifetime, typically some tens of nanoseconds, instead of a few picoseconds which is the characteristic interaction time for a binary collision.

The spin interaction Hamiltonian for an alkali-noble gas pair is

$$H = A\,\vec{I}\cdot\vec{S} + \gamma\,\vec{N}\cdot\vec{S} + \alpha\,\vec{K}\cdot\vec{S} + \ldots \qquad (7)$$

we expect to find a large coupling constant A between the nuclear spin $\vec{I}$ and the electron spin $\vec{S}$ of the alkali atom. The coefficient A should be about the same as that of a free alkali atom. The next largest interaction is $\gamma\,\vec{N}\cdot\vec{S}$ between $\vec{S}$ and the rotational angular momentum $\vec{N}$ of the alkali-noble gas

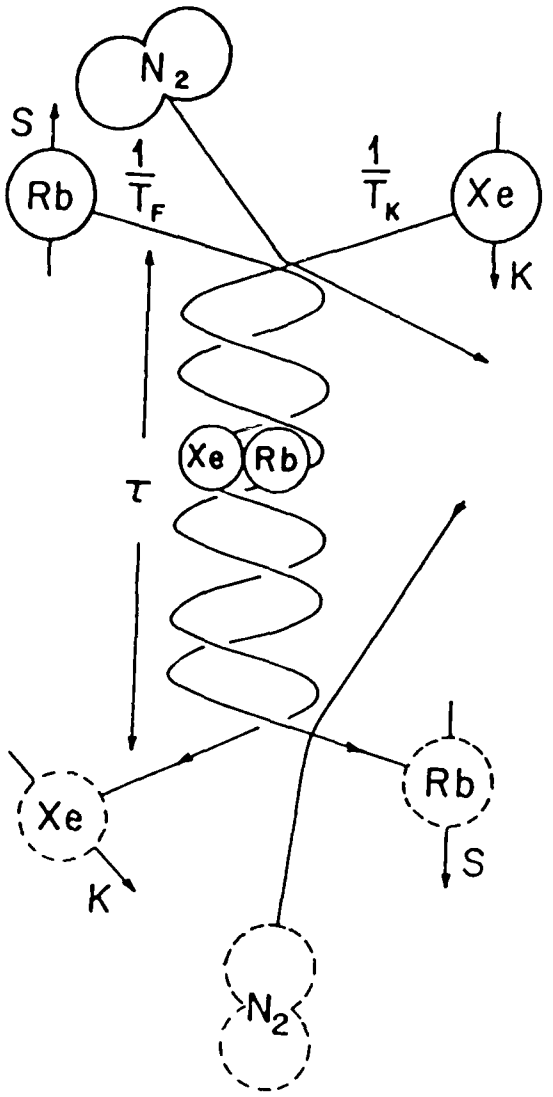

Fig. 3. Alkali-noble-gas van der Waals molecules are formed in three body collisions at a rate T_F^{-1} per alkali atom and T_K^{-1} per noble gas atom. They are broken up at a rate τ^{-1} by collisions with other atoms or molecules. Electron-nuclear spin exchange is greatly enhanced by the long-lived moleucles.

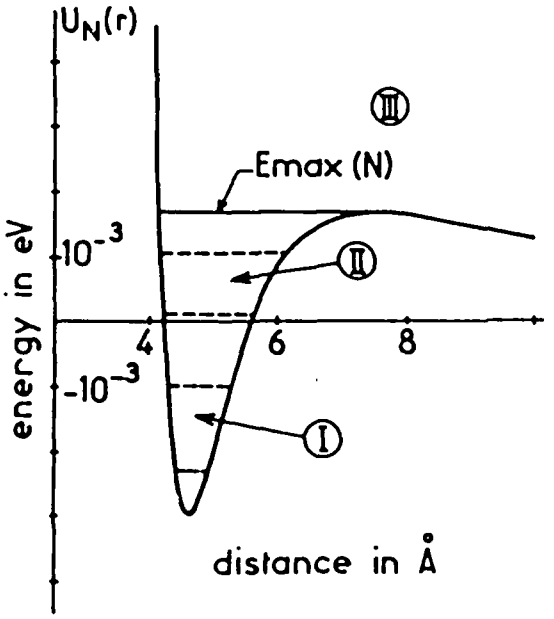

Fig. 4. Interaction potential for an alkali atom and a noble gas atom (RbKr) with a relative angualr momentum N. The pair can be absolutely bound as in region I, quasibound as in region II or free as in region III. From C.C. Bouchiat, M.A. Bouchiat and L.C.L. Pottier, Phys. Rev. 181, 144 (1969).

pair. The importance of this interaction for electron spin relaxation of optically pumped alkali atoms was first pointed out by Bernheim[22]. Systematic experimental studies by Bouchiat, Pottier and Brossel[23] showed that the spin rotation coupling constant γ ranges from about 0.1 MHz for RbAr to about 1.6 MHz for RbXe. Recent experiments by Wu have shown that γ is about the same for the series of van der Waals molecules KXe, RbXe and CsXe. Thus, experiments show clearly that the spin rotation interaction is controlled by the spin orbit interaction in the noble gas, and this conclusion is supported by recent theoretical calculations by Wu, Walker and Happer[24]. Electron-nuclear spin exchange is caused by the Fermi contact interaction $\alpha \vec{K}\cdot\vec{S}$ between $\vec{S}$ and the nuclear spin $\vec{K}$ of the noble gas. Experiments by Zeng et al.[25] have shown that for the series of molecules $K^{129}Xe$, $Rb^{129}Xe$ and $Cs^{129}Xe$

$$x = \frac{\gamma N}{\alpha} \simeq 3 \tag{8}$$

Since the rotational angular momentum $\vec{N}$ is very large for typical van der Waals molecules, say $N \gtrsim 50$, the rotational angular momentum can be thought of as a fixed classical vector and the Hamiltonian (7) is therefore equivalent to a Breit-Rabi Hamiltonian with the Breit-Rabi parameter (8) substantially greater than unity.

The Hamiltonian (7) differs in an unwelcome way from the electron spin exchange Hamiltonian (1) since the total internal spin $\vec{S}+\vec{I}+\vec{K}$ does not commute with the Hamiltonian (7) and in fact

$$[\vec{S}+\vec{I}+\vec{K},H] = i\gamma \vec{N}\times\vec{S} \tag{9}$$

Physically (9) implies that spin angular momentum $\vec{S}$ is lost to $\vec{N}$, and $\vec{N}$ is dissipated to translational motion in the gas after the van der Waals molecules break up. In contrast to electron-electron spin exchange collisions where more than 99% of the spin angular momentum is transferred from one atom to another, only about 8% of the electron spin angular momentum can be transferred from alkali atoms to the nuclei of ^{129}Xe, the most efficient receptor of angular moment known so far. However, in spite of the substantial loss of spin angular momentum to $\vec{N}$ for electron nuclear spin exchange, very large amounts of nuclear spin angular momentum can be accumulated because of the high efficiency of Kastler's optical pumping method[1], which deposits about one unit of spin angular momentum in the alkali vapor for each absorbed photon, and because of the long nuclear spin relaxation times which are characteristic of noble gases. The original experiments of Bouchiat et al.[18] in 1960 already showed that nuclear spin relaxation times of several hours could be observed and later experiments by Schearer and Walters[26] at Rice University and by Carver and Gamblin[27] at Princeton University showed that ^3He nuclear spin relaxation times as long as one day were feasible. Thus one can pump angular momentum into a ^3He sample for as long as one day before the spin polarization saturates. The long relaxation time was exploited by Daniels et al.[28] to make an optically pumped target of nuclear spin polarized ^3He.

As an illustration of current work on spin exchange I would like to describe experiments in our laboratory[25] to learn about the physics of molecule-assisted spin exchange in noble-gas-alkali-atom mixtures. The physics can be naturally divided into two categories: studies of the formation and breakup rates of van der Waals molecules, and studies of the spin interaction in the van der Waals molecules. The relatively simple

apparatus used to study these questions is shown in Fig. 5. Glass cells containing a few torr to as much as an atmosphere of Xe gas, about 50 torr of N_2, and a small amount of alkali metal are pumped for 10 to 15 minutes with light from an alkali resonance lamp or from a dye laser. During this pumping phase of the experiment angular momentum flows from the photons to the alkali atoms and finally to the noble gas nuclei. Once an equilibrium polrization of the noble gas nuclei is achieved, the pumping light is removed and the sample cell is probed with unpolarized light from an alkali resonance lamp. The flow of angular momentum is reversed in this probe phase and the probing photons become slightly circularly polarized. This small circular polarization can be measured with great sensitivity with a photoelastic modulator. Some representatiave nulear spin relaxation curves of ^{129}Xe in various alkali vapors are shown in Fig. 6. The decay is so slow that we find it useful to periodically invert the spin polarization with a chirped audio frequency pulse to eliminate the effects of slow drifts in the gains of the electronics or in the stray polarization of the optical system.

To understand the significance of transient decays like those of Fig. 6 and to extract the maximum amount of physics from them we find it useful to model the spin exchange process with the RC network[29] shown in Fig. 7. The extensive, conserved quantity, angular momentum, is equivalent to the electrical charge stored in the network. The spin angular momentum is stored in two different atomic species, in the electronic and nuclear spins of the dilute alkali vapor and in the nuclear spins of the much more dense noble gas. These two types of atoms are represented by two capacitors whose magnitudes are proportional to the numbers of the respective atoms. The various terms in the Hamiltonian which allow angular momentum to be transferred from one spin to another are represented by resistors, whose values are determined

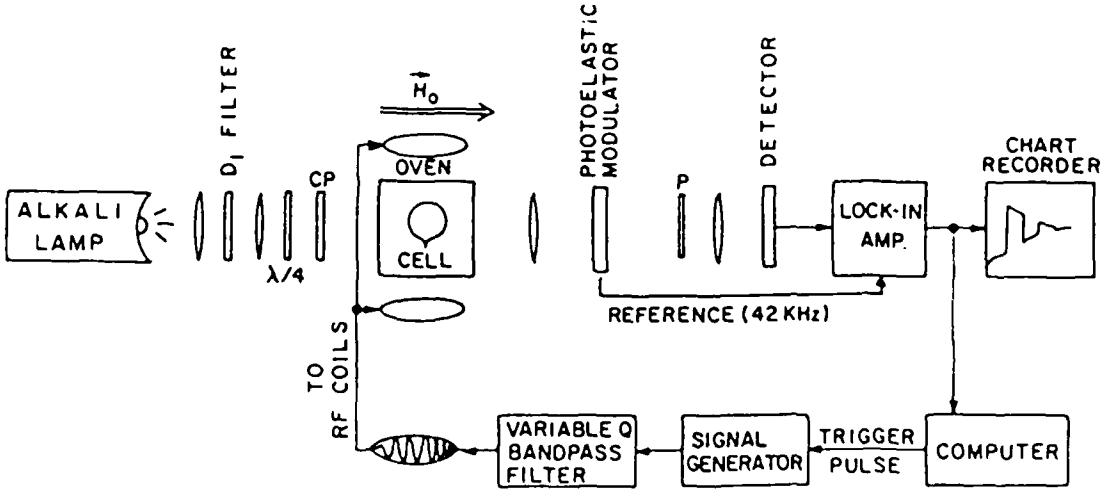

Fig. 5. Representative apparatus to study spin exchange between optically pumped alkali atoms and noble gas nuclei.

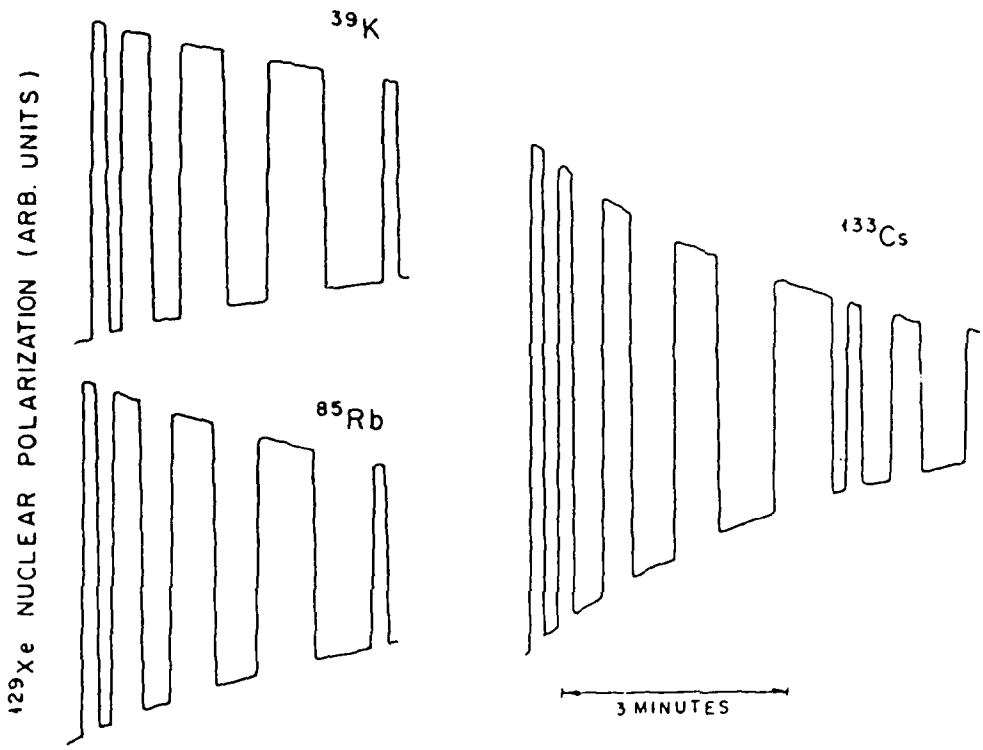

Fig. 6. Representative ^{129}Xe nuclear spin relaxation transients in various alkali vapors as observed with the apparatus of Fig. 5.

Table I. Spin-Rotation Coupling Factors G

Noble Gas	G/h (10^{-31} MHz cm^5)
Ne	0.062
Ar	0.49
Kr	3.0
Xe	9.8
Rn	31

To directly test the dependence of γ on the fine structure of the alkali atom we determined[6] the spin rotation coupling constants from measured magnetic slowing down curves for the ^{129}Xe nuclear spin relaxation in the series of van der Waals molecules KXe, RbXe and CsXe. The experimental method was similar to that described by Bhaskar et al.[7] and we refer to that paper for more experimental detail. The basic experimental measurement is the width ΔH_0 of the magnetic slowing-down curve at low buffer gas pressure. The widths for KXe, RbXe and CsXe along with the mean coupling constants γ inferred from these widths are shown in Table II. Since Herman's formula for γ is proportional to the D-line splitting $\Delta\nu_{fs}$ of the alkali atom, a substantial increase of γ would be expected for the series K, Rb, Cs, which have the splittings 58 cm^{-1}, 237 cm^{-1} and 554 cm^{-1}. No such increase is evident from the experimental data. We have also listed in Table II characteristic fields H_1^* for the magnetic slowing-down curves of the electronic spin relaxation and the inferred values of γ for the series RbAr, RbKr, RbXe measured by Bouchiat[8] et al. Although the D line splitting of the alkali atom is the same for this series there is a very substantial variation of γ. Thus, it is clear from the experimental data that the spin rotation constant γ depends on

derived.

$$\gamma(R) = \frac{mG}{MR} \frac{d}{dR} |\phi_1(R)|^2 \qquad (1)$$

Here m and M are the electron mass and the reduced mass of the alkali atom noble gas pair, respectively, R is the internuclear separation, $\phi_1(R)$ is the unperturbed valence electron wave function of the alkali atom at a distance R from the alkali nucleus, and the factor

$$G = \frac{1}{2} \left(\frac{\hbar}{mc}\right)^2 \int_0^\infty \left(\sum_n C_{np} R_{np}(r)\right)^2 \frac{1}{r} \frac{dV}{dr} dr \qquad (2)$$

depends only on the spin-orbit interaction of the noble gas. The effective central potential in which the noble gas electrons move is denoted by V, r is the distance from the noble gas nucleus, $\psi_{np0}(r\theta\phi) = \frac{R_{np}(r)}{r} Y_{10}(\theta,\phi)$ is the wave function of a noble gas p electron of principle quantum number n, and the sum on n in (2) extends over all filled shells of the noble gas. The coefficient C_{np} is the overlap integral

$$C_{np} = \int_0^\infty z\, \psi_{np0}(\vec{r})\, d^3r \qquad (3)$$

In all numerical evaluations of G, $\phi_1(R)$ and ψ_{np0} used in this paper we have used the Hartree-Fock-Slater wave functions tabulated by Herman and Skillman.[5] The values of G calculated for Ne, Ar, Kr, Xe and Rn are given in Table 1.

Recently it has become clear that large amounts of angular momentum can be transferred from optically pumped alkali atoms to the nuclei of the heavier noble gases by spin exchange interactions.[1,2] Only a few of the thirty or so possible pairs of different alkali atoms with different noble gas atoms have been investigated experimentally, and it would be very useful to be able to predict the spin interactions well enough to tell which pairs are particularly promising for applications to nuclear spin polarization. The most important spin interactions in these molecules are the Fermi contact hyperfine interaction $\alpha\vec{I}\cdot\vec{S}$ between the nuclear spin $\vec{I}$ of the noble gas and the electron spin $\vec{S}$ of the alkali atom and the spin rotation interaction $\gamma\vec{N}\cdot\vec{S}$ between $\vec{S}$ and the rotational angular momentum $\vec{N}$ of the noble gas and alkali atom about each other. Here we present a simple new formula which accounts very well for the systematic variation of the spin-rotation interaction for different alkali atoms or noble gas atoms, and which predicts for the first time how γ varies with internuclear separation.

As Bernheim[3] first pointed out, the spin rotation interaction is responsible for most of the spin relaxation of alkali atoms in noble gases. So far there has been no reliable way to calculate the coupling coefficient γ. The most serious attempt has been made by Herman,[4] who concluded that γ was short range and was mainly due to the alkali ionic field. Herman[4] derived expressions for γ which were proportional to the fine structure splitting of the alkali atom and not directly dependent on the fine structure of the noble gas atom.

As we shall discuss in detail below, Herman's[4] formulas are in qualitative and quantitative disagreement with the most reliable experimental determinations of γ. If certain terms which Herman neglected in his analysis are retained, we shall show that the following new expression for γ can be

The Spin Rotation Interaction of Noble Gas Alkali Atom Pairs

Z. Wu, T.G. Walker and W. Happer

Department of Physics

Princeton University

Princeton, NJ 08544

Abstract

Recent experimental data show that the spin rotation coupling for alkali-noble-gas van der Waals molecules is mainly due to the spin-orbit interaction of the alkali valence electron within the core of the noble gas. We present a simple formula which accounts very well for the systematic variation of the spin rotation interaction with different noble gas or alkali atoms.

References Continued:

22. R.A. Bernheim, J. Chem. Phys. 36, 135 (1962).

23. M.A. Bouchiat, J. Brossel and L.C. Pottier, J. Chem. Phys. 56, 3703 (1972).

24. Z. Wu, T. Walker and W. Happer, "The Spin Rotation Interaction of Noble-Gas-Alkali-Atom Pairs" preprint 1985.

25. X. Zeng, Z. Wu, T. Call, E. Miron, D. Schreiber and W. Happer, Phys. Rev. A 31, 260 (1985).

26. L.D. Schearer and G.K. Walters, Phys. Rev. 139, A1398 (1965).

27. R.L. Gamblin and T.R. Carver, Phys. Rev. 138, A946 (1965).

28. R.S. Timsit, J.M. Daniels, E.I. Denning, A.K.C. Kiang and A.D. May, Can. J. Phys. 49, 508 (1971).

29. W. Happer, E. Miron, S. Schaefer, D. Schreiber, W.A. van Wijngaarden and X. Zeng, Phys. Rev. A29 3092 (1984).

30. N.D. Bhaskar, W. Happer, M. Larsson and X. Zeng, Phys. Rev. Letters 50, 105 (1983).

31. F.P. Calaprice, W. Happer, D.F. Schreiber, M.M. Lowry, E. Miron and X. Zeng, Phys. Rev. Letters 54, 174 (1985).

32. E.W. Weber, Physics Reports 32, 123 (1977).

33. T.G. Vold, F.J. Raab, B. Heckel and E.N. Fortson, Phys. Rev. Letters 52, 2229 (1984).

34. V.W. Hughes, H.G. Robinson and V. Bertran-Lopez, Phys. Rev. Letters 4 342 (1960); R.W.P. Drever, Phil. Mag. 6, 683 (1961).

References

1. A. Kastler, J. Phys. Radium 11, 225 (1950).

2. W. Heisenberg, Z. Physik 39, 499 (1927).

3. E.M. Purcell and G.B. Field, Astrophys. J. 124, 542 (1956).

4. J.P. Wittke and R.H. Dicke, Phys. Rev. 103, 620 (1956).

5. H.G. Dehmelt, Phys. Rev. 109, 381 (1958).

6. W.W. Holloway, Jr. and R. Novick, Phys. Rev. Letters 1, 367 (1958).

7. R.H. Lambert and F.M. Pipkin, Phys. Rev. 128, 198 (1962).

8. F. Grossetete, Dissertation, University of Paris, 1967 (unpublished); F. Grossetete and J. Brossel, Compt. Rend. 264, 381 (1967).

9. F. Grossetete, J. Physique 29, 456 (1968).

10. H. Gibbs, Phys. Rev. 139, A1374 (1965).

11. L.W. Anderson, F.M. Pipkin and J.C. Baird, Phys. Rev. 116, 87 (1958).

12. L.W. Anderson and A.T. Ramsey, Phys. Rev. 132, 712 (1963).

13. W. Happer and H. Tang, Phys. Rev. Letters 31, 273 (1973).

14. M. Tinkham and M.W.P. Strandberg, Phys. Rev. 97, 937 (1955); J.M. Daniels and P.B. Dorain, J. Chem. Phys. 45, 26 (1966).

15. N.D. Bhaskar, J. Pietras, J. Camparo, W. Happer and J. Liran, Phys. Rev. Letters 44, 930 (1980).

16. R.M. Kulsrud, H.P. Furth, E.J. Valeo and M. Goldhaber, Phys. Rev. Letters 50, 1248 (1983).

17. W. Happer, E. Miron, R. Knize and J. Cecehi, AIP Conference Proceedings No. 117, "Polarized Proton Ion Sources" p. 114.

18. M.A. Bouchiat, T.R. Carver and C.M. Varnum, Phys. Rev. Letters 5, 374 (1960).

19. G.K. Walters, F.D. Colegrove and L.D. Schearer, Phys. Rev. Letters 8, 439 (1962).

20. B.C. Grover, Phys. Rev. Letters 40, 391 (1978).

21. M. Aymar, M.A. Bouchiat and J. Brossel, Physics Letters 24A, 753 (1967).

Figure Captions

Fig. 1. Electron-electron spin exchange occurs at a rate proportional to the difference between the singlet and triplet potential curves of the interacting pair. The exchange is basically of an electrostatic nature. From T.R. Carver, Science 141, 598 (1963).

Fig. 2. A typical experiment with spin exchange spectroscopy. Strontium ions are polarized by spin exchange with optically pumped rubidium. Changes in the Sr^+ polarization produce corresponding changes in the Rb polarization which is detected by optical pumping methods. From H.M. Gibbs and G.C. Churchill, Phys. Rev. 3, 1617 (1971).

Fig. 3. Alkali-noble-gas van der Waals molecules are formed in three body collisions at a rate T_F^{-1} per alkali atom and T_K^{-1} per noble gas atom. They are broken up at a rate τ^{-1} by collisions with other atoms or molecules. Electron-nuclear spin exchange is greatly enhanced by the long-lived moleucles.

Fig. 4. Interaction potential for an alkali atom and a noble gas atom (RbKr) with a relative angualr momentum N. The pair can be absolutely bound as in region I, quasibound as in region II or free as in region III. From C.C. Bouchiat, M.A. Bouchiat and L.C.L. Pottier, Phys. Rev. 181, 144 (1969).

Fig. 5. Representative apparatus to study spin exchange between optically pumped alkali atoms and noble gas nuclei.

Fig. 6. Representative ^{129}Xe nuclear spin relaxation transients in various alkali vapors as observed with the apparatus of Fig. 5.

Fig. 7. RC network model for spin exchange between optically pumped alkali atoms and noble gas nuclei. Angular momentum is analogous to electrical charge and the alkali atoms and noble gas atoms in which the angular momentum is stored are represented by capacitors. Various spin interactions in the Hamiltonian are represented by resistors and the optical pumping light source is represented by an EMF with an internal resistance.

Fig. 8. Magnetic slowing down of the nuclear spin relaxaiton rate of ^{129}Xe. The strong dependence of the relaxation rate on the external magnetic field is characteristic of relaxation due to van der Waals molecules and can be used to infer the magnitudes of the spin coupling coefficients.

Fig. 9. Experimental apparatus for polarizing radioactive xenon isotopes. From Calaprice et al. Phys. Rev. Letters 54, 174 (1985).

Fig. 10. The nuclear magnetic resonance line shape observed with the apparatus of Fig. 9.

Finally, nuclear spin polarized noble gases, because of their extremely long spin relaxaiton times, are ideally suited for studies of tiny interactions of fundamental importance. An example is the recent search by Fortson[33] and his coworkers at the University of Washingto for a permanent electric dipole moment of ^{129}Xe. Chupp at Princeton is designing an experiment to use ^{21}Ne to search for a small anisotropy of space by a variant of the Hughes-Drever[34] experiment. The key to all such precision experiments is the extremely narrow magnetic resonance linewidths attainable with noble gases which have been polarized by spin exchange optical pumping. Line widths of a few microhertz should be attainable for ^{3}He and ^{21}Ne.

None of the fascinating experiments on spin exchange mentioned above would have been possible without the invention of optical pumping by Alfred Kastler.

This work was supported by the U.S. Air Force Office of Scientific Research under Grant No. AFOSR 81-0104-C.

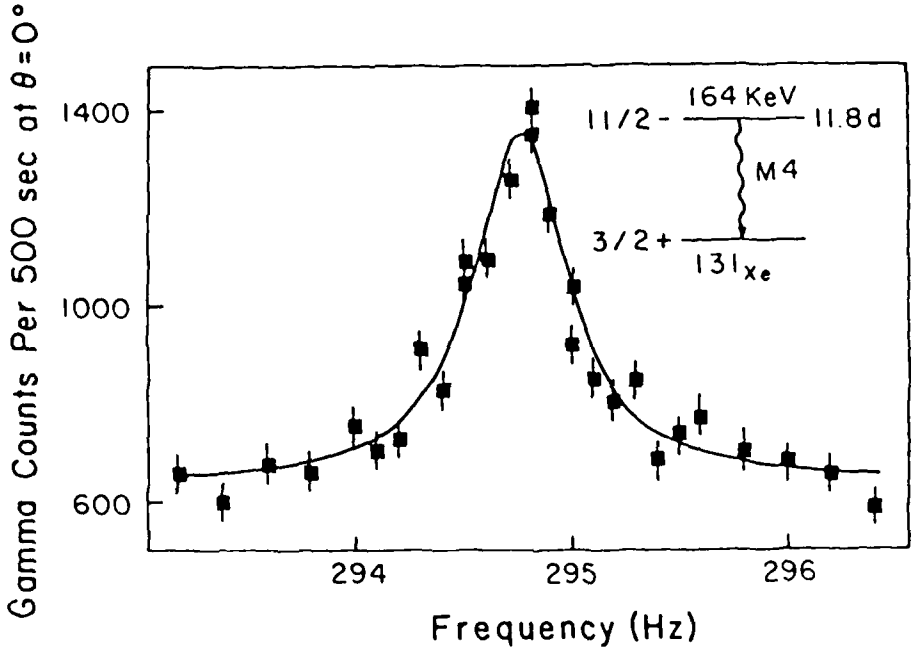

Fig. 10. The nuclear magnetic resonance line shape observed with the apparatus of Fig. 9.

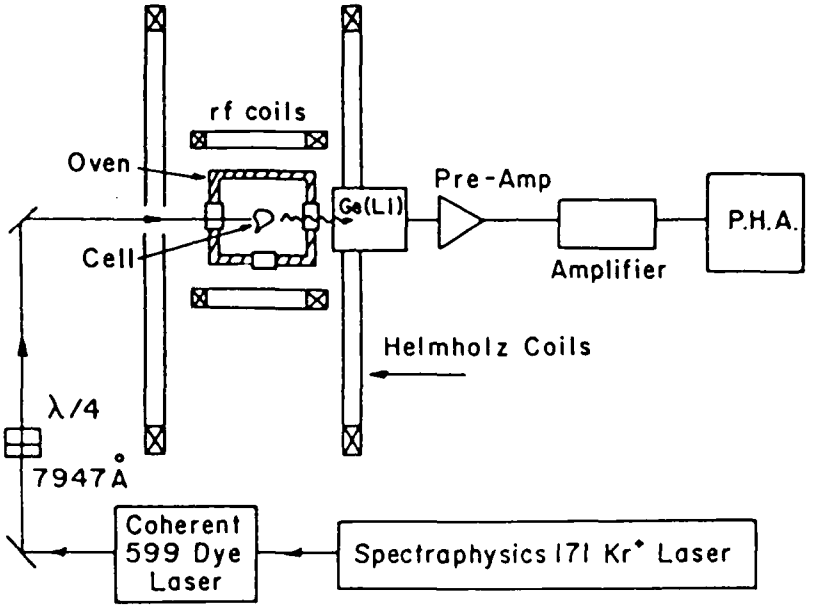

Fig. 9. Experimental apparatus for polarizing radioactive xenon isotopes. From Calaprice et al. Phys. Rev. Letters 54, 174 (1985).

future of the field. Many interesting radioactive noble gases can be polarized by spin exchange with optically pumped alkali vapors and a representative experiment done by Calaprice and his coworkers[31] at Princeton is sketched in Fig. 9. The nuclear moment of the radioactive noble gas atom ^{133m}Xe can be measured with very high precision by observing the change in the γ-ray count rate when a small audiofrequency field is applied at the nuclear magnetic resonance frequency of the atom. The resulting resonance is shown in Fig. 10. The natural width of the resonance, which is determined by the spin relaxation time of several minutes, is on the order of 10^{-3} Hz and the 0.5 Hz width of Fig. 10 is entirely due to magnetic noise in the laboratory.

Electron-nuclear spin exchange could also be used to produce polarized noble gas targets for nuclear scattering experiments. The most interestig targets would be the light noble gases ^{3}He and ^{21}Ne. Neither of these gases is easy to polarize by electron-nuclear spin exchange because neither ^{3}He nor ^{21}Ne forms van der Waals molecules readil, with alkali atoms and in both cases the Fermi contact interaction $\alpha \vec{K}\cdot\vec{S}$ is small. One way to overcome these difficulties would be to use optically pumped alkaline earth ions to polarize the light noble gases. Because of the polarization forces between a positive ion and a neutral atom the formation of molecular ions, e.g.

$$Ba^+ + 2He \rightarrow Ba^+He + He \qquad (11)$$

should proceed with an efficiency comparable to that for the formation of van der Waals molecules like RbXe. Very promising early work on optically pumped alkaline earth ions has been carried out by Weber[32] and his colleagues at Heidelberg.

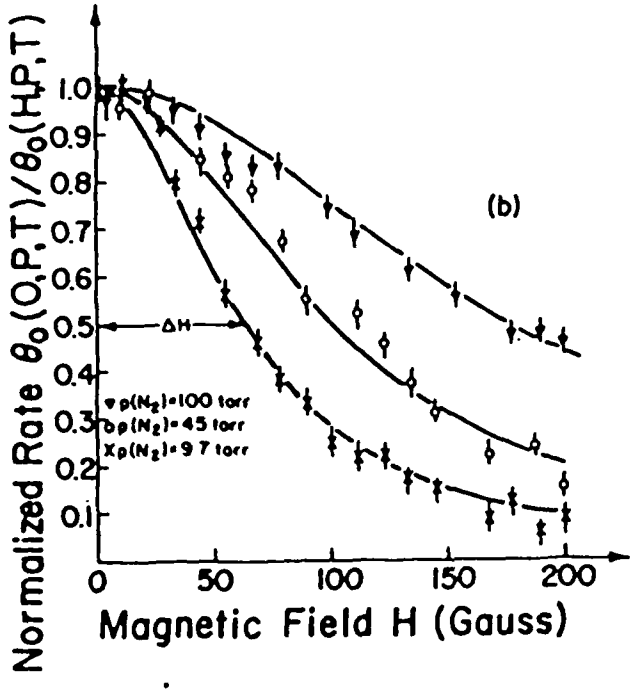

Fig. 8. Magnetic slowing down of the nuclear spin relaxaiton rate of ^{129}Xe. The strong dependence of the relaxation rate on the external magnetic field is characteristic of relaxation due to van der Waals molecules and can be used to infer the magnitudes of the spin coupling coefficients.

from Fermi's Golden Rule. The pumping light is represented by a battery whose EMF is equal to the mean spin of the pumping photons and whose internal resistance is inversely proportional to the intensity of the pumping light. The network model of Fig. 7 is completely quantitative and the various RC time constants of the network, in particular a time constant on the order of a millisecond which is associated with the charging or discharging of the alkali atom capacitor and a time constant of many minutes associated with the charging or discharging of the very large noble gas capacitor give useful information about the system. By comparing fast and slow time constants of the spin system it is possible to infer ratios of the various coupling terms in Eq. (7), in particular the important Breit-Rabi parameter x of Eq. (8).

To deduce the absolute values of the coupling coefficents of Eq. 7 we analyze the effects of a magnetic field on the spin relaxation of the noble gas nuciei[30]. As is shown in Fig. 8 a magnetic field of a few hundred gauss is sufficient to eliminate most of the nuclear spin relaxation of ^{129}Xe. The relaxation slows down to half of its zero-field value at a magnetic field ΔH given by

$$\gamma N = 2n\ \mu_B\ \Delta H_0 \qquad (10)$$

where n is a numerical coefficient on the order of unity which can be calculated for noble gas relaxaiton in terms of the alkali nuclear spin I and the Breit-Rabi parameter x.

Having discussed the history of spin exchange optical pumping and some of the current work in this area, let me make a few predictions about the

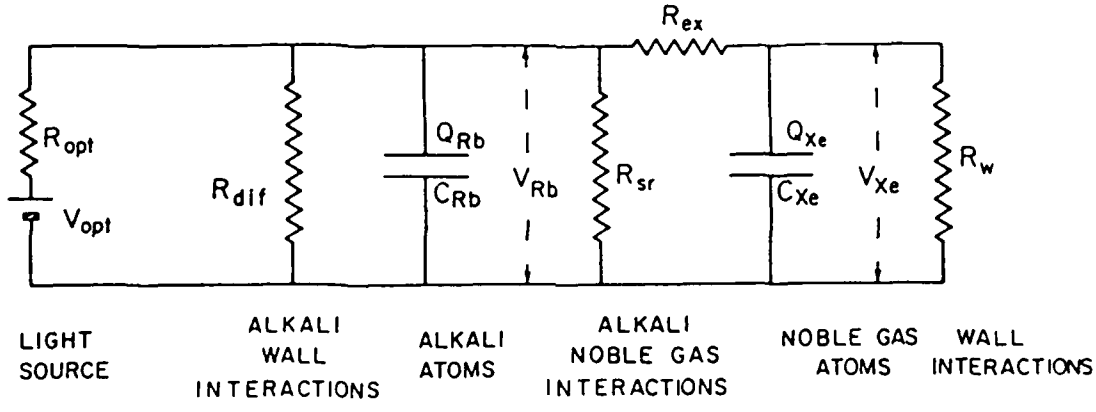

Fig. 7. RC network model for spin exchange between optically pumped alkali atoms and noble gas nuclei. Angular momentum is analogous to electrical charge and the alkali atoms and noble gas atoms in which the angular momentum is stored are represented by capacitors. Various spin interactions in the Hamiltonian are represented by resistors and the optical pumping light source is represented by an EMF with an internal resistance.

the spin orbit interaction in the noble gas and is nearly independent of the spin orbit interaction of the alkali atom. For completeness, we have also listed in Table II the value of γ inferred by Freeman et al.[9] for the v=0, N=0 state of the KAr molecule. This value was deduced from molecular beam magnetic resonance experiments and should be quite reliable although it is not directly comparable to the gas cell measurements of Bouchiat[8] and our group[6] which give the mean value of γ for all bound and quasi bound vibration and rotation states of the van der Waals molecule.

Table II

Comparison of γ/h inferred from experiment with γ/h calculated from (1). Also shown are the widths ΔH_0 of the magnetic slowing-down curves from Ref. 6 or the characteristic fields H_1^* for the magnetic slowing-down curves of the electronic spin relaxation from Ref. 8.

Molecule	ΔHo or H_1^* (Gauss)	$\left\|\frac{\gamma_{expt}}{h}\right\|$ (MHz)	$-\frac{\gamma_{theory}}{h}$ (MHz)	Ref
$^{39}K^{129}Xe$	65±4	2.5±0.2	3.6	6
$^{85}Rb^{129}Xe$	74±8	1.7±0.2	2.4	6
$^{133}Cs^{129}Xe$	109±15	1.8±0.2	2.9	6
$^{87}RbAr$	1.0-1.2	0.09-0.11	0.14	8
$^{87}RbKr$	9.59±.28	0.647	0.88	8
$^{8}RbXe$	38.1±1.0	1.4 -1.7	2.4	8
^{39}KAr		0.240	0.3[illegible]	9

We have used the new formula (1) to estimate γ for the molecules listed in Table II. The steps involved are illustrated in Fig. 1 which shows a van der Waals potential curve U(R) for KAr, the classical probability P(R)dR of finding a bound or quasibound molecule between R and R+dR, and the spin rotation coefficient γ calculated from (1). The potential U(R) has the form $ar^{-12}-br^{-6}$ with the constants a and b chosen to reproduce the well depth E and equilibrium separation R_0 given by Baylis[10]. To good approximation the value of γ for KAr should be $-\gamma(R_0) = -\gamma(5.27\text{Å}) = 0.31$ MHz. This is larger than the experimental value of 0.24 MHz by 30%. However, as one can see from Fig. 1, $|\gamma(R)|$ drops so rapidly with internuclear separation that one would get perfect agreement between experiment and theory if the internuclear separation were 5.40Å, 2.5% larger than the value given by Baylis.[10] For the first six entries in Table II we have computed the mean value

$$\bar{\gamma} = \int_0^\infty \gamma(R)\ P(R)\ dR \qquad (4)$$

for curves like those of Fig. 1. There is excellent agreement with the systematic variation of γ for the six van der Waals molecules but again the absolute value of γ is too large, by about a factor of 1.5. This discrepancy would be eliminated if the van der Waals potential had a minimum at an internuclear separation which was a few percent larger than those tabulated by Baylis[10]. We note also that the computed values of γ would be about 10% smaller if instead of using the valence electron wave functions $\phi_1(R)$ tabulated in Ref. 5, we were to use Coulomb approximation wave functons.[11] The systematic discrepancy between the calculated and experimental values of γ is therefore well within the expected systematic uncertainty of the parameters used to evaluate (1) and (4).

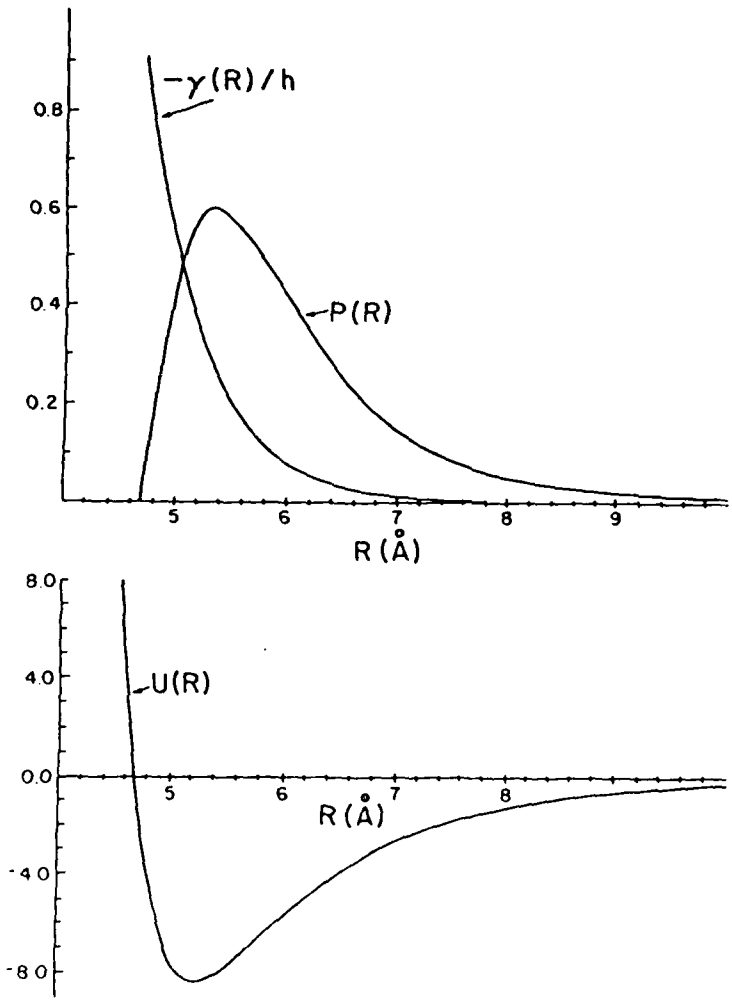

Fig. 1 The spin rotation constant $\frac{\gamma}{h}$ in MHz calculated from Eq. (1) as a function of internuclear separation R in Å for a KAr pair. Also shown is the classical probability density P(R) in $Å^{-1}$ for finding a bound or quasibound KAr pair with an internuclear separation R. The van der Waals potential U, in units of 10^{-14} erg, from which P was calculated for a temperature of 100 C is shown in the lower sketch.

The derivation of (1) is straightforward. We imagine an alkali atom at rest with an unperturbed valence electron wave function ϕ_1. A noble gas atom moves by the alkali atom with a velocity $\vec{v}$. The alkali valence electron will scatter in the Coulomb potential V of the noble gas atom. We account for the scattering to first approximation by orthogonalizing the alkali valence electron wave function to the core electron orbitals $\psi_i(\vec{r})\, e^{\frac{im\vec{v}\cdot\vec{r}}{h}}$ of the moving noble gas atom. The orbital of the resting noble gas is $\psi_i(\vec{r})$ where $\vec{r}$ is the distance from the noble gas nucleus, and the phase factor $e^{\frac{im\vec{v}\cdot\vec{r}}{h}}$ accounts for the motion. This is analogous to the orthogonalized plane wave method used to calculate conduction electron wave functions in solids[12] except that the translational phase factor does not normally occur in solids. Then the orthogonalized valence electron wave function is

$$\phi(\vec{r}) = \phi_1(\vec{r}) - \sum_i \psi_i(\vec{r}) e^{\frac{im\vec{v}\cdot\vec{r}}{h}} \int \psi_i^*(\vec{r}') e^{\frac{-im\vec{v}\cdot\vec{r}'}{h}} \phi_1(\vec{r}') d^3r' \qquad (5)$$

The alkali wave function $\phi_1(\vec{r})$ and the translational phase factor $e^{\frac{im\vec{v}\cdot\vec{r}}{h}}$ will vary slowly in the neighborhood of the noble gas core and their product can be expanded as a power series in $\vec{r}$ so the integral in (5) becomes

$$\int \psi_i^*(\vec{r}') \, [\phi_1(R) + \vec{A}\cdot\vec{r}' + \ldots] d^3\vec{r}' \qquad (6)$$

where the complex vector $\vec{A}$ is

$$\vec{A} = \frac{\vec{R}}{R} \frac{d\phi_1(R)}{dR} - \frac{im\vec{v}}{h} \phi_1(R) \qquad (7)$$

Then the orthogonalized wave function (5) becomes

$$\phi(\vec{r}) = \phi_1(\vec{r}) - \sum_n C_{np}\, \vec{A}\cdot\vec{\psi}_{np}\, e^{\frac{im\vec{v}\cdot\vec{r}}{\hbar}} + \ldots \tag{8}$$

where we have focused attention on the p orbitals of the noble gas core and C_{np} was defined by (3). For convenience we have denoted the three substates of the np orbital with the Cartesian vector $\vec{\psi}_{np} = \hat{x}\psi_{npx} + \hat{y}\psi_{npy} + \hat{z}\psi_{npz}$. The expectation value of the spin-orbit interaction is then

$$-\langle\phi|\, \frac{\mu_B}{mc}\, \vec{\nabla}V\times\vec{p}\cdot\vec{S}|\phi\rangle = i\, G\, \vec{A}\times\vec{A}^*\cdot\vec{S} = \gamma\vec{N}\cdot\vec{S} \tag{9}$$

where G was defined by (2). Substituting for $\vec{A}$ from (7) into (9) we find the expression for γ given in (1). One can easily verify that the same formula (1) for γ is obtained if both the alkali atom and the noble gas atom are moving in such a way that the relative velocity of the noble gas atom with respect to the alkali atom is $\vec{v}$. Formula (1) can also be obtained by the method outlined by Herman[4] if rotational excitation of the core orbitals of the noble gas is included. These terms were neglected by Herman with the result that the alkali valence electron orbital was orthogonalized to the resting noble gas orbitals rather than to the moving orbitals.

The formula (1) for γ is closely analogous to Herman's formula[13] for the Fermi contact interaction coefficient.

$$\alpha(R) = \frac{16\pi}{3}\, \frac{\mu_B\mu_K}{K}\, n^2|\phi_1(R)|^2 \tag{10}$$

The enhancement factor η^2, like the factor G of (2), depends only on the properties of the noble gas through overlap integrals with noble-gas core electron orbitals. The dependence of both γ and α on the internuclear separation R is dominated by the exponential decrease of the unperturbed alkali valence electron wave function $\phi_1(R)$.

In conclusion, we have shown how to derive a simple formula (1) for the spin-rotation coupling constant γ of alkali-noble gas van der Waals molecules. Although (1) could be refined, for example, by including the distortion of the alkali valence electron outside of the noble gas core or by replacing the orthogonalization procedure (7) with a solution of the wave equation within the noble gas core and proper boundary matching, the simplest approximation (1) already gives reasonable agreement with experiments. It should be possible to use the closely analogous formulas (1) and (10) to reliably estimate the key spin coupling parameters γ and α for many untested noble-gas-alkali-atom pairs and their isoelectronic analogs (e.g. KRn, Ba^+Ne, etc.).

It is a pleasure to acknowledge useful discussions with P.W. Anderson and S.Treiman.

This work was supported by the U.S. Air Force Office of Scientific Research under Grant No. AFOSR 81-0104-C.

References

1. B.C. Grover, Phys. Rev. Lett. 40, 391 (1978); C.H. Volk, T.M. Kwon and J.G. Mark, Phys. Rev. A21 1549 (1980).

2. W. Happer, E. Miron, S. Schaefer, D. Schreiber, W.A. van Wijngaarden, and X. Zeng, Phys. Rev. A 29, 3092 (1984); X. Zeng, Z. Wu, T. Call, E. Miron, D. Schreiber and W. Happer, Phys. Rev. A31, 260 (1985).

3. R.A. Bernheim, J. Chem. Phys. 36, 135 (1962).

4. R.M. Herman, Phys. Rev. 136, A1576 (1964).

5. Frank Herman and Sherwood Skillman, Atomic Structure Calculations, Prentice Hall 1963.

6. Z. Wu and W. Happer, Proceedings of the Workshop on Polarized Targets in Storage Rings, Argonne National Laboratory, May 17-18, 1984.

7. N.D. Bhaskar, W. Happer and T. McClelland, Phys. Rev. Lett. 49, 25 (1982).

8. M.A. Bouchiat, J. Brossel and L.C. Pottier, J. Chem. Phys. 56, 3703 (1972).

9. E.M. Mattison, D.E. Pritchard and D. Kleppner, Phys. Rev. Lett. 32, 507 (1974); R.R. Freeman, E.M. Mattison, D.E. Pritchard and D. Kleppner, J. Chem. Phys. 64 1194 (1976).

10. W.E. Baylis, J. Chem. Phys. 51, 2665 (1969).

11. D.R. Bates and A. Damgaard, Phil. Trans. Roy. Soc. Lon. 242, 101 (1949).

12. C. Herring, Phys. Rev. 57, 1169 (1940); M.H. Cohen and V. Heine, Phys. 122, 1821 (1961).

13. R.M. Herman, Phys. Rev. 137, A1062 (1965).

Figure Caption

Fig. 1 The spin rotation constant $\frac{\gamma}{h}$ in MHz calculated from Eq. (1) as a function of internuclear separation R in Å for KAr pair. Also shown is the classical probability density P(R) in $Å^{-1}$ for finding a bound or quasibound KAr pair with an internuclear separation R. The van der Waals potential U, in units of 10^{-14} erg, from which P was calculated for a temperature of 100 C is shown in the lower sketch.

END
FILMED
4-86
DTIC